Alma Mater Studiorum – Università degli Studi di Bologna

FACOLTÀ DI SCIENZE MATEMATICHE, FISICHE E NATURALI
Dipartimento di Chimica "G. Ciamician"

DOTTORATO DI RICERCA IN
SCIENZE CHIMICHE
Ciclo XXIV

Settore scientifico-disciplinare di afferenza: CHIM 03

Preparation of new crystal forms *via* photochemical mechanochemical and sol-gel methods

Presentata da:
Dott.
SIMONE D'AGOSTINO

Relatore:
Chiar.mo Prof.
DARIO BRAGA

Coordinatore Dottorato:
Chiar.ma Prof.ssa
ADRIANA BIGI

Esame finale - Anno 2012

Welcome Sophia

A crystal is a chemical graveyard.

L. Ruzička

Nothing could be further from the truth.

Preparation of new crystal forms via photochemical mechanochemical and sol-gel methods

Chapter 4 - Design of Low Molecular Weight Gelators and MetalloGelators

Chapter 1 - Caesium crown ether complexes with aromatic polycarboxylate anions

Preface

Crystal engineering is the rational design of molecular solids,[1] i.e. the synthesis of functional solid-state structures from neutral or ionic building blocks. Design strategies make use of a pletora of intermolecular interactions, from coordination bonds between ligands and metal centers to coulombic attractions and repulsions between ions, interactions of the van der Waals type, π-stacking and interactions between halogen atoms as well as hydrogen bonds in the whole range of strength from weak interactions of the C—H···O type to strong "charge assisted" bonds between ions; all these interactions can be used in many different combinations.[2]

Crystal engineering can be regarded as a solid-state supramolecular chemistry and it goes far beyond the traditional divisions of organic and inorganic chemistry, thus resulting in an extraordinary blend of ideas and techniques.

This work involves various aspects of this branch of chemistry. Chapter 1 focuses on crystals containing crown ether complexes. Aspects such as the possibility of preparing these materials by *non-solution methods*, *i.e.* by direct reaction of the solid components,[3] thermal behavior and also isomorphism and interconversion between hydrates are taken into account.

In chapter 2 a study is presented aimed to understanding the relationship between hydrogen bonding capability and *shape* of the building blocks chosen to construct crystals. The focus is on the control exerted by shape on the organization of sandwich cations such as cobalticinium, decamethylcobalticinium and bisbenzenchromium(I) and on the aggregation of monoanions all containing carboxylic and carboxylate groups, into 0-D, 1-D, 2-D and 3-D networks.

Reactions conducted in multi-component molecular assemblies or co-crystals have been recognized as a way to control reactivity in the solid state. The [2+2] photodimerization of olefins[4] is a successful demonstration of how templated solid state synthesis can efficiently synthesize unique materials with remarkable stereoselectivity and under environment-friendly conditions.[5] A demonstration of this synthetic strategy is given in chapter 3.

The combination of various types of intermolecular linkages, leading to formation of high order aggregation and crystalline materials or to a random aggregation resulting in an amorphous precipitate, may not go to completeness. In such rare cases an aggregation process intermediate between crystalline and amorphous materials is observed, resulting in the formation of a gel, i.e. a viscoelastic solid-like or liquid-like material.[6]

Supramolecular gels[7] represent a blooming field in the more general area of crystal engineering; potential applications have been and are being found in the design of a new class of functional materials: Low Molecular Weight Gelators (LMWGs) are molecular or coordination network materials able to gel solvents under the application of appropriate stimuli.

In chapter 4 design of new LMWGs is presented. Aspects such as the relationships between molecular structure, crystal packing and gelation properties and the application of this kind of gels as a medium for crystal growth[8] of organic molecules, such as APIs, are also discussed.

References

[1] G. R. Desiraju, *Angew. Chem. Int. Ed.*, 2007, **46**, 8342-8356. (b) D. Braga and F. Grepioni Eds., *Making Crystal by Design: Methods, Techniques and Applications*. WILEY-VCH, Weinheim, 2007.

[2] (a) D. Braga, Chem. Commun., 2003, 2751-2754 . (b) D. Braga, F. Grepioni and L. Maini, Chem. Commun., 46, 6232-6242.

[3] (a) D. Braga, L. Maini, S. L. Giaffreda, F. Grepioni, M. R. Chierotti and R. Gobetto, *Chem.–Eur. J.*, 2004, **10**, 3261; (*c*) D. Braga, M. Curzi, F. Grepioni and M. Polito, *Chem. Commun.*, 2005, 2915; (*d*) D. Braga, M. Curzi, A. Johansson, M. Polito, K.Rubini and F.Grepioni, *Angew. Chem., Int. Ed.*, 2006, **45**, 142.

[4] M. D. Cohen and G. M. J. Schmidt, J. Chem. Soc., 1964, 2000–2013; (b) G. M. J. Schmidt, Pure Appl. Chem., 1971, 27, 647–678.

[5] (a) S. Anderson AND H. L. Anderson, in *Templated Organic Synthesis*; F. Diederich, P. J. Stang, Eds. Wiley-VCH: New York, pp. 1–38, 2000. (b) X. Gao, T. Friscic, L. R. MacGillivray, *Angew. Chem. Int. Ed.* 2004, **43***,* 232-236.

[7] (a) P. Sahoo, D. Krishna kumar, D. R. Trivedi, P. Dastidar, *Tetrahedron Lett*. 2008, **49**, 3052 (b) P. Dastidar*, Chem. Soc. Rev.,* 2008, **37**, 2699-2715. (c)) D. K. Smith, in *Organic Nanostructures*, Eds. J. L. Atwood, J. W. Steed, WILEY-VCH, Weinheim, 2008, pp. 111-148.

[8] J. A. Foster, M.O. Piepenbrock, G. O. Lloyd, N. Clarke, J. A. K. Howard and J. W. Steed, N*ature Chemistry*, 2010, **2**, 1037-1043.

1 Introduction

Crown ethers constitute a popular class of compounds. First prepared by Pedersen[1] in 1967, the number of their derivatives and complexes are nowadays known by the thousands.[2] This wealth is also a consequence of the stability of the complexes that crown ethers form with a variety of metal and other inorganic cations. Crown ethers complexes have been amply utilized in supramolecular chemistry[3] and crystal engineering[4] as modules for the construction of complex superstructures.

Braga *et. al.* have shown in a series of publications[5-10] that crown ethers can also be used in solid-solid and solid-liquid processes to capture alkali metal and ammonium cations in extended hydrogen bonded networks formed by inorganic acid anions, such as the hydrogen sulphate and the di-hydrogen phosphate as well as by organic acid anions. These compounds constitute the subject matter of this first chapter with a focus on the preparation methods and on crystal to crystal transformations[11] and isomorphism.

2 Aim of the work

In the last decade the group has reported a number of publications on non-solution methods to prepare novel supramolecular materials;[5-10] manual grinding in the air of solid 18-crown[6] with solid hydrogen sulfate salts of alkali metals, dihydrogen phosphate salts of alkali metals and hydrogen sulfate salts of Cd^{2+}, Mn^{2+}, Pb^{2+} leads to formation of hydrated crown ether complexes, the water molecules being taken up from ambient humidity during grinding.

The basic idea is to extend the strategy to the complexation of the metal cation Cs^{+} with the crown ether 18-crown[6] and anions derived from aromatic polycarboxylic acids as those shown in scheme 1, which are of interest in the construction of coordination networks and hydrogen-bonds between ions, a relevant supramolecular chemistry and crystal engineering issue.[12] In the second section of this chapter also the investigation of isomorphous crystals is taken into account since it is usually very informative on the robustness of a given packing arrangement and/or of given sets of bonding and supramolecular bonding interactions.

Moreover, this study provides an additional example of the use of mechanochemical methods as an alternative to conventional solution chemistry to prepare new solids (molecular crystals and co-crystals, but also coordination networks and metal complexes) by mechanical mixing of the reactants (grinding) or in the presence of a catalytic amount of solvent (kneading).[13]

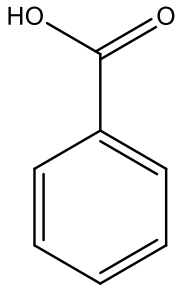

Benzoic acid (benH)

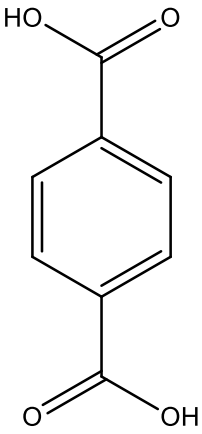

Terephthalic acid (tereH$_2$)

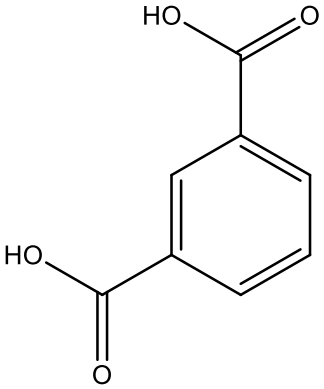

Isophthalic acid (isoH$_2$)

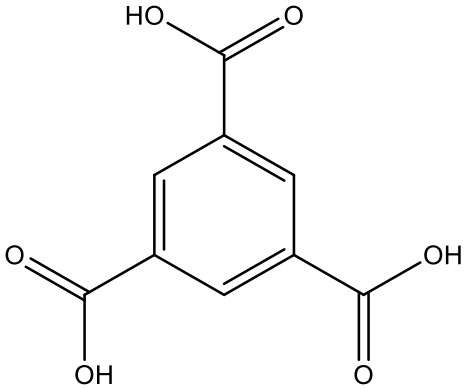

Trimesic acid (trmH$_3$)

Scheme 1. Aromatic mono-, di- and tri-carboxylic acids used in the present study. Throughout the text the following abbreviations are used: $[ben]^-$ = $[C_7H_5O_2]^-$, $[tereH]^-$ = $[C_8H_5O_4]^-$, $[isoH]^-$ = $[C_8H_5O_4]^-$, $[trimH_2]^-$ = $[C_9H_5O_6]^-$, $[trim]^{3-}$ = $[C_9H_3O_6]^{3-}$.

These complexes have all been obtained by mechanical mixing of the reactants in the solid state, followed by dissolution in bidistilled water. This strategy allowed us to obtain six complexes, of formula: 18-crown[6]·Cs[trimH$_2$] (**1**), 18- crown[6]·Cs[isoH] (**2**) and 18-crown[6]·Cs$_2$[isoH]$_2$·2H$_2$O (**3**), (18-crown[6])3·Cs$_3$[trim]·9H$_2$O (**4**), 18-crown[6]·Cs[ben]·(H$_2$O) (**5**) and (18-crown[6])$_6$·Cs$_4$[tereH]$_2$[tere]·5H$_2$O (**6**). The thermal behaviour of **1**, **2** and **4** has been investigated *via* DSC, TGA and variable-temperature X-ray diffraction experiments.

3 Structural description

*3.1 - 18-crown[6]·Cs[trimH_2] (**1**).* In crystalline **1** the Cs^+ cation is coordinated to six oxygen atoms of the crown ether [$Cs^+\cdots O_{crown}$ = 3.063(3)–3.258(3) Å] and two oxygen atoms of di-hydrogen trimesates [$Cs^+\cdots O^-$ = 3.145(3) Å and $Cs^+\cdots O_{C=O}$ = 2.917(3) Å] (figure 1a), while an oxygen atom from a second crown ether completes the coordination sphere of Cs^+ [$Cs^+\cdots O_{crown}$ = 3.488(3) Å] as shown in figure 1b.

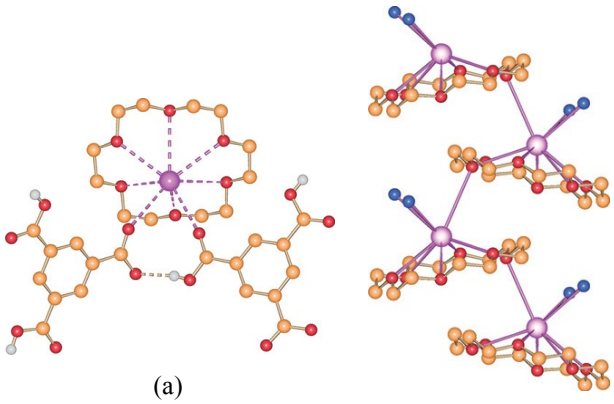

(a) (b)

Fig.1. (a) Coordination geometry of the crown ether and two dihydrogen trimesate anions (referred by symmetry) around the Cs+ ion in crystalline **1**. (b) Chain arrangement in crystalline **1**, as one oxygen atom in a second crown ether completes the coordination sphere of Cs^+. Blue spheres represent the metal-coordinated trimesate oxygen atoms in (a). H_{CH} atoms omitted for clarity.

The structure of **1** is characterized by the presence of chains of dihydrogen trimesate anions linked via C=O···H–O hydrogen bonds [$O_O\cdots O_{C=O}$ = 2.598(4) Å], see Fig. 6a. Thermal gravimetric analysis on solid 1 shows a weight loss of ca. 43 % in the temperature range 210–280 °C, in agreement with the evaporation of the crown ether. A VT-XRPD experiment (figure 2) shows that crystalline **1** is stable at least up to 100 °C.

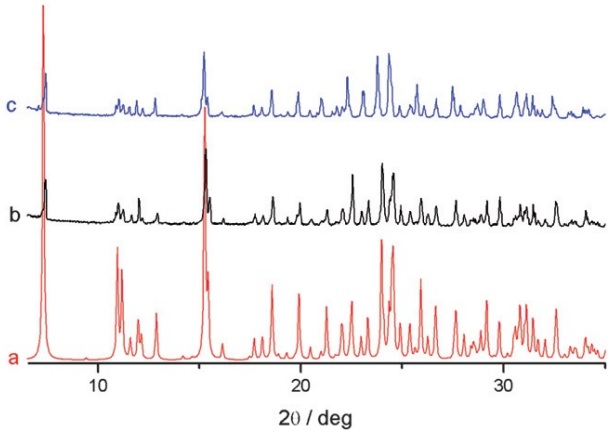

Fig.2. (a) Calculated (on the basis of single crystal data) XRPD pattern for **1** (b) and (c) experimental XRPD patterns at RT and at 100 °C, respectively.

*3.2 - 18-crown[6] ·Cs[isoH] (**2**)*. In crystalline **2** the Cs^+ cation is coordinated to six oxygen atoms of the crown ether [$Cs^+\cdots O_{crown}$ = 3.090(2)–3.285(3) Å] and two oxygen atoms of hydrogen isophthalates ($Cs^+\cdots O^-$ = 3.046(2) Å and $Cs^+\cdots O_{C=O}$ = 3.057(3) Å]; an oxygen atom from a second crown ether completes the coordination sphere of Cs^+ [$Cs^+\cdots O_{crown}$ = 3.445(3) Å], as shown in figure 3. Also the structure of **2** is characterized by the presence of chains of hydrogen isophthalate anions linked *via* C=O···H–O hydrogen bonds [$O_{OH}\cdots OC=O$ = 2. 456(3) Å], in a very similar manner to that observed in complex 1 (see Fig. 4 and 5). It is worth noting that **1** and **2** crystallize in the same space group with very close cell parameters (see Table 1) and that their packings are very similar, which is unexpected in view of the difference in size and shape of the anions and the different number of carboxylic groups in the two anions.

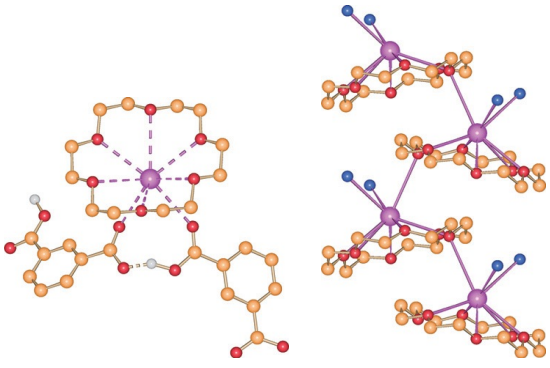

(a) (b)

Fig.3. (a) Coordination geometry of the crown ether and two hydrogenisophthalate (referred by a symmetry operation) around the Cs^+ ion in crystalline **2** (compare with Fig. 1). (b) Chain arrangement in crystalline **2**, as one oxygen atom in a second crown ether completes the coordination sphere of Cs^+. Blue spheres represent the coordinated trimesate oxygen atoms in (a). H_{CH} atoms omitted for clarity. Note the similarities between the packing of **1** (fig. 1) and **2**.

Figure 4 shows a comparison of the hydrogen bonding patterns involving the dihydrogen trimesate and hydrogen isophthalate anions in crystalline **1** and **2**. In crystalline **1** each carboxylic group not involved in the inter-row hydrogen bonds (figure 4a) forms an out-of-plane hydrogen-bond with a carboxylate fragment belonging to a different row, as the two groups are lying in planes that are tilted with respect to each other, see figure 4c. This last bond originates a 2-D network of anions, see figure 4a. No additional hydrogen bond is possible, however, in crystalline **2** (see figure 4b and 4d), and only a 1-D network is present in this structure.

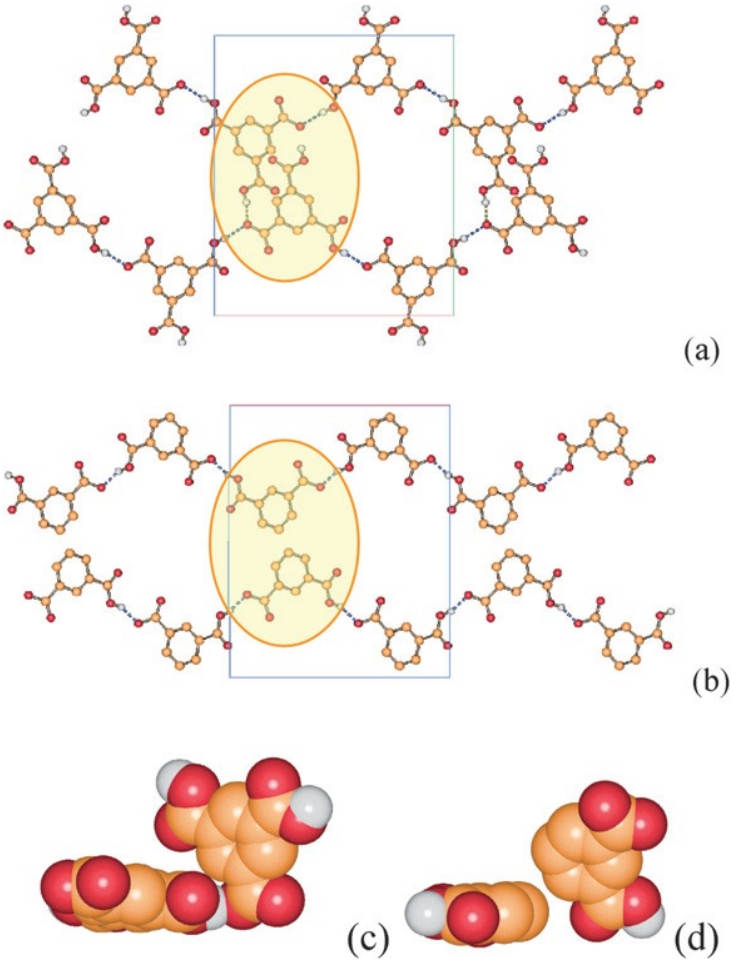

Fig.4. 2-D (a) and 1-D (b) hydrogen bonding anionic networks in crystalline **1** and **2**. Note the close similarity of the two arrangements, in spite of the fact that the hydrogen isophthalate anions possess one carboxylic group less with respect to the dihydrogen trimesate anion. (c) The extra COOH group in **1** allows formation of the 2-D network via an out-of-plane hydrogen bond with a carboxylate group belonging to a second row of anions; the same bond cannot be formed in **2** (d).

Thermal behaviour of crystalline **2** is also of some interest because the thermogravimetric measurements indicate a total weight loss of ca. 47 % in the interval 175–275 °C, which is in agreement with the loss (for evaporation) of 1 mol of crown ether as observed in **1**, although this process occurs in two steps (figure 5). If the process is investigated by hot stage microscopy, the formation of liquid crown ether at 190 °C can be observed. The liquid then rapidly evaporates leaving a crystalline residue, which could corresponds to Cs[isoH] or to an intermediate phase still containing a fraction of crown ether. The hot stage process is shown in figure 6. The DSC trace of **2** on heating (first cycle, see figure 7) shows a single endothermic peak at 181 °C (ΔH = 86 J g^{-1}). After cooling, a second heating cycle (see figure 7) reveals an endothermic peak at 173 °C, associated with a lower ΔH value (53 J g^{-1}).

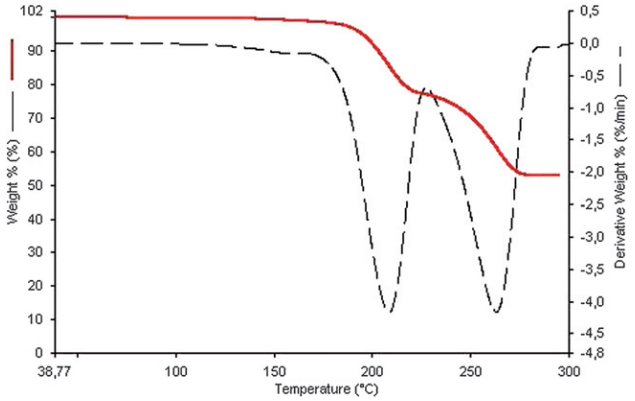

Fig.5. TGA trace for complex **2**: the extrusion of the crown ether occurs in two well defined steps.

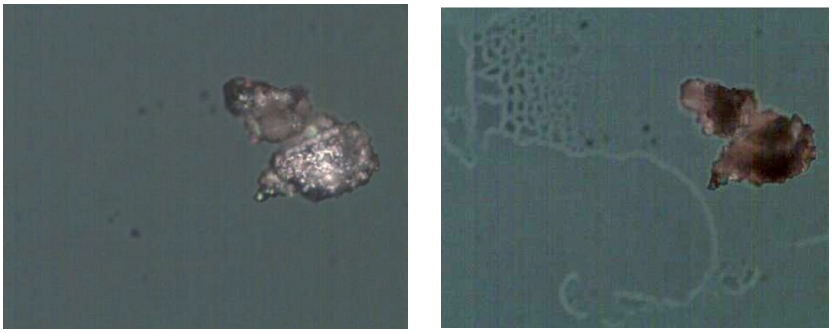

(a) (b)

Fig.6. Hot Stage Microscopy images taken on crystalline fragment of a solid sample of **2**, on heating from 25 °C (top) to 190 °C (bottom): note the formation of a liquid phase at high temperature, due to partial extrusion (and melting) of 18- crown(6) from crystalline **2**.

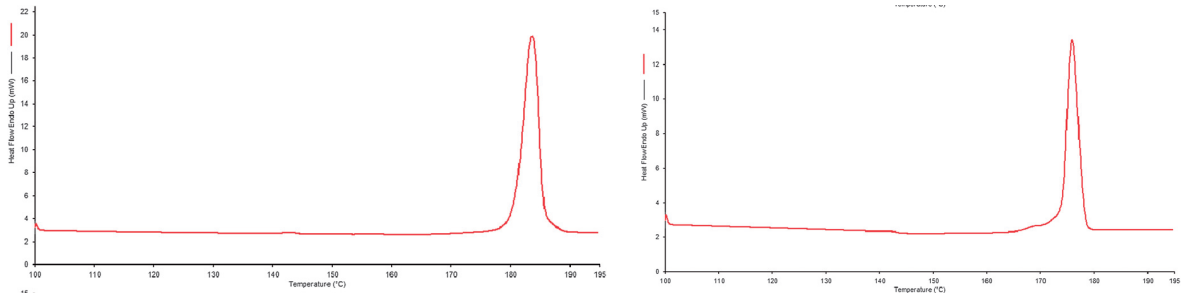

(a) (b)

Fig.7. DSC trace for complex **2** (a) first heating cycle and (b) second heating cycle.

Variable temperature X-ray powder diffraction on complex **2** (figure 8) indicates some changes in the crystalline structure of **2** after 20 min at 190 °C. These changes are irreversible, since the new compound does not revert to the original form on standing or if mechanically mixed.

*3.3 - 18-crown[6]·Cs_2[isoH]$_2$·2H_2O (**3**).* Recrystallization of this product from water yields a crystalline solid of formula 18-crown[6] ·Cs_2[isoH]$_2$·2H_2O (**3**), see figure 9, that confirms our assumption about the partial loss of the crown ether; at the same time, the diffractogram calculated on the basis of single crystal data of **3** and the experimental one measured at 190 °C for **2** do not compare well, so we cannot be more precise about the exact formula/structure of the crystalline residue from the hot-stage experiment.

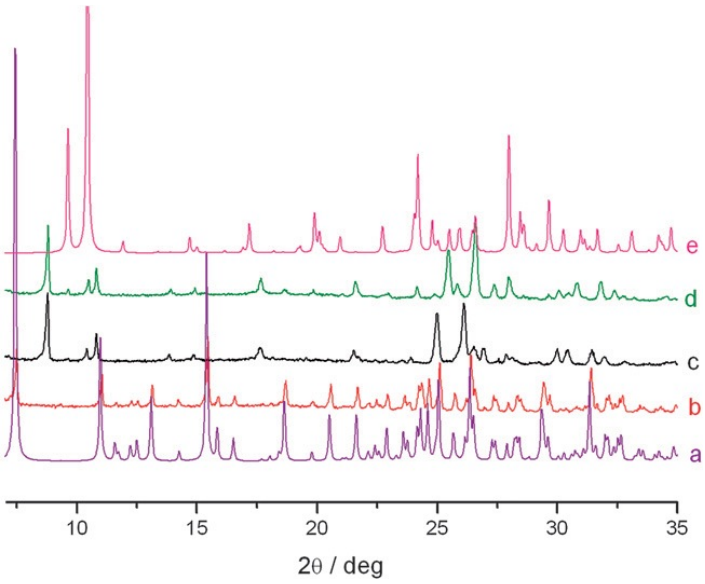

Fig.8. (a) Calculated (on the basis of single crystal data) XRPD pattern for **2**; (b–d) experimental XRPD patterns at RT, after heating at 190 °C for 20 min and after cooling back to RT, respectively; (e) calculated (on the basis of single crystal data) XRPD pattern for **3**.

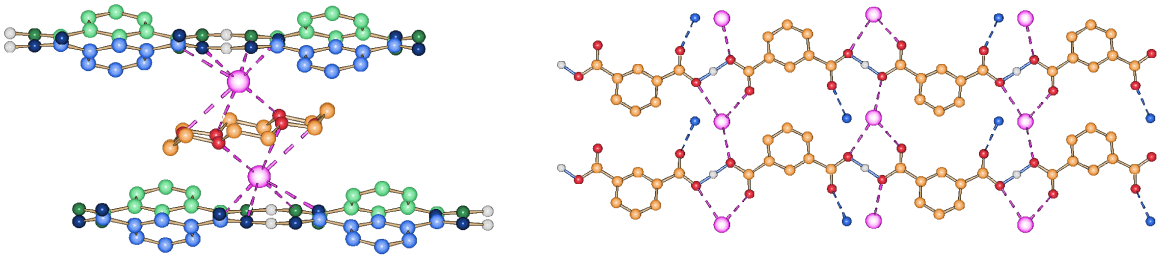

(a) (b)

Fig.9. Structure of crystalline 18-crown[6]·Cs_2[isoH]$_2$·2H_2O (**3**). (a) The Cs^+ cations, which are referred by a crystallographic inversion centre, are linked to three oxygen atoms of the crown ether [$Cs^+\cdots O_{crown}$ = 3.225(3)–3.336(3) Å] and an oxygen atom from the hydrogen-isophthalate anion [$Cs^+\cdots O^-$ = 3.072(3)–3.494(3) Å]. (b) The hydrogen isophthalate anion forms also a hydrogen bond with a water molecule (represented by a blue sphere) [$O_{water}\cdots O_{C=O}$ = 2.915(3) Å]. $H_{CH/water}$ atoms not shown for clarity.

The diffraction, thermogravimetric, calorimetric and hot stage measurements allow to construct a simple model for the thermal behaviour of **2** (see Scheme 2).

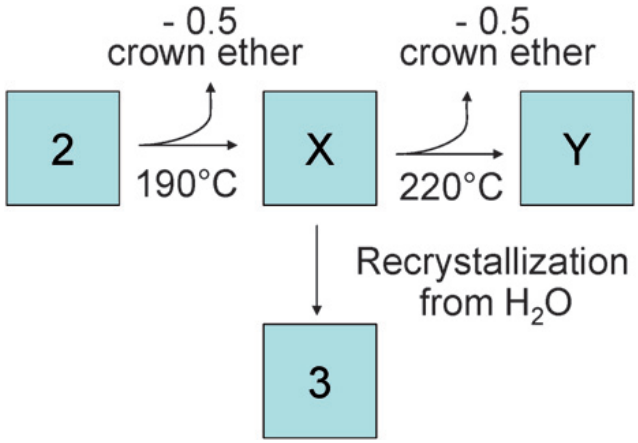

Scheme 2. Representation of the thermal behaviour of **2**. Extrusion of half a mole of crown ether at 190 °C produces a form X (presumably anhydrous), that recrystallizes from water to yield complex **3**. A further heating on X induces the extrusion of the second half mole of crown ether, and yields the unknown phase Y.

*3.4 - (18-crown[6])$_3$·Cs_3[trim]·9H_2O (**4**).* In crystalline **4** each Cs^+ ion is coordinated to six oxygen atoms of the crown ether [$Cs^+\cdots O_{crown}$ = 2.989(4)–3.403(5) Å]. The resulting supramolecular units are all interconnected via oxygen atoms belonging to water molecules and trimesate carboxylate groups [$Cs^+\cdots O_{trim}$ = 3.189(3)–3.230(4) Å]; $Cs^+\cdots O_{water}$ = 3.159(5)–3.58(6) Å] (figure 10). Figure 10b shows the complex 2-D hydrogen bonding network formed by water molecules and trimesate anions [$O_{trim}\cdots O_{water}$ = 2.690(7)–3.070(6) Å; $O_{water}\cdots O_{water}$ = 2.688(8)–3.030(2) Å].

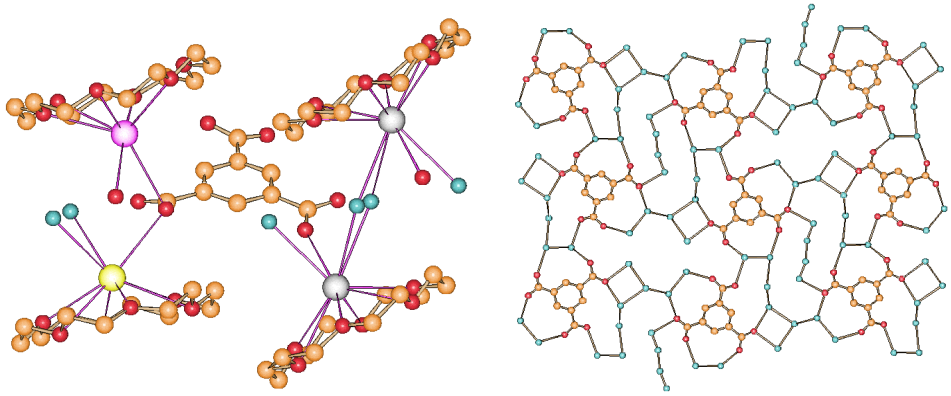

(a) (b)

Fig.10. (a) Coordination of crown ethers, water molecules and trimesate anions around the caesium cations in crystalline 4. Stars indicate oxygen atoms belonging to trimesate anions (not shown for clarity). (b) The 2-D hydrogen bonding network formed by water molecules and trimesate anions (H atoms not shown for clarity).

TGA measurements on compound **4** indicate three weight losses (figure 11), the first (ca. 6.4 %) in the range 50–80 °C, the second (ca. 2.5%) in the range 90–125 °C, and the third (ca. 52%) in the range 130–250 °C. The first two processes are consistent with the loss of 5.5 and 2.5 water molecules per formula unit, respectively, while the third is probably associated with the loss (evaporation) of 18-crown[6] and of the residual water molecule. The DSC trace on heating (first cycle) shows two broad endothermic peaks at 67 °C ($\Delta H = 119$ J g^{-1}) and at 101 °C ($\Delta H = 48$ J g^{-1}), see figure 11. Peak shape and enthalpic balance are consistent with water evaporation processes, corresponding to the loss of the 8 water molecules observed in the TGA measurement. No further transformation is observed upon cooling and reheating of the same sample.

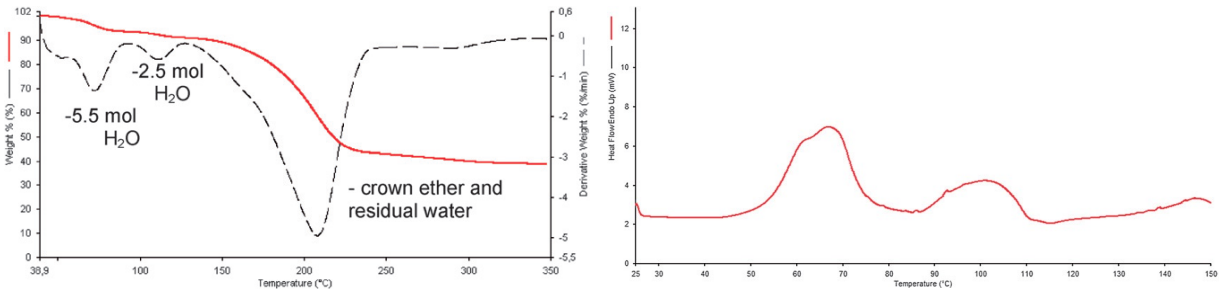

(a) (b)

Fig.11. (a) TGA trace of crystalline **4** and (b) DSC trace of complex **4** (first heating cycle).

VT-XRPD experiments were particularly useful to investigate these dehydration processes; the loss of 5.5 water molecules after heating to 85 °C leads to the partially hydrated product A and is fully reversible: after mechanical mixing A reverts in *ca.* 45 minutes to the original form **4** *via* uptake of air humidity, as it can be seen in figure 12. Further heating to 115 °C is associated to the loss of 2.5 water molecules, leading to the monohydrated product B. This process is also fully reversible: after mechanical mixing B reverts overnight to the original form **4** via uptake of air humidity (figure 13). Unfortunately, we did not succeed in growing single crystals of the two dehydration products A and B, and could not characterize them. The whole process is depicted in Scheme 3. Both A and B revert to the starting solid **4** via water uptake from air humidity; the process is accelerated by grinding.

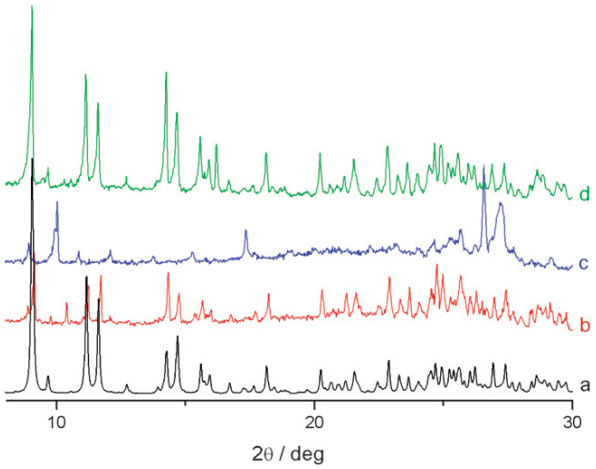

Fig.12. (a) Calculated (on the basis of single crystal data) XRPD pattern of **4**; (b)–(d) experimental XRPD pattern measured at RT, after heating to 85 °C and after mechanical mixing of the solid back at RT.

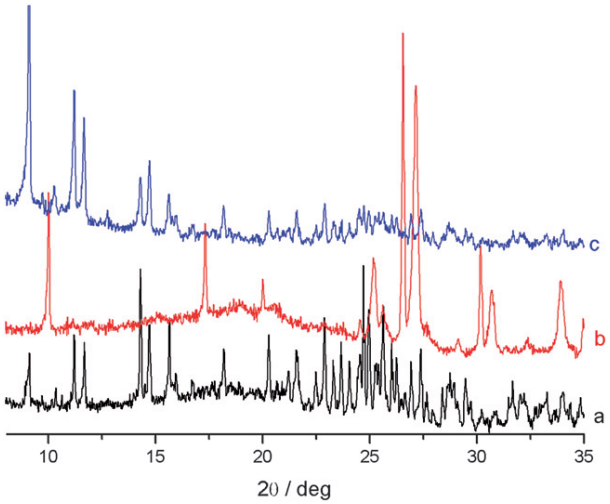

Fig.13. Comparison between the diffraction patterns measured on **4**: (a) starting diffractogram at RT; (b) diffractogram after heating the complex **4** to 115 °C and (c) diffractogram after mechanical mixing of B.

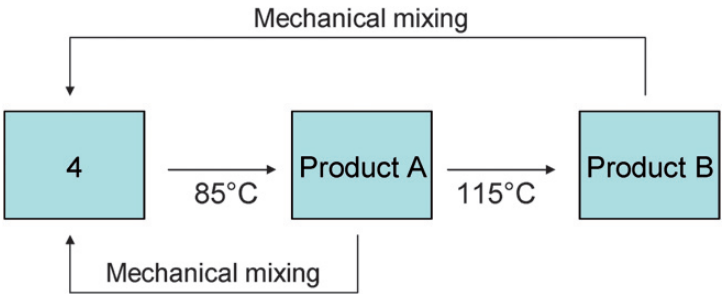

Scheme 3. Schematic representation of the two-steps thermal behavior of **4**. A sample of 4 is heated to 85 °C: 5.5 moles of water molecules are released and the partially dehydrated product A is formed; upon further heating of A to 115 °C, other 2.5 moles of water are released, and the monohydrate product B is formed. Further heating (not shown in the scheme) leads to evaporation of the crown ether and of the residual water molecule.

*3.5 - 18-crown[6]·Cs[ben]·H_2O (**5**)*. In crystalline 5 two caesium ions, which are referred by a crystallographic inversion centre, are each sandwiched between a crown ether [$Cs^+\cdots O_{crown}$ = 3.050(2)–3.293(2) Å] and an hydrogen-bonded ring formed by two benzoate anions and two water molecules [$O_{ben}\cdots O_{water}$ = 2.752(4)–2.772(4) Å; $Cs^+\cdots O_{ben}$ = 3.369(2)–3.535(2) Å; $Cs^+\cdots O_{water}$ = 3.511(3) Å], thus constituting a supramolecular ‘‘triple-decker’’ unit (figure 14). The overall crystal packing results from the arrangement of these neutral units (figure 14).

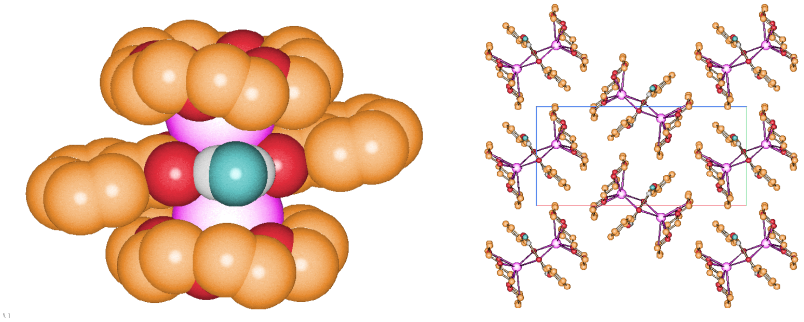

(a) (b)

Fig.14. (a) The supramolecular ‘‘triple-decker’’ unit in crystalline **5**, constituted of two caesium ions, each linked to a crown ether and to an hydrogen-bonded ring formed by two benzoate anions and two water molecules. (b) The resulting crystal packing. H_{CH} atoms omitted for clarity.

*3.6 - (18-crown[6])$_6$·Cs_4[tereH]$_2$[tere]·5H_2O (**6**)*. The same supramolecular unit of **5** is present in crystalline **6** [$Cs^+\cdots O_{crown}$ = 3.096(4)–3.310(4) Å; $O_{tereH}\cdots O_{water}$ = 2.744(8)–2.778(7) Å; $Cs^+\cdots O_{tereH}$ = 3.354(5)–3.441(6) Å; $Cs^+\cdots O_{water}$= 3.650(4)–3.752(6) Å]; as observed in **5**, the two caesiumions are referred by a crystallographic centre of inversion. In this case, though, the additional presence of a carboxylic group on the hydrogen-terephthalate

anions causes the formation of an extended 1-D hydrogen bonding network, by insertion of a second anion not bound to the crown ether moieties [$O_{tereH}\cdots O_{tereH}$ =2.439(6) Å], see figure 15. ‘‘Traditional’’ sandwich units, with caesium ions encapsulated between two crown ethers, are also detectable in the crystal, and they are connected to the 1-D network via hydrogen bonding interactions involving the remaining water molecules [$O_{crown}\cdots O_{water}$ = 2.915(2) Å, $O_{water}\cdots O_{water}$ = 2.406(2) Å, $O_{water}\cdots O_{tereH}$ = 2.809(1)–2.741(2) Å], see figure 15b.

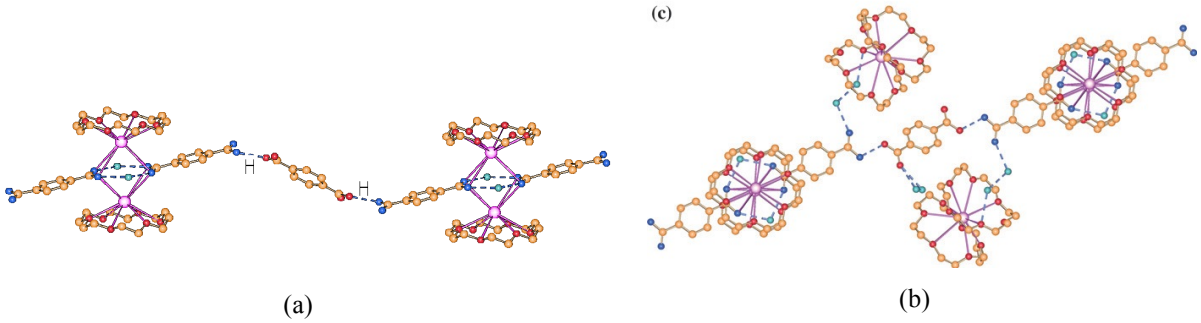

(a) (b)

Fig.15. (a) The supramolecular ‘‘triple-decker’’ unit in crystalline **6**, constituted of two caesium ions, each linked to a crown ether and to an hydrogen-bonded ring formed by two hydrogen-terephthalate anions and two water molecules (compare with Fig. 14a), the 1-D hydrogen bonding network formed via insertion, in between the supramolecular units, of a second anion not bound to the crown ether moieties. (b) ‘‘Traditional’’ sandwich units are connected to the 1-D network via hydrogen bonding interactions involving the remaining water molecules. No H_{OH} atoms observed. H_{CH} atoms omitted for clarity.

4 Isomorphism in caesium crown ether complexes with substituted isophthalates

The investigation of isomorphous crystals is usually very informative on the robustness of a given packing arrangement and/or of given sets of bonding and supramolecular bonding interactions.

It is worth noting that complexes **1** and **2** crystallize in the same space group with very close cell parameters (see Table 1) and that their packings are very similar, which is unexpected in view of the difference in size and shape of the anions , as the number of the *carboxylic* groups on the hydrogen-isophthalate and dihydrogen-trimesate monoanions is one and two for the two anions, respectively.

Intrigued by this feature, we decided to further explore differences and similarities in shape and function of 18-crown[6] caesium complexes containing anions derived from a series of 5-substituted isophthalic acids (scheme 4), in order to detect packing relations and verify to which extent the isomorphic features are dependent on the nature of the substituent, i.e. on its size, shape and ability to form hydrogen bonds.

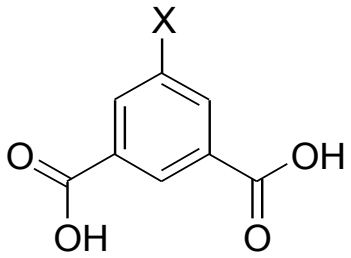

Scheme 4. The aromatic dicarboxylic acids $C_8H_4O_4X$ used in the present part of this study for the synthesis of 18-crown[6]·Cs[X-isoH] complexes [X = OH (**7**), CH_3 (**8**), Br (**9**), OCH_3 (**10**), NO_2 (**11**), t-butyl (**12**)].

In this section is reported the synthesis and characterization of six novel complexes, namely 18-crown[6]·Cs[OH-isoH] (**7**), 18-crown[6]·Cs[CH_3-isoH] (**8**), 18-crown[6]·Cs[Br-isoH] (**9**), 18-crown[6]·Cs[OCH_3-isoH] (**10**), 18-crown[6]·Cs[NO_2-isoH] (**11**) and 18-crown[6]·Cs[t-Butyl-isoH] (**12**). All complexes have been obtained by mechanical mixing of the reactants in the solid state and/or by reaction in aqueous solution.

The six complexes share the following features: (i) with the exception of **12** they are isomorphous to each other and with complexes **1** and 2; (ii) they are all anhydrous, (iii) they are stable up to *ca.* 220°C, temperature at which they decompose with loss of the crown ether and (iv) they can be obtained by grinding, *i.e.* by direct reaction in the solid state.

5 Structural description of the isomorphous crystals

The coordination sphere of the caesium cations in crystalline **7**, **8**, **9**, **10** and **11** closely resembles the one observed in complexes **1** and **2** (figure 16): the Cs^+ ion interacts with the six oxygen atoms of the crown ether and two oxygen atoms of the $[X\text{-isoH}]^-$ anions, with the exception of **7**, in which only one anion is linked to the cation trough the carboxylate group, while the other anion interacts with Cs^+ via the hydroxyl lone pair, see figure 16b. As it had been observed for complexes **1** and **2**, an oxygen atom from a second crown ether completes the coordination sphere of the caesium cation, as it can be seen in figure 17. In complex **12** the caesium ion coordination is completely filled by a single crown ether and two $[\text{t-Butyl-isoH}]^-$ anions (figure 17b). Relevant $Cs^+\cdots O$ interactions are listed in Table 2.

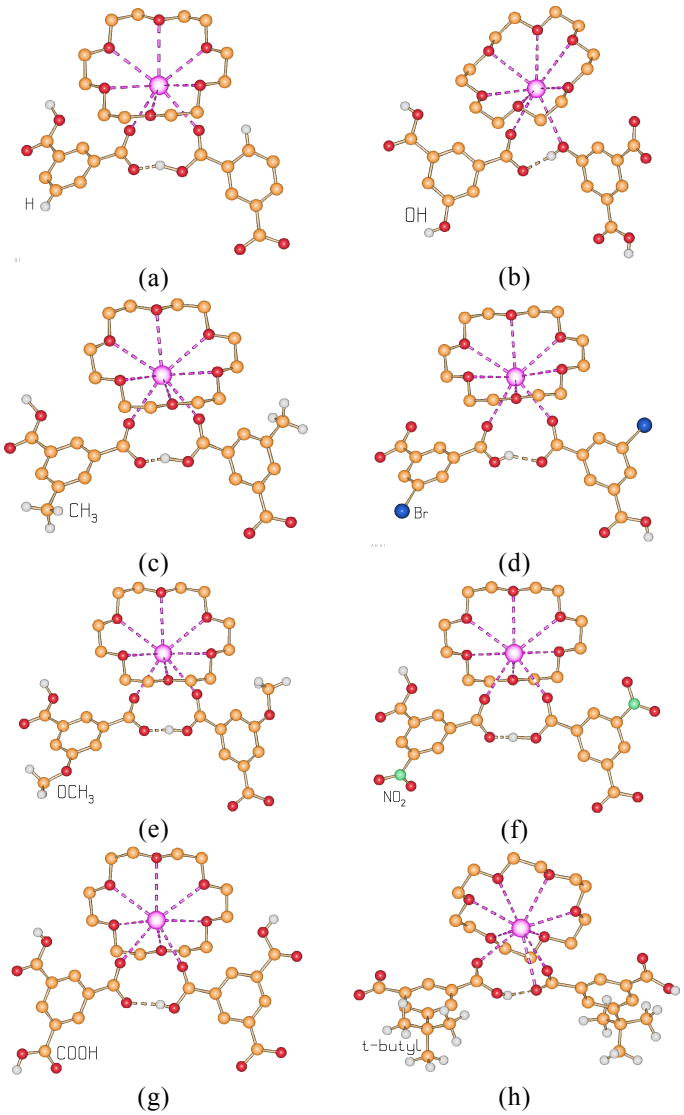

Fig.16. The coordination geometry of the 18-crown[6] molecule and of the $[X\text{-isoH}]^-$ anions (referred by symmetry) around the Cs^+ ion in crystalline **1** and **2** and in the complexes **7** – **11** and **12**. [$X\text{-isoH}_2$, X = COOH (**1**), H (**2**), OH (**7**), CH_3 (**8**), Br (**9**), OCH_3 (**10**), NO_2 (**11**), t-butyl (**12)**].

Table 2. Relevant Cs^+···O interactions and O(H)···O hydrogen bonds for **7**, **8**, **9**, **10**, **11**, and **12**. (a) The interaction between Cs^+ and the oxygen of a *second* crown ether; (b) $O(H)_{OH}$···O_{COO}- ; (c) bifurcated hydrogen bond.

Complex	Cs^+···O_{crown} Cs^+···O'_{crown} [a]	Cs^+···O_{anion}	$O(H)_{COOH}$···O_{COO}-
7	3.195(2) – 3.479(2) 3.686(2)	3.100(2) 3.375(2) 3.790(2)	2.604(3) 2.614(4)[b]
8	3.092(2) – 3.284(2) 3.424(2)	3.008(3) 3.051(2)	2.466(3)
9	3.101(5) – 3.275(4) 3.456(5)	2.998(5) 3.053(5)	2.446(6)
10	3.083(3) – 3.291(2) 3.408(2)	3.044(2) 3.088(2)	2.431(3)
11	3.080(2) – 3.283(2) 3.412(2)	2.991(2) 3.080(2)	2.447(3)
12	3.047(5) – 3.192(6) ---	3.051(4) 3.289(5) 3.292(6)	2.833(9)[c] 2.862(8)[c]

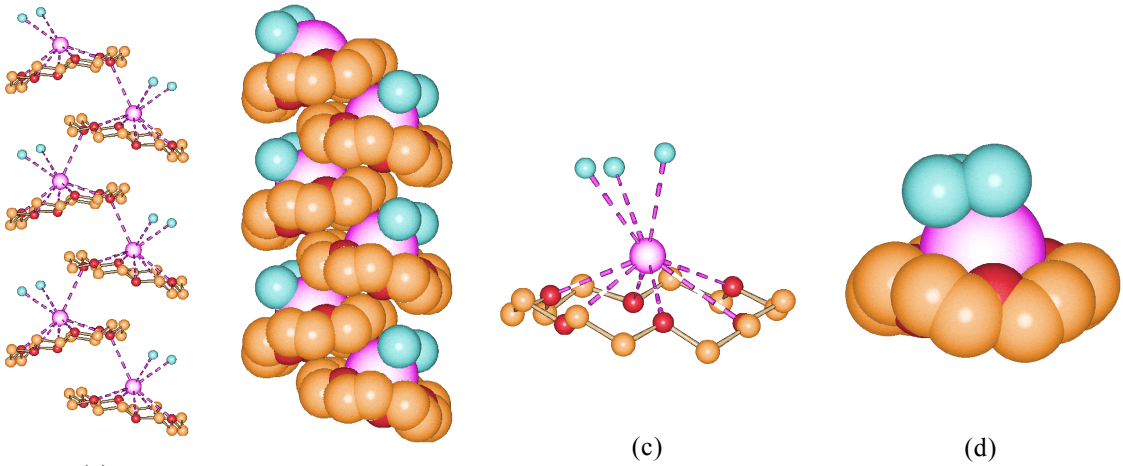

Fig.17. (a) Chain arrangement in crystalline **11**, as one oxygen atom in a second crown ether completes the coordination sphere of Cs^+. The same kind of pattern is observed in complexes **1**, **2**, **7**, **8**, **9** and **10**. (b) The chain arrangement is not observed in crystalline **12**, as the coordination sphere of Cs^+ is completed by the crown ether and two [t-Butyl-isoH]$^-$ anions. Light blue spheres represent the metal-coordinated oxygen atoms belonging to the [X-isoH]$^-$ anion. H_{CH} atoms omitted for clarity.

All structures are characterized by the presence of chains of $[X\text{-}isoH]^-$ anions linked *via* C=O···H—O hydrogen bonds (see Figures 18, 19 and Table 2); in the case of crystalline **7** the presence of an OH function allows the formation of a 2-D network (figure 18a).

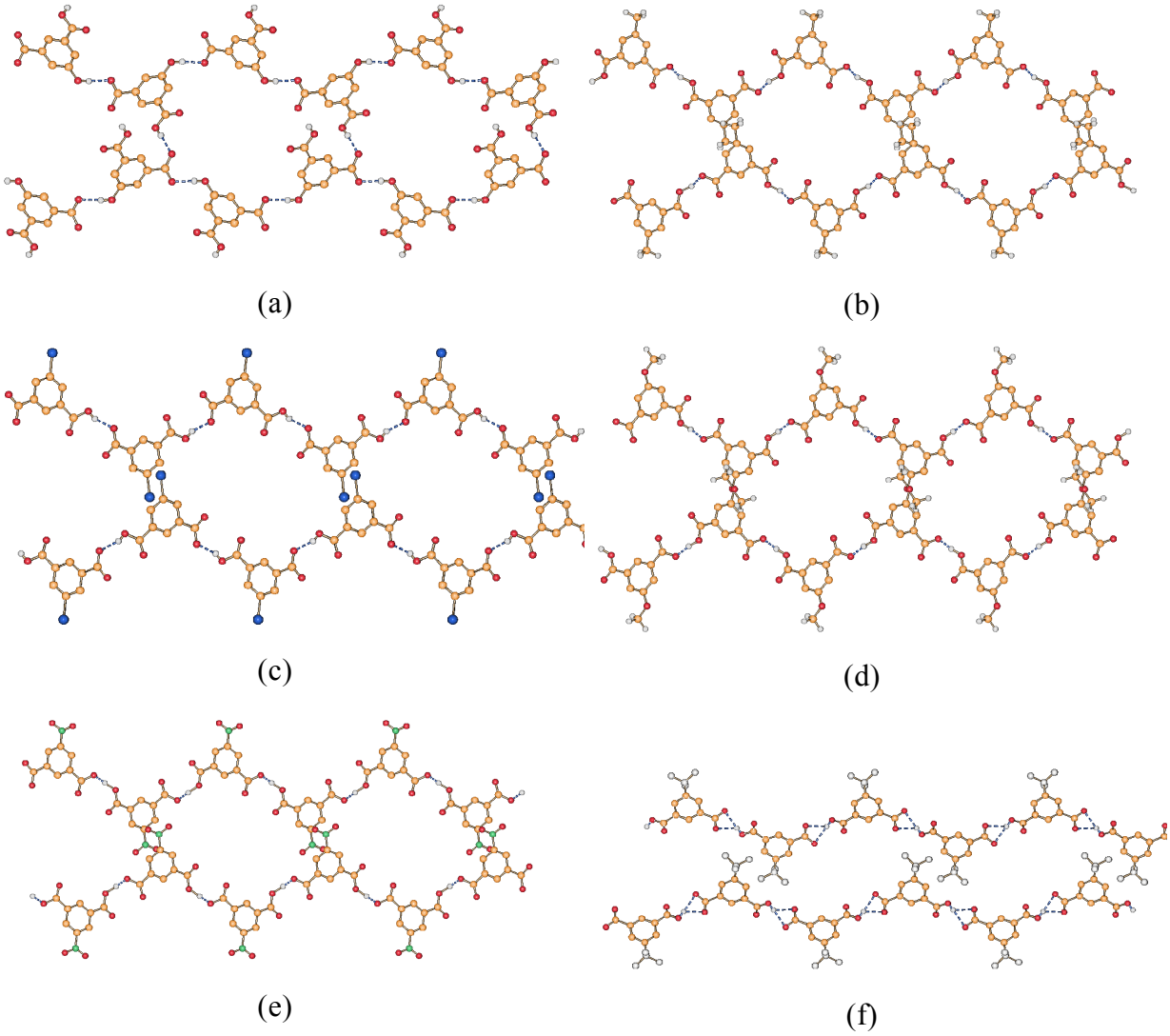

Fig.18. (a) 2-D hydrogen bonding anionic network in crystalline **7** viewed in the *bc*-plane; (b) 1-D hydrogen bonding anionic network in crystalline **8** viewed in the *bc*-plane; (c) 1-D hydrogen bonding anionic network in crystalline **9** viewed in the *bc*-plane; (d) 1-D hydrogen bonding anionic network in crystalline **10** viewed in the *bc*-plane; (e) 1-D hydrogen bonding anionic network in crystalline **11** viewed in the *bc*-plane and (f) 1-D hydrogen bonding anionic network in crystalline **12** showing the similarity in the chains arrangement with the main packing motif of complexes **1**, **2** and **7-11**. H_{CH} atoms omitted for clarity.

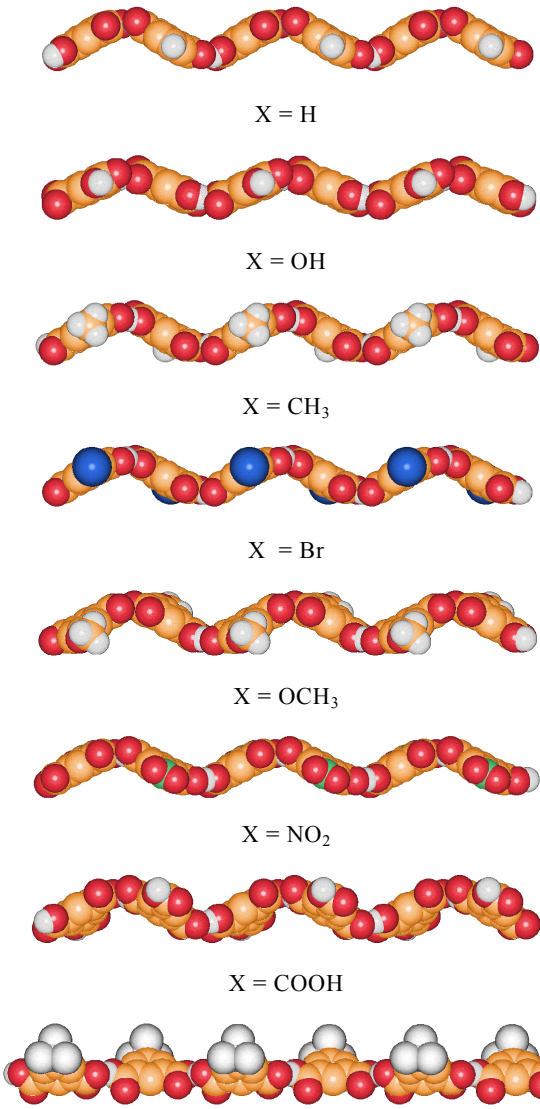

Fig.19. Comparison of the hydrogen bonded chains of anions in crystalline **1,2** and **7** – **12**. Note how the relative orientation of the anions along the chain is markedly different for X = t-butyl (light grey moieties in the bottom chain). [H_{ring} atoms not shown for clarity, except for the H_X atom in compound **1**.]

6 Robustness of the a unit cell

The two complexes 18-crown[6]·Cs[trimH_2] (**1**) and 18-crown[6]·Cs[isoH] (**2**) are isomorphous. The complexes **7**, **8**, **9**, **10** and **11** also crystallize in the same space group $P2_12_12_1$, with very close cell parameters (see Table 1) and a similar organization in their solids (figures 17 and 18),[16] while the same does not occur when we use a very bulky group such as the t-butyl in complex **12** and both similarities and differences can be observed for the main packing motifs (figure 19). Therefore these crystals are conservative in terms of packings but capable of some flexibility, and this is reflected in the fact that the cell constants are essentially independent on the nature of the substituent or on its ability of forming hydrogen bonds, while they depend only on its *size*. Below a certain threshold the crystal is able to adjust itself, therefore the cell parameters are very similar, while above the same threshold the transition from an orthorhombic to a monoclinic system is observed. Table 3 lists the anionic volumes[15] and the increasing ΔVol with respect to the smallest anion, i.e. the one with X = H, while in figure 20 the anionic volumes for all compounds are plotted.

Table 3. Values of anionic volumes and ΔVol[a] for compounds **1**, **2** and **7** – **12**. [a]ΔVol = V_{anion} - V_{anion}(H).

compound	X	V_{anion} (Å^3)	Δ Vol (Å
1	**H**	140.39	-
2	**OH**	149.54	9.15
3	**CH_3**	154.87	14.48
4	**Br**	159.76	19.37
5	**OCH_3**	164.26	23.87
6	**NO_2**	166.49	26.10
7	**COOH**	169.64	29.25
8	**t-butyl**	201.19	60.80

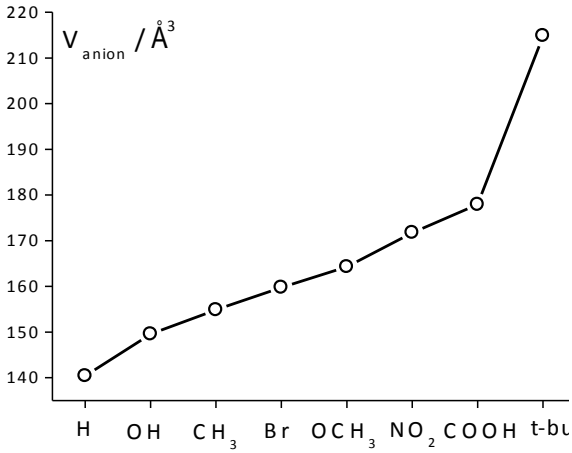

Fig.20. Plot of V_{anion} values for compounds **1,2** and **7** – **12**

Figure 21 show the variation of cell parameters, cell volume and percentage of filled space (packing coefficients) on increasing the Van de Waals volume of the anions. As it can be seen from figure 21a, on increasing the anion size from [isoH]$^-$ to [trimH_2]$^-$ the cell parameters *b* and *c* are the ones that vary most. On passing from [trimH_2]$^-$ < [t-butyl-isoH]$^-$, on the other hand, a dramatic change is observed for the *a* and *c* axes; the *b*-axis

remains *only apparently* unaffected, as in crystalline **12** the packing arrangement along this axis is not the same as the one observed for compounds **1**,**2,** and **7**– **12**.

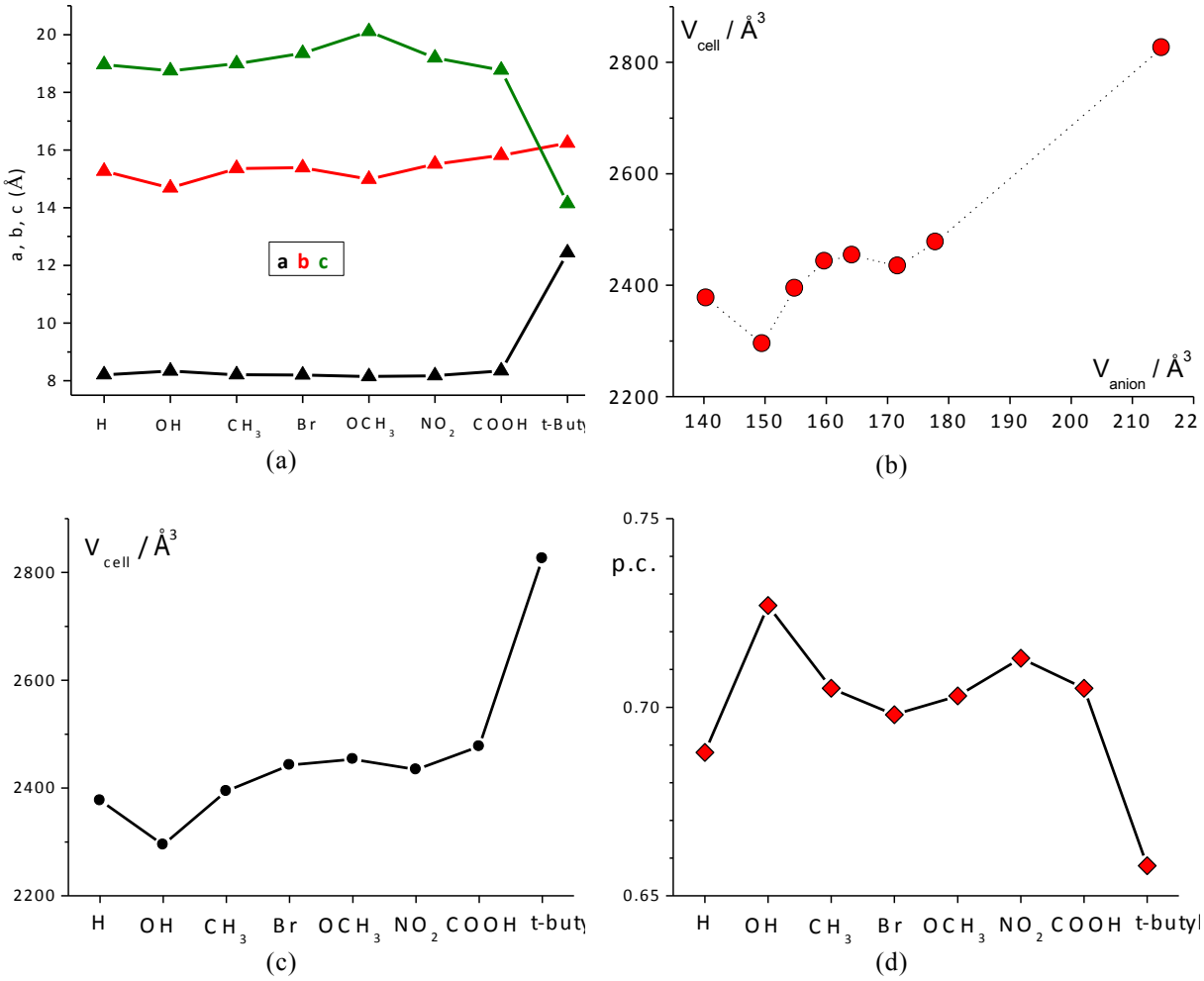

Fig.21. (a) Plot of cell axes values for compounds **1**,**2,** and **7**– **12**; (b) Plot of V_{cell} as a function of V_{anion}; (c) Plot of V_{cell} values for compounds **1**,**2,** and **7**– **12** and (d) Plot of packing coefficient[5] values for compounds **1**,**2,** and **7**– **12**.

The cell volume grows almost linearly on increasing the anion size (see Figure 21bc), with the exception of complex 18-crown[6]·Cs[OH-isoH] (**7**) that experiences a sort of contraction, likely due to the fact that the OH groups are engaged in a hydrogen bond with a carboxylic function belonging to the same chain, while an oxygen lone-pair coordinates a Cs^+ ion, as it can be seen in figure 16a. This also affects the values of the packing coefficent, which remarkably high (figure 21d). On the contrary, the packing coefficient reacheas a minium for compound **12**, for which large anisotropic displacement parameters are observed.

7 Mechanochemistry

Synthesis of 18-crown[6]·Cs[OH-isoH] (**7**), 18-crown[6]·Cs[CH_3-isoH] (**8**), 18-crown[6]·Cs[Br-isoH] (**9**), 18-crown[6]·Cs[OCH_3-isoH] (**10**), 18-crown[6]·Cs[NO_2-isoH] (**11**) and 18-crown[6]·Cs[t-Butyl-isoH] (**12**). Cs_2CO_3, 18-crown[6] and X-isoH$_2$ acid were mixed together in stoichiometric ratio 0.5:1:1. The amount of reagents was chosen so that 100 – 200 mg of solid product could be obtained (see experimental section for details). The solid reagents were manually mixed in an agate mortar for ten minutes; as the crown ether readily adsorbs water from the atmosphere, the solid-state product was actually the result of a kneading process.

Powder diffraction patterns of the solid-state reaction outcome and solution products were compared with the patterns calculated on the basis of single crystals data, see figure 22.

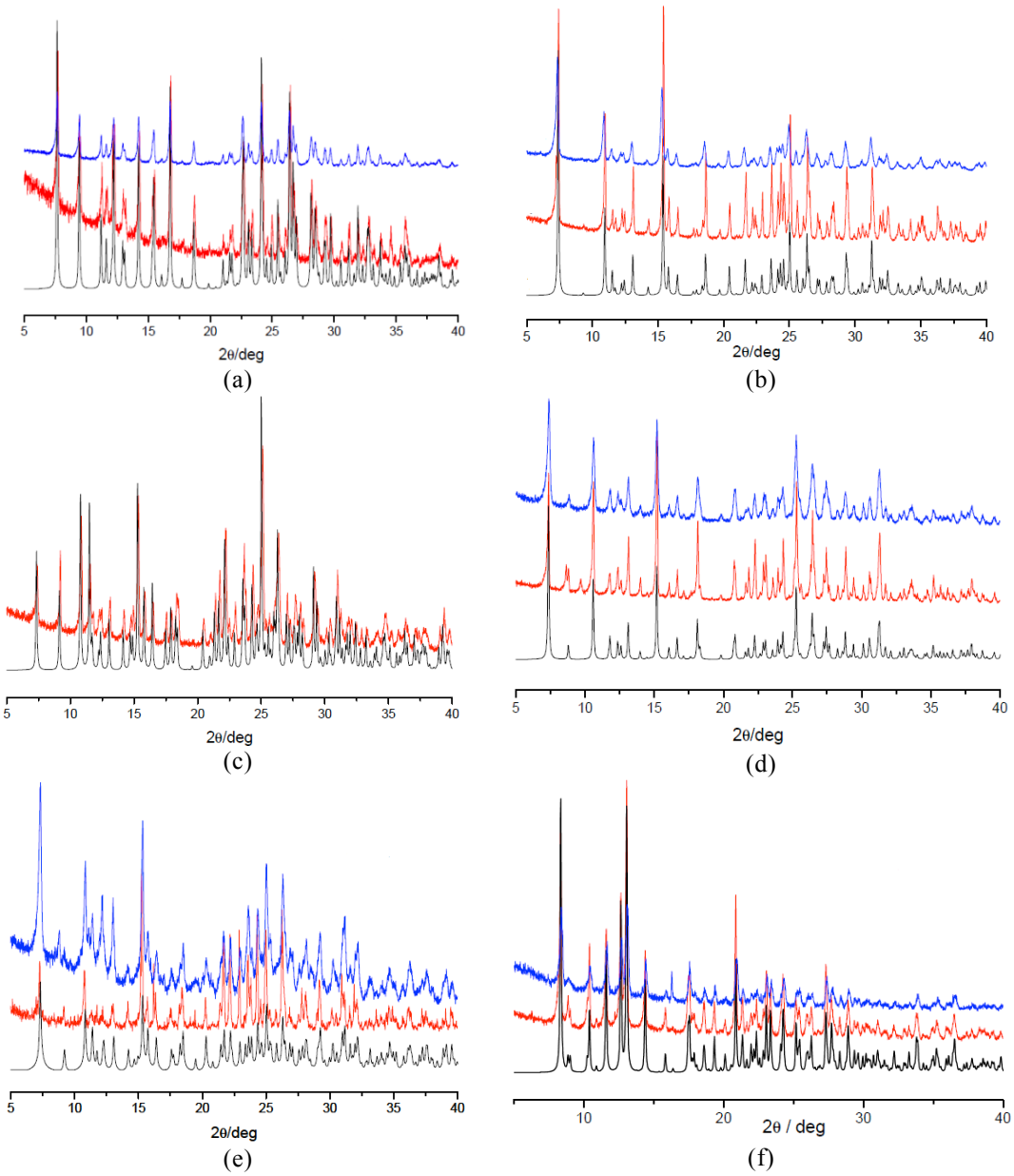

Fig.22. Comparison of the XRPD patterns computed on the basis of single crystal structure data (black-line) and measured on the solution (red-line) and solid-state reaction products (blue-line) for complexes: (a) **7**, (b) **8**, (c) **9**, (d) **10**, (e) **11** and (f) **12**.

8 Conclusions

In the first section of this chapter are reported the preparation and characterization of six novel organic–inorganic compounds belonging to the family of crown ether complexes.

In particular the following compounds: 18-crown[6]·Cs[trimH_2] (**1**), 18-crown[6]·Cs[isoH] (**2**) and 18-crown[6] ·Cs_2[isoH]$_2$·2H_2O (**3**), (18-crown[6])$_3$·Cs_3[trim]·9 H2O (**4**), 18-crown[6]·Cs[ben]·H2O (**5**) and (18-crown[6])$_6$·Cs_4[tereH]$_2$[tere]·5H_2O (**6**) have been synthesized and characterized.

Crystalline **1** and **2** are isomorphous despite the difference in shape and supramolecular bonding of the anions. We have investigated their behaviour upon heating, showing that **1** and **2** are very stable under ca. 200 °C, temperature at which the crown ether extrusion process takes place. Interestingly, for **2** this process occurs in two steps. We have been able to crystallize the product corresponding to the first loss (half crown ether), although the recrystallization is accompanied by the uptake of two water molecules. By varying the reagents molar ratio used in preparation of **1** we were able to obtain complex **4**, which behaves in a similar manner when heated up to 200°C, but at lower temperatures shows two subsequent dehydration processes yielding two different products, namely A and B, that reconvert to the original form **4**. Crystallization of complex **5** was only possible by an unusual method, i.e. ‘‘cooking’’ it in the oven at 90°C, since its nature is that of an highly hygroscopic salt.

A deeper view about the role of shape and function of hydrogen bonding network formers in determining structural behaviour of systems containing 18-Crown[6] is given in the second part of this chapter, in which is reported the preparation and structural characterization of the crown ether complexes 18-crown[6] ·Cs[OH-isoH] (**7**), 18-crown[6]·Cs[CH_3-isoH] (**8**), 18-crown[6]·Cs[Br-isoH] (**9**) and 18- crown[6]·Cs[CH_3O-isoH] (**10**), 18-crown[6]·Cs[NO_2-isoH] (**11**) and 18-crown[6]·Cs[t-Butyl-isoH] (**12**).[16] All complexes have been obtained by mechanical mixing of the reactants in the solid state and by direct crystallization from water. The complexes, with the the exception of **12**, are all isomorphous among themselves and with the complexes 18-crown[6]·Cs[trimH_2] (**1**) and 18-crown[6]·Cs[isoH] (**2**),[10] irrespective of the size, shape and chemical nature of the substuìtuent. In the case of complex **12** the very bulky t-butyl ligand is no longer compatible with the arrangement available to all other substituents, and the crystal structures switches to a more “lousy” packing. The cell choice is neither dictated, nor affected by the hydrogen bonding donor or acceptor capability of the substituent.

Moreover, this study provides an additional example of the use of mechanochemical methods as an alternative to conventional solution chemistry to prepare new solids by mechanical mixing of the reactants (grinding) or in the presence of a catalytic amount of solvent (kneading).[3]

Experimental section

All reactants and solvents were purchased from Sigma-Aldrich and used without further purification. Bi-distilled water was used.

*Synthesis of 18-crown[6]·Cs[trimH$_2$] (**1**).* Cs_2CO_3 (179 mg, 0.54 mmol), 18-crown[6] (290 mg, 1.0 mmol) and trimesic acid (173 mg, 0.8 mmol) were manually mixed in an agate mortar for 10 min. The ground material was dissolved in 10 mL water, the solution was then heated until clear and left to evaporate in the air at room temperature; after a few days single crystals of **1** suitable for X-ray diffraction were obtained.

*Synthesis of 18-crown[6]·Cs[isoH] (**2**).* Cs_2CO_3 (183 mg, 0.56 mmol), 18-crown[6] (297 mg, 1.12 mmol) and isophthalic acid (183 mg, 1.10 mmol) were manually mixed in an agate mortar for 10 min. Single crystals of **2** were obtained by slow evaporation at RT of a solution obtained by dissolving the ground material in 10 mL of bi-distilled water and heating up to a clear solution.

*Synthesis 18-crown[6]·Cs$_2$[isoH]$_2$·2H$_2$O (**3**).* A polycrystalline sample of **2** is warmed up to 190°C and allowed to cool to room temperature. Recrystallization from water yields crystals of **3** suitables for X-ray diffraction.

*Synthesis of (18-crown[6])$_3$·Cs$_3$[trim]·9H$_2$O (**4**).* Cs_2CO_3 (208 mg, 0.64 mmol), 18-crown[6] (336 mg, 1.27 mmol) and trimesic acid (87 mg, 0.41 mmol) were manually mixed in an agate mortar for 10 min. The ground material was dissolved in 10 mL of water, the solution was then heated until clear and left to evaporate in the air at room temperature; after a few days single crystals of **4** suitable for X-ray diffraction were obtained.

*Synthesis of 18-crown[6]·Cs[ben]·H$_2$O (**5**).* Cs_2CO_3 (183 mg, 0.56 mmol), 18-crown[6] (300 mg, 1.13 mmol) and benzoic acid (136 mg, 1.12 mmol) were manually mixed in an agate

mortar for 10 min and then dissolved in 5 mL of bi-distilled water. Complex **5** is ighly hygroscopic and does not crystallize at ambient temperature and humidity; single crystals could only be obtained by leaving the product in an oven at 90°C for ca. 12 h.

*Synthesis of (18-crown[6])$_6$·Cs$_4$[tereH]$_2$[tere]·5H$_2$O (**6**)*. Cs_2CO_3 (201 mg, 0.61 mmol), 18-crown[6] (326 mg, 1.22 mmol) and terephthalic acid (205 mg, 1.22 mmol) were manually mixed in an agate mortar for 10 min. The ground material was dissolved in 10 mL of water, the solution was then heated until clear and left to evaporate in the air at room temperature; after a few days single crystals of **6** suitable for X-ray diffraction were obtained.

Synthesis of 18-crown[6]·Cs[OH-isoH] (7). Cs_2CO_3 (66.6 mg, 0.307 mmol), 18-crown[6] (109.9 mg, 0.416 mmol) and 5-hydroxyl-isophthalic acid (76.1 mg, 0.418 mmol) were manually mixed in an agate mortar for 10 min. The ground material was dissolved in 10 mL water, the solution was then heated until clear and left to evaporate in the air at room temperature; after a few days single crystals of **7** suitable for X-ray diffraction were obtained.

*Synthesis of 18-crown[6]·Cs[CH$_3$-isoH] (**8**)*. Cs_2CO_3 (85.3 mg, 0.262 mmol), 18-crown[6] (139.5 mg, 0.528 mmol) and 5-methyl-isophthalic acid (94.2 mg, 0.523 mmol) were manually mixed in an agate mortar for 10 min. The ground material was dissolved in 10 mL water, the solution was then heated until clear and left to evaporate in the air at room temperature; after a few days single crystals of **8** suitable for X-ray diffraction were obtained.

*Synthesis of 18-crown[6]·Cs[Br-isoH] (**9**)*. Cs_2CO_3 (18.7 mg, 0.574 mmol), 18-crown[6] (31.0 mg, 0.117 mmol) and 5-bromo-isophthalic acid (27.0 mg, 0.112 mmol) were manually mixed in an agate mortar for 10 min. The ground material was dissolved in 10 mL water, the solution was then heated until clear and left to evaporate in the air at room temperature; after a few days single crystals of **9** suitable for X-ray diffraction were obtained.

*Synthesis of 18-crown[6]·Cs[CH$_3$O-isoH] (**10**)*. Cs_2CO_3 (68.7 mg, 0.211 mmol), 18-crown[6] (110.5 mg, 0.418 mmol) and 5-methoxy-isophthalic acid (81.8 mg, 0.417 mmol) were manually mixed in an agate mortar for 10 min. The ground material was dissolved in 10 mL water, the solution was then heated until clear and left to evaporate in the air at room

temperature; after a few days single crystals of **10** suitable for X-ray diffraction were obtained.

*Synthesis of 18-crown[6]·Cs[trimH_2] (**11**).* Cs_2CO_3 (85.3 mg, 0.262 mmol), 18-crown[6] (139.5 mg, 0.528 mmol) and 5-methyl-isophthalic acid (94.2 mg, 0.523 mmol) were manually mixed in an agate mortar for 10 min. The ground material was dissolved in 10 mL water, the solution was then heated until clear and left to evaporate in the air at room temperature; after a few days single crystals of **10** suitable for X-ray diffraction were obtained.

*Synthesis of 18-crown[6]·Cs[t-Butyl-isoH] (**12**).* Cs_2CO_3 (94.0 mg, 0.289 mmol), 18-crown[6] (152.9 mg, 0.578 mmol) and 5-ter-butyl-isophthalic acid (127.3 mg, 0.573 mmol) were manually mixed in an agate mortar for ten minutes. The ground material was dissolved at RT in 5 mL of *n*PrOH, and "seeds" of complexes **1** or **2** were added to the solution. Crystals of **12** suitable for X-ray diffraction were grown by vapour diffusion of *i*-Pr_2O into the alcoholic solution on a period of 2 weeks. In the absence of seeds the product **8** could be obtained only as a polycrystalline material.

Thermogravimetric analysis (TGA). TGA analyses were performed with a Perkin-Elmer TGA-7. Each sample, contained in a platinum crucible, was heated in a nitrogen flow (20 cm3 min^{-1}) at a rate of 5 °C min^{-1}, up to decomposition. Samples weights were in the range 5–10 mg.

Differential scanning calorimetry (DSC). Calorimetric measurements were performed with a Perkin-Elmer DSC-7 equipped with a PII intracooler. Temperature and enthalpy calibrations were performed using high-purity standards (n-decane, enzene and indium). Heating of the aluminium open pans containing the samples (3–5 mg) was carried out at 5 °C min^{-1} in the temperature range 40–300 °C.

Hot stage microscopy. Hot Stage experiments were carried out using a Linkam TMS94 device connected to a Linkam LTS350 platinum plate. Images were collected with the imaging software Cell, from an Olympus BX41 stereomicroscope.

Calculation of van der Waals volumes. Evaluation of vdW volumes for all the acids used in this work was performed with Gavezzotti's program OPIX.[15]

X-ray diffraction. Single-crystal data for compounds **1—12** were collected on an Oxford X'Calibur S CCD diffractometer equipped with a graphite monochromator (Mo-Kα radiation, λ = 0.71073) and operated at room temperature. Data collection and refinement details are listed in Table 1. All non-hydrogen atoms were refined anisotropically; H_{OH} atoms were either directly located or added in calculated positions; H_{CH} atoms for all compounds were added in calculated positions and refined riding on their respective carbon atoms. SHELX97[17a] was used for structure solution and refinement on F^2, PLATON[17b] and SCHAKAL99[17c] were used for hydrogen bonding analysis and molecular graphics, respectively. Powder data were collected on a Philips X'Pert automated diffractometer with Cu-Kα radiation. The program PowderCell[17d] was used for calculation of X-ray powder patterns on the basis of single crystal data. The identity between the bulk material obtained via the solution and solid-state processes was verified by comparing calculated and observed powder diffraction patterns.

Mechanochemistry. Complexes **1-12** were quantitatively obtained as polycrystalline materials by manual grinding (ca. 10 minutes) of solid Cs_2CO_3, 18-crown[6] and the corresponding polycarboxyllic aromatic acid in a 0.5:1:1 ratio. Powder diffraction patterns of the solid-state reaction and solution products were compared with the patterns calculated on the basis of single crystals data.

Table 1a. Crystallographic data and details of measurements for compounds **1**–**6**.

	1	**2**	**3**	**4**	**5**	**6**
formula	$C_{21}H_{29}CsO_{12}$	$C_{20}H_{29}CsO_{10}$	$C_{28}H_{38}O_{16}Cs_2$	$C_{45}H_{93}Cs_3O_{23}$	$C_{38}H_{62}O_{18}Cs_2$	$C_{96}H_{168}O_{53}Cs_4$
fw	606.35	562.34	896.40	1551.92	1072.70	2701.94
Cryst. System	Orthorhombic	Orthorhombic	Orthorhombic	Monoclinic	Monoclinic	Monoclinic
Space group	$P2_12_12_1$	$P2_12_12_1$	Pbca	$P2_1/n$	$P2_1/c$	$P2_1/c$
Z	4	4	8	4	2	2
a (Å)	8.3466(2)	8.2125(3)	14.8028(4)	14.6690(5)	11.0263(3)	27.2991(4)
b (Å)	15.8125(3)	15.2641(4)	12.4245(4)	27.0044(9)	21.5415(5)	10.4306(2)
c (Å)	18.7686(4)	18.9603(6)	18.3359(5)	17.2458(4)	10.2369(3)	22.0035(4)
α (deg)	90	90	90	90	90	90
β (deg)	90	90	90	103.860(3)	97.333(2)	101.003(2)
γ (deg)	90	90	90	90	90	90
V ($Å^3$)	2477.09(9)	2376.80(1)	3372.3(2)	6632.6(4)	2411.6(1)	6150.2(2)
D_{calc} (Mg/m^3)	1.626	1.572	1.766	1.544	1.477	1.488
μ (mm^{-1})	1.555	1.608	2.233	0.431	1.577	1.267
measured reflns	10828	7761	10325	33893	13828	146555
indep. reflns	5314	4063	3410	12936	5500	15581
R1[onF_0^2,I>2sigma(I)]	0.0344	0.0260	0.0450	0.0526	0.0323	0.0637
wR2 (all data)	0.0583	0.0412	0.0805	0.1364	0.0413	0.1817
Flack parameter	0.02(1)	-0.04(9)	-	-	-	-

Table 1b. Crystal data and details of measurements for the **18-crown[6]·Cs[X-isoH]** complexes **7**–**12**.

	7 X = OH	**8 X = CH_3**	**9 X = Br**	**10 X = OCH_3**	**11 X = NO_2**	**12 X = t-But**
formula	$C_{20}H_{29}CsO_{11}$	$C_{21}H_{31}CsO_{10}$	$C_{20}H_{28}BrCsO_{10}$	$C_{21}H_{31}CsO_{11}$	$C_{20}H_{28}CsNO_{12}$	$C_{24}H_{37}CsO_{10}$
fw	578.34	576.37	641.23	592.37	607.34	618.45
Cryst. System	orthorhombic	orthorhombic	orthorhombic	orthorhombic	orthorhombic	monoclinic
Space group	$P2_12_12_1$	$P2_12_12_1$	$P2_12_12_1$	$P2_12_12_1$	$P2_12_12_1$	$P2_1/n$
Z	4	4	4	4	4	4
a (Å)	8.3337(3)	8.2066(2)	8.2041(2)	8.1436(2)	8.176(2)	12.441(3)
b (Å)	14.6878(4)	15.3598(4)	15.3854(4)	14.9847(2)	15.512(3)	16.237(5)
c (Å)	18.7462(5)	18.9926(4)	19.3495(6)	20.1066(4)	19.195(3)	14.139(4)
α (deg)	90	90	90	90	90	90
β (deg)	90	90	90	90	90	98.318(2)
γ (deg)	90	90	90	90	90	90
V ($Å^3$)	2294.6(1)	2394.1(1)	2442.4(1)	2453.60(8)	2434.28(8)	2826.1(1)
D_{calc} (Mg/m^3)	1.674	1.599	1.744	1.604	1.657	1.454
μ (mm^{-1})	1.671	1.598	3.202	1.565	1.584	1.359
measured reflns	9234	9890	15842	16810	9551	7825
indep. reflns	6594	6901	6528	5785	5200	4077
R1[on F_0^2,I>2sigma(I)]	0.0328	0.0361	0.0547	0.0276	0.0295	0.0407
wR2 (all data)	0.0472	0.0538	0.1498	0.0529	0.0422	0.0955
Flack parameter	-0.028(11)	0.015(12)	0.05(2)	-0.071(2)	0.1951(1)	-

References

[1] (a) C. J. Pedersen, *J. Am. Chem. Soc.*, 1967, **89**, 7017; (b) C. J. Pedersen and H. K. Frensdorff, *Angew. Chem.*, 1972, **84**, 16; (c) C. J. Pedersen and H. K. Frensdorff, *Angew. Chem., Int. Ed. Engl.*, 1972, **11**, 16.

[2] The CSD (version 5.31, November 2011) contains 4427 crystal structures of crown ether derivatives and complexes.

[3] (a) J. M. Lehn, *Supramolecular Chemistry: Concepts and Perspectives*, VCH, Weinheim, 1995; (b) J. L. Atwood, K. T. Holman and J. W. Steed, *Chem. Commun.*, 1996, 1401; (c) J. W. Steed and J. L. Atwood, *Supramolecular Chemistry*, Wiley & Sons, New York, 2000

[4] (a) J. W. Steed, *Coord. Chem. Rev.*, 2001, **215**, 171; (b) P. C. Junk, B. J. McCool, B. Moubaraki, K. S. Murray, L. Spiccia, J. D. Cashion and J. W. Steed, *J. Chem. Soc., Dalton Trans.*, 2002, **6**, 1024; (c) M. Calleja, S. A. Mason, P. D. Prince, J. W. Steed and C. Wilkinson, *New J. Chem.*, 2003, **27**, 28; (d) J. M. Harrington, S. B. Jones, P. H. White and R. D. Hancock, *Inorg. Chem.*, 2004, **43**, 4456; (e) J. M. Dou, X. K. Gao, F. Y. Dong, D. C. Li and D. Q. Wang, *Dalton Trans.*, 2004, **18**, 2918; (f) D. R. Turner, S. Nee Pek and S. R. Batten, *New J. Chem.*, 2008, **32**, 719; (g) P. C. Junk, *New J. Chem.*, 2008, **10**, 1039; (h) K. M. Fromm and R. D. Bergougnant, *Solid State Sci.*, 2008, **9**, 580; (i) O. Ermer and J. Neudorfl, *Chem. Eur. J.*, 2001, **7**, 4961. (l) A. Clearfield, C. V. K. Sharma, B. P. Zhang, Chem. Mat. 2001, **13,** 3099; **(m)** S. Wishkerman, J. Bernstein, M. B. Hickey, *Crystal Growth & Design* 2009, **9**, 3204.

[5] D. Braga, M. Gandolfi, M. Lusi, M. Polito, K. Rubini, and F. Grepioni, *Crystal Growth & Design,* 2007, **7**, 919.

[6] D. Braga, M. Gandolfi, M. Lusi, D. Paolucci, M. Polito, K. Rubini, and F. Grepioni, *Chem. Eur. J.*, 2007, **13**, 5249.

[7] D. Braga, M. Curzi, M. Lusi and F. Grepioni, *CrystEngComm.*, 2005, **7**, 276.

[8] D. Braga, E. Modena, M. Polito, K. Rubini and F. Grepioni, *New J. Chem.*, 2008, **32**, 1718.

[9] D. Braga, M. Polito, E. Dichiarante, K. Rubini and F. Grepioni, *Chem. Commun.*, 2007, 1594.

10) D. Braga, S. D'Agostino, M. Polito, K. Rubini and F. Grepioni, *CrystEngComm.*, 2009, **11**, 1994.

[11] (a) D. Braga, F. Grepioni, l. Maini and M. Polito, *Struct. Bonding* 2009, **132**, 25; (b) D. Braga D, D. D'Addario, S. L. Giaffreda, F. Grepioni, *Topics in Curr. Chem*. 2005, **254**, 71;

(c) D. Braga, S. L. Giaffreda, F. Grepioni, A. Pettersen, L. Maini, M. Curzi, M. Polito, *Dalton Trans.* 2006, **10**, 1249; (d) F. Herbstein, *Acta Crystallogr., Sect. B*, 2006, **62**, 341; (e) G. Kaupp, in *Prediction of Reactivity in Solid-State Chemistry*, eds. D. Braga and F. Grepioni, Wiley-Vch, Weinheim, 2006, pp. 87; (f) J. W. Lauher, F. W. Fowler, N. S. Goroff, *Acc. Chem Res*. 2008, **41**, 1215; (g) C. M. Reddy, G. R. Krishna, S. Ghosh, *CrystEngComm* 2010, **12**, 2296.

[12] (a) D. Braga, E. D'Oria, F. Grepioni, F. Mota and J. J. Novoa, *Chem.– Eur. J.*, 2002, **8**, 1173; (b) D. Braga, L. Maini, M. Polito and F. Grepioni, *Struct. Bonding*, 2004, **111**, 1; (c) F. Braga and

G. R. GrepioniDesiraju, *Chem. Rev.*, 1998, **98**, 1375; (d) A. J. Blake, N. R. Champness, P. Hubberstey, W. S. Li, M. A. Withersby and M. Schroder, Coord. *Chem. Rev.*, 1999, **183**, 117; (e) D. Braga, G. R. Desiraju, J. Miller, A. G. Orpen and S. Price, *CrystEngComm*, 2002, **4**, 500; (f) M. D. Hollingsworth, Science, 2002, **295**, 2410; (g) L. Brammer, *Chem. Soc. ReV.*, 2004, **33**, 476; (h) M. W. Hosseini, *CrystEngComm*, 2004, **6**, 318; (i) D. Braga, L. Brammer and N. Champness, CrystEngComm, 2005, **7**, 1; (j) R. B. Moulton and M. J. Zaworotko, *Chem. Rev.*, 2001, **101**, 1629; (k) O. R. Evans and W. Lin., *Acc. Chem. Res.*, 2002, **35**, 511; (l) M. Oh, G. B. Carpenter and D. A. Sweigart, *Acc. Chem. Res.*, 2004, **37**, 1; (m) L. Carlucci, G. Ciani and D. M. Proserpio, *CrystEngComm*, 2003, **5**, 269; (n) C. Janiak, *Dalton Trans.*, 2003, 2781; (o) R. Robson, J. Chem. *Soc., Dalton Trans.*, 2000, 3735; (p) L. R. MacGillivray, *CrystEngCo*mm, 2000, **2**, 1; (q) K. Chadwick, G. Sadiq, R. J. Davey, C. C. Seaton, R. G. Pritchard and A. Parkin, *Cryst. Growth Des.*, 2009, **9**, 1278; (r) D. Braga, F. Grepioni, L. Maini, M. Polito, K. Rubini, M. Chierotti and R. Gobetto, *Chem.–Eur. J.*, 2009, **15**, 1508; (s) R. Santra, N. Ghosh and K. Biradha, *New J. Chem.*, 2008, **32**, 1673.

[13] T. Friscic, *J. Mat. Chem.,* 2010, **20**, 7599-7605; S. Karki, T. Friscic and W. Jones, *CrystEngComm*, 2009, **11**, 470-481; L. R. MacGillivray, G. S. Papaefstathiou, T. Friščić, D. B. Varshney and T. D. Hamilton, *Top. Curr. Chem.*, 2005, **248**, 201; D. R. Weyna, T. Shattock and M. J. Zaworotko, *Cryst. Growth Des.*, 2009, **9**, 1106-1123; M. J. Zaworotko, *Cryst. Growth Des.*, 2007, **7**, 4; G. M. J. Schmidt, *Pure Appl. Chem.*, 1971, **27**, 647; D. Braga, G. Palladino, M. Polito, K. Rubini, F. Grepioni, M. Chierotti and R. Gobetto, *Chem. Eur. J.*, 2008, **14**, 10149 – 10159; V. Andre, D. Braga, F. Grepioni and M. T. Duarte, *Cryst. Grow. Des.*, 2009, **9**, 5108-5116; T. Friscic and W. Jones, *Cryst. Grow. Des.,* 2009, **9**, 1621-1637; D. Braga, S. L. Giaffreda, F. Grepioni, M. R. Chierotti, R. Gobetto, G. Palladino and M. Polito, *CrystEngComm*, 2007, **9**, 879-881; D. Braga, S. L. Giaffreda, F. Grepioni, G.

Palladino and M. Polito, *New J. Chem.*, 2008, **32**, 820-828; D. Braga, F. Grepioni, M. Polito, M. R. Chierotti, S. Ellena and R. Gobetto, *Organometallics*, 2006, **25**, 4627-4633; M. R. Chierotti, L. Ferrero, N. Garino, R. Gobetto, L. Pellegrino, D. Braga, F. Grepioni and L. Maini, *Chem. Eur. J.*, 2010, **16**, 4347-4358; G. Kaupp, *CrystEngComm*, 2009, **11**, 388-403; G. Kaupp, in *Prediction of Reactivity in Solid-State Chemistry*, eds. D. Braga and F. Grepioni, Wiley-Vch, Weinheim, 2006, pp. 87-148; D. Braga, M. Gandolfi, M. Lusi, D. Paolucci, M. Polito, K. Rubini and F. Grepioni, *Chem. Eur. J.*, 2007, **13**, 5249-5255; A. D. Bond, *CrystEngComm*, 2007, **9**, 833-834.

[14] The IUCr Online Dictionary of Crystallography reports the following definition of isomorphism: "Two crystals are said to be isomorphous if (*a*) both have the same space group and unit-cell dimensions and (*b*) the types and the positions of atoms in both are the same except for a replacement of one or more atoms in one structure with different types of atoms in the other (*isomorphous replacement*), such as heavy atoms, or the presence of one or more additional atoms in one of them (*isomorphous addition*). Isomorphous crystals can form *solid solutions*." According to this definition, then, compound 7 is not, strictly speaking, truely isomorphous, as the coordination of the isophthalate ligand to the caesium cations is different with the respect to that of the other compounds; at the same time, given that cell parameters are comparable and all main supramolecular packing features are mantained, we can treat compound **7** as a case of *quasi-isomorphism*, and discuss it together with compounds **12** and **7-11**.

[15] A.Gavezzotti, *OPiX*, *A computer program package for the calculation of intermolecularinteractions and crystal energies*, University of Milano, Italy, 2003.

[16] D. Braga, S. d'Agostino and F. Grepioni, *CrystEngComm.*, 2011, **13**, 1366–1372.

[17] (a) Sheldrick, G. M. SHELXL97, Program for Crystal Structure Determination; University of Go¨ ttingen: Göttingen, Germany, 1997. (b) Speck, A. L. PLATON; Acta Crystallogr., Sect. A **1990**, 46, C34. (c) Keller, E. SCHAKAL99, Graphical Representation of Molecular Models; University of Freiburg: Freiburg, Germany, 1999. (d) Kraus, W.; Nolze, G. PowderCell; BAM: Berlin; subgroups developed by Müller, U.; Universität Gh Kassel: Kassel, Germany.

Chapter 2 - Anionic networks templated around organometallic cations

1 Introduction

Making crystals by design is the paradigm of crystal engineering, an area of solid state chemistry that encompasses molecular crystals and materials.[1] The assembly of building blocks into frameworks with predefined architectural (hence functional) features requires *control* over the interactions that are chosen to glue together the molecular or ionic components. It is unquestionable that, although the attention of researchers has been and is attracted by the whole range of possible supramolecular interactions, the hydrogen bond has taken the lion's share in crystal engineering studies.[2] The role of strong π-π stacking interactions in the stabilization of homochiral, helical metal-organic frameworks has also been recently explored.[3] The number of papers dealing with hydrogen bonded organic, inorganic and organometallic building blocks is very large and still increasing. The reason for this interest stems from the potential applications of organometallic and metal-organic frameworks in diverse areas such as gas storage[4] and sensing,[5] but also catalysis[6] and separations,[7] among others.

We have contributed with a number of studies dealing with hydrogen bonded networks formed by organic or inorganic molecules and ions *templated* by organometallic sandwich cations such as $[Co(\eta^5\text{-}C_5H_5)_2]^+$, $[Cr(\eta^6\text{-}C_6H_6)_2]^+$, $[Fe(\eta^5\text{-}C_5Me_5)_2]^+$ and $[Co(\eta^5\text{-}C_5Me_5)_2]^+$.[8,9,10] In all these cases the design criterion was based on the idea of *confining* all strong donor/acceptor hydrogen bonding groups on the organic or inorganic (usually anionic) networks while *excluding* the organometallic fragments (usually cationic) from the direct participation in the hydrogen bonds. This strategy has led to hydrogen bonded superstructures, whose topology depends on the size, shape, number and geometry of the -OH/-COOH/COO^- groups *around* the cationic sandwich. The regular cylindrical shape of these cations appeared to play a role in directing the assembly of the anionic frameworks, also with the participation of C-H ···O interactions between the acceptor sites on the networks and the C-H groups protruding from the complex surface.[11] The relevance of inter-anionic hydrogen bonds sustained by the presence of non-participating cations (such as the organometallic sandwiches) has also been addressed by computational studies.[12] Early examples of this strategy are the compounds $[Co(\eta^5\text{-}C_5H_5)_2][(D,L\text{-}taH)\cdot(D,L\text{-}taH_2]$ and $[Co(\eta^5\text{-}C_5H_5)_2][L\text{-}taH]$, which were obtained with D,L- and L-tartaric acid (D,L-taH_2 and L-taH_2) respectively.[13] With oxalic acid ($oxaH_2$), compounds $[Fe(\eta^5\text{-}C_5Me_5)_2][(oxaH)(oxaH_2)_{0.5}]$ and $[Cr(\eta^6\text{-}C_6H_6)_2][oxaH]\cdot H_2O$ were prepared,[14] while compounds $[Cr(\eta^6\text{-}C_6H_6)_2][sqaH]$ and $\{[Cr(\eta^6\text{-}C_6H_6)_2]\}_2[sqa]\cdot 6H_2O$ were prepared with

squaric acid ($sqaH_2$).[15] With phthalic (paH_2) and terephthalic acids ($tpaH_2$) the compounds $\{[Co(\eta^5\text{-}C_5H_5)_2]\}_4[(paH_2)(pa)]\cdot 4H_2O$, $[Cr(\eta^6\text{-}C_6H_6)_2][(paH)(paH_2)]$, and $\{[Co(\eta^5\text{-}C_5H_5)_2]\}_2[tpa]\cdot 6H_2O$ were prepared,[16] while with trimesic acid ($tmaH_3$) $[Co(\eta^5\text{-}C_5H_5)_2][(tmaH_2)(tmaH_3)]\cdot 2H_2O$ was obtained[17] and with R-binaphtol (R-bnH_2) were prepared $[Co(\eta^5\text{-}C_5H_5)_2][(R\text{-}bnH)(RbnH_2)]$, and $[Co(\eta^5\text{-}C_5H_5)_2][(R\text{-}bnH)(R\text{-}bnH_2)0.5]$.[18,19]

2 Aim of the work

This section reports an extension of these studies aimed to understanding the relationship between hydrogen bonding capability and *shape* of the building blocks and how the shape of the sandwich cation may act as a template for the aggregation of monoanions, all containing carboxylic and carboxylate groups, in 3-D networks. In the cases discussed herein the hydrogen bonding interaction is either confined *within* the discrete units (0-D bricks) or between ions in the formation of 1-D stripes and channels, while the global architecture depends on *shape recognition* between building blocks. In other words, we attempt to address the question on whether the absence of extra-molecular hydrogen bonding capacity because of the formation exclusively of intramolecular bonds of to no hydrogen bonding capacity within organic dicarboxylic acids or anhydrates would lead, in the presence of the same sandwich cations as used in all cases referred to above, to different architectures. To this end we have selected and synthesized[20] two organic building blocks, namely the dicarboxylic acid *trans*-9,10-dihydro-ethanoanthracene-11,12-dicarboxylic acid (*trans*-$deccaH_2$) and the anhydrate *cis*-9,10-dihydroanthracene-9,10-α,β-succinic acid anhydride (*cis*-decca). Sketches are provided in scheme 1. Upon hydrolysis this latter generates the monoanion *cis*-9,10-dihydro-9,10- ethanoanthracene-11-carboxylate-12-carboxylic acid (*cis*-$deccaH)^-$.

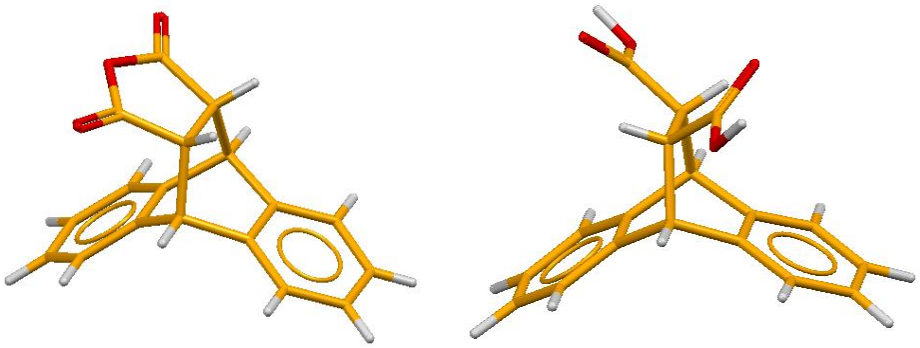

(a) (b)

Scheme 1. (a): 9,10-dihydroanthracene-9,10-α,β-succinic acid anhydride (the corresponding *cis*-acid is *cis*-$deccaH_2$); (b): *trans*-9,10-dihydro-ethanoanthracene-11,12-dicarboxylic acid (*trans*-$deccaH_2$).

3 Synthetic strategy

In order to promote assembly around the organometallic cations a combination of redox and acid-base processes are exploited. More specifically the spontaneous oxidation by oxygen of the neutral complexes cobaltocene, decamethyl cobaltocene and bisbenzene chromium generates the strongly basic anion O_2^-, which is able to fully or partially deprotonate the polyprotic acids, depending on the stoichiometric ratio. Since the oxidation products, namely the cations $[(\eta^5\text{-}C_5H_5)_2Co]^+$, $[Co(\eta^5\text{-}C_5Me_5)_2]^+$ and $[(\eta^5\text{-}C_6H_6)_2Cr]^+$, are not suitable for coordination by the $-COO^-$ groups, self-assembly of the neutral or deprotonated polycarboxylic acid moieties is promoted.

4 Structural description of anionic networks

Table 1 summarizes chemical information for the compounds part of this study. A brief description of the salient structural features will be provided in the following.

Table 1.

Formula	No.
$[(\eta^5\text{-}C_5H_5)_2Co][(cis\text{-deccaH})(cis\text{-deccaH}_2)]$	**1**
$[(\eta^5\text{-}C_5H_5)_2Co][(cis\text{-deccaH})(cis\text{-deccaH}_2)]\cdot H_2O$	**2**
$[(\eta^5\text{-}C_5H_5)_2Co][trans\text{-deccaH}]$	**3**
$[(\eta^5\text{-}C_5H_5)_2Co][(trans\text{-deccaH})(trans\text{-deccaH}_2)]$	**4**
$[(\eta^5\text{-}C_5Me_5)_2Co][cis\text{-deccaH}]$	**5**
$[(\eta^5\text{-}C_5Me_5)_2Co][(trans\text{-deccaH})]\cdot 4H_2O$	**6**
$[(\eta^6\text{-}C_6H_6)_2Cr][(trans\text{-deccaH})]$	**7**

4.1 Anionic networks derived from cis-decca

4.1.1 - $[(\eta^5\text{-}C_5H_5)_2Co][(cis\text{-deccaH})(cis\text{-deccaH}_2)]$ (1) and $[(\eta^5\text{-}C_5H_5)_2Co][(cis\text{-deccaH})(cis\text{-deccaH}_2)]\cdot H_2O$ (**2**). The anhydrous $[(\eta^5\text{-}C_5H_5)_2Co][(cis\text{-deccaH})(cis\text{-deccaH}_2)]$ (**1**) and the monohydrate $[(\eta^5\text{-}C_5H_5)_2Co][(cis\text{-deccaH})(cis\text{-deccaH}_2)]\cdot H_2O$ (**2**) crystalline salts share similar features and will be discussed together. In both crystalline **1** and **2** a neutral diacid molecule and a monodeprotonated unit interact via an $O(H)_{COOH}\cdots O_{COO^-}$ hydrogen bond [O···O distances 2.604(2) and 2.691(3) Å for **1** and **2**, respectively], thus forming the supramolecular anion $[(cis\text{-deccaH})(cis\text{-deccaH}_2)]^-$ shown in Figure 1. These supramolecular anions are all connected via intermolecular hydrogen bonds of the kind $O(H)_{COOH}\cdots O_{COO^-}$ [O···O distances 2.595(2), 2.666(3) and 2.619(3) Å for **1** and **2**, respectively], originating tape motifs that extend along the crystallographic *a*-axis, as shown

in Figure 2. The two moieties are oriented differently with respect to each other within the two supramolecular anions (Figure 1); this is probably a consequence of the presence of one water molecule in **2**, which participates in the hydrogen bonds along the tape (Figure 2b). One of the two COO(H) groups on the two moieties in **2** (which are related by symmetry) is affected by disorder over two positions; only one of the possible images of the supramolecular anion is shown in both Figures 1b and 2b.

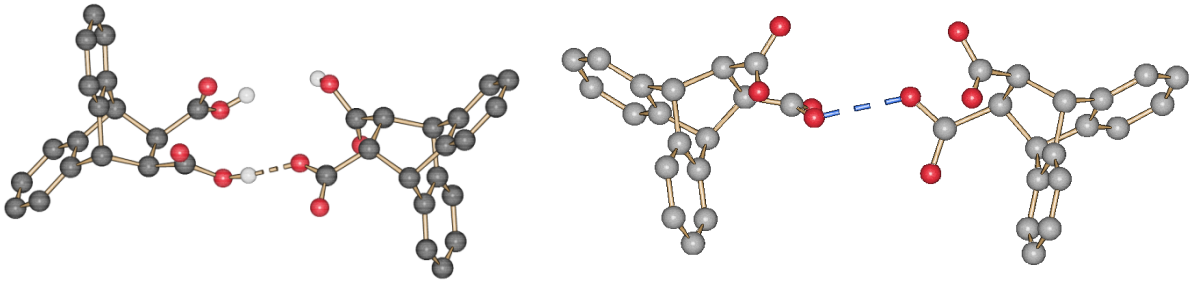

(a) (b)

Fig.1. (a) Ball and stick representation of the supramolecular anion [(*cis*-deccaH)(*cis*-deccaH$_2$)]$^-$ in crystalline **1** and **2** (only one of the possible images due to COOH/COO$^-$ disorder is shown here for **2**). H_{CH} omitted for clarity.

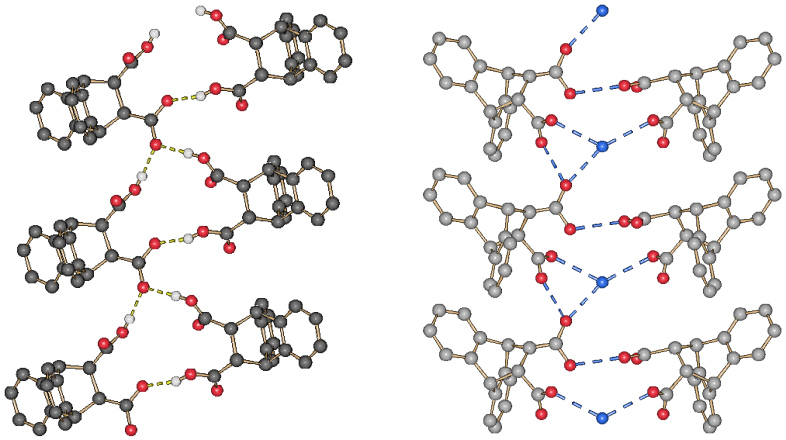

(a) (b)

Fig.2. Ball and stick representation of the hydrogen bonded tapes extending along the crystallographic *a*-axis in (a) anhydrous (**1**) and (b) monohydrated (**2**) [(η^5-C_5H_5)$_2$Co][(*cis*-deccaH)(*cis*-deccaH$_2$)]·H_2O (only one of the possible images due to COOH/COO$^-$ groups disorder is shown here for **2**). Blue spheres in **2** represent water molecules. H_{CH} atoms omitted for clarity.

The tapes are interlocked, taking advantage of the shape factor: the aromatic rings belonging to adjacent tapes are juxtaposed, so that geometrical complementarity is satisfied; no π-stacking interactions, though, are present, as in **1** and **2** the distance between the phenyl groups is 3.7 and 3.9 Å, respectively, therefore much larger than the one usually associated with π-stacking interactions[22] (see also Figure 3); this is not surprising, as the interacting dimers are both negatively charged, i.e. their interaction has to be repulsive.

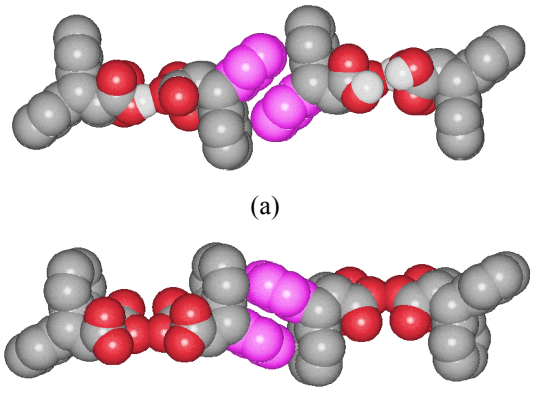

(a)

(b)

Fig.3. Space-filling representation of the juxtaposition of phenyl groups on adjacent tapes in (a) **1** and (b) **2**. H_{CH} atoms omitted for clarity.

The tape interlocking generates walls and channels, in which the cations are accommodated in infinite piles that run along the *a*-axis (see Figure 4). In compound $[(\eta^5\text{-}C_5H_5)_2Co][(cis\text{-}deccaH)(cis\text{-}deccaH_2)]\cdot H_2O$ (**2**), which is affected by orientational disorder of the cobalticinium moieties, the channels are wider and accommodate the disordered cations with their molecular axes perpendicular to the channel direction (see Figure 4b).

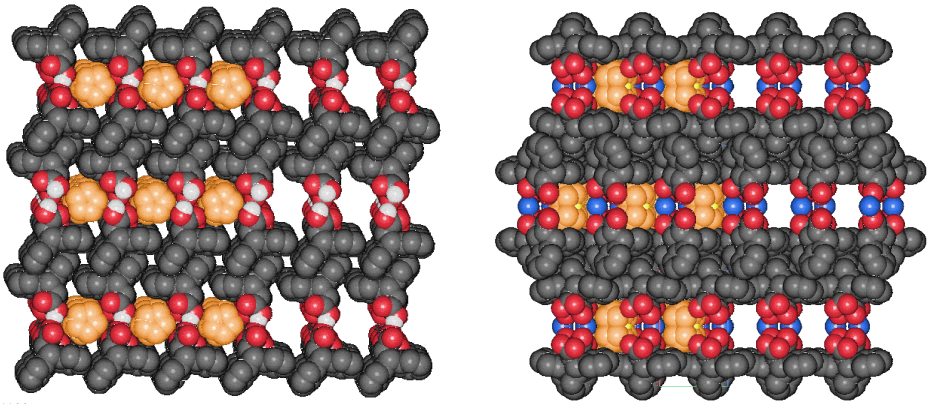

(a) (b)

Fig.4. Projections along the crystallographic *a*-axis of the crystalline packing in **1** (a) and **2** (b); the walls and channels generated via tapes interlocking are filled with the $[(\eta^5\text{-}C_5H_5)_2Co]$ cations. On the right side of each

figure the cations (carbon atoms in orange) have been artificially removed, to show the anionic superstructures; H_{CH} atoms omitted for clarity. The cations in **2** are disordered over two equivalent positions.

Crystallization in the presence of one equivalent or an excess (two equivalents) of anhydride invariably results in the formation of **2**, and it has not been possible, so far, to obtain a salt in which the neutral form of the acid is absent.

*4.1.2 - [(η^5-C_5Me_5)$_2$Co][cis-deccaH] (**3**).* The decamethylcobalticinium cations are much more demanding in terms of space with respect to the smaller cobalticinium ones. This results in a different superstructure consisting of adjacent cationic $[(\eta^5\text{-}C_5Me_5)_2Co]^+$ piles forming an almost layered packing alternated by organic anionic planes. In addition to this, the carboxylic/carboxylate functions, localized on the anion, form very short intramolecular hydrogen bonds [$O_{COOH}\cdots O_{COO}^-$ = 2.395(8) and 2.384(10) Å]. See figure 5.

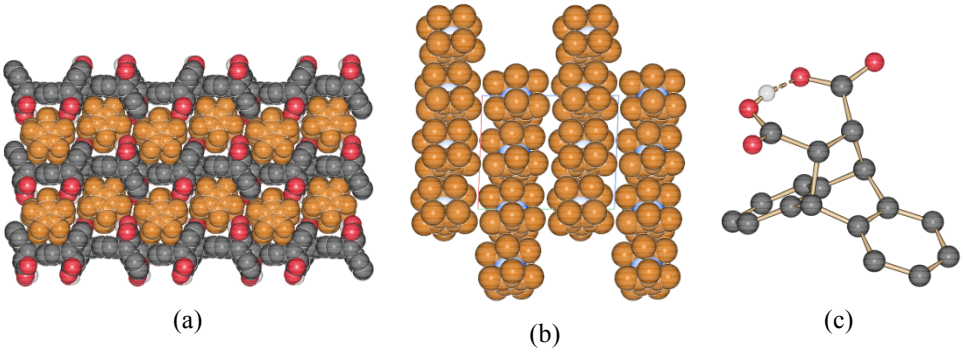

Fig.5. (a) Space-filling representation of the layered structure of compound $[(\eta^5\text{-}C_5Me_5)_2Co]$[*cis*-deccaH] (**3**) viewed along the *b*-axis; (b) projection along the *a*-axis of the cationic piles formed by the decamethylcobalticinium cations and (c) the intramolecular hydrogen bond observed in the (*cis*-deccaH)$^-$ anion. H_{CH} atoms omitted for clarity.

4.2 Anionic networks derived from the Trans-deccaH$_2$

4.2.1 - [(η^5-C_5H_5)$_2$Co][(trans-deccaH)] (4). In the crystal architecture of **4** the organic superstructure recalls a honeycomb scaffold with large and almost hexagonal channels extending along the *c*-axis. The channels are occupied by columnar piles of organometallic cations, as represented in figure 6.

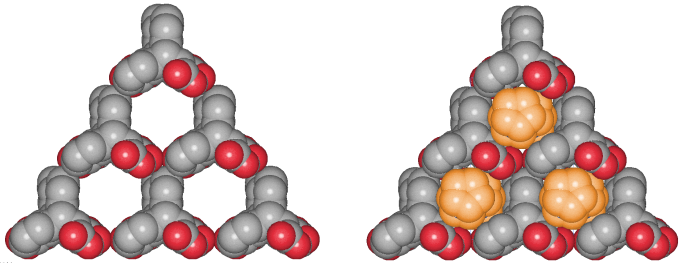

(a) (b)

Fig.6. (a) Space-filling representation of the channels formed by the [*trans*-deccaH]$^-$anions in crystalline **4**; (b) the channels are accommodating the cobalticinium piles extending along the *c*-axis. H_{CH} atoms omitted for clarity.

The carboxylic and carboxylate groups do not participate in significant interactions between the anions, but are involved in a short intramolecular hydrogen bond ($O_{COO^-}\cdots O_{COOH}$ = 2.473(6) Å, see figure 7); in this respect the system behaves quite differently from other geometrically related systems, i.e. tartaric, terephthalic, etc,[13,16] in which inter-molecular hydrogen bonds are responsible for the generation of the 3D superanion networks. Contrary to what observed earlier in the case of the adduct between cobalticinium and D,L, tartaric acid, for example, where the honeycomb superstructure is held together by interanionic hydrogen bonds, in the case of **4** it is only the combination of the shape of the cation (a cylinder) and of the anionic three-spikes stars that yields the honeycomb structure. A comparison (see Figure 8) between the two packings shows the strong analogy between the two compounds.

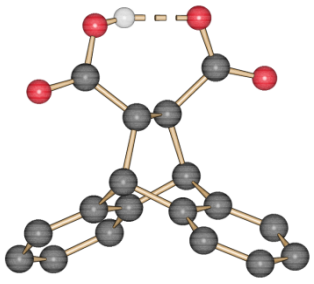

Fig.7. The intramolecular hydrogen bond observed in the (*trans*-deccaH)$^-$ anion. H_{CH} omitted for clarity.

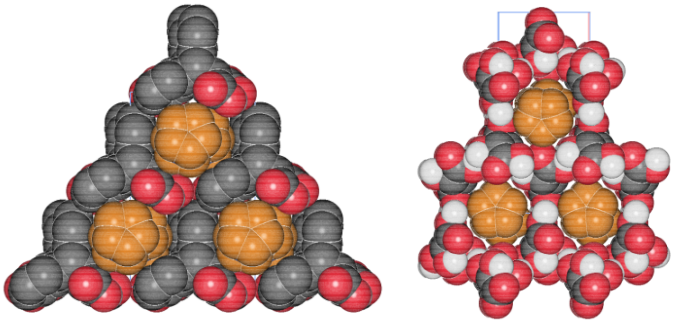

(a) (b)

Fig.8. (a) A comparison of the packings for crystalline **4** (a) and $[Co(\eta^5\text{-}C_5H_5)_2][(D,L\text{-taH})\cdot(D,L\text{-taH}_2]$ (b), showing how the same honeycomb motif is generated only by the matching shapes of cations and anions in **4**, while it is sustained by the presence of interanionic hydrogen bonds in $[Co(\eta^5\text{-}C_5H_5)_2][(D,L\text{-taH})\cdot(D,L\text{-taH}_2]$. H_{CH} atoms not shown for clarity.

*4.2.2 - [(η^5-C_5H_5)$_2$Co][(trans-deccaH)(trans-deccaH$_2$)] (**5**)*. If the cobalticinium cation $[(\eta^5\text{-}C_5H_5)_2Co]^+$ is crystallized in the presence of two equivalents of *trans*-deccaH$_2$, the co-crystalline derivative **5** is obtained, analogously to what observed in the case of the *cis*-decca derivative **2**. In crystalline $[(\eta^5\text{-}C_5H_5)_2Co][(trans\text{-deccaH})(trans\text{-deccaH}_2)]$ (**5**) we observe the presence of supramolecular anions held together by inter-molecular hydrogen bonds ($O_{COO^-}\cdots O_{COOH}$ = 2.603(6) Å). The superanions, in turn, participate in a hydrogen bonded network ($O_{COO^-}\cdots O_{COOH}$ = 2.557(6) – 2.759(7) Å) that yields connected cavities along the *a*-axis, as shown in Figure 9. Two cobalticinium cations fit within each cavity with their axes perpendicular to the *a*-axis direction.

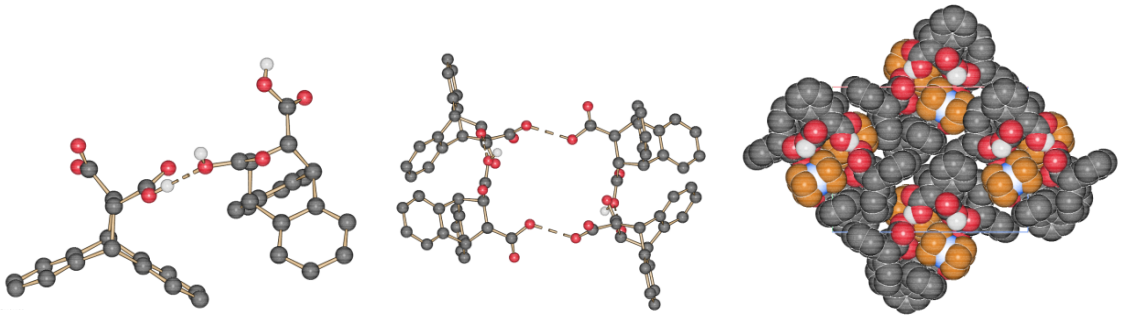

(a) (b) (c)

Fig.9. (a) Ball and stick representation of the supramolecular anion $[(cis\text{-deccaH})(cis\text{-deccaH}_2)]^-$ in crystalline **5**; (b) hydrogen bonding interactions network and (c) how the cations fit inside the niches, both viewed along the *a*-axis. H_{CH} atoms omitted for clarity.

*4.2.3 - [(η^5-C_5Me_5)$_2$Co][(trans-deccaH)]·4H_2O (**6**)*. In the crystal structure of compound **6** we observe the presence of an R4 cyclic water tetramer (shown in blue in Figure 10a)[22] held together by hydrogen bonds [$O_w\cdots O_w$ distances in the range 2.882(10) – 2.992(8) Å, $O_w\cdots O_w\cdots O_w$ angles in the range 101.7(4) - 103.9(7)° and 71.1(5) - 74.0(6)°], in a sort of a "butterfly" conformation (dihedral angle *ca.* 151°). To the best of our knowledge this conformation is unusual because: (i) it strongly deviates from planarity and (ii) two angles are much smaller than those usually observed for these kinds of clusters. The majority of water tetramers either predicted[23] or observed[24] are planar or quasi-planar, with angles ranging from *ca.* 90° to *ca.* 125°. In crystalline **6** H-atoms could not be directly located from a Fourier difference map, but a possible distribution is presented in Figure 10: as it can be seen, the small $O_w\cdots O_w\cdots O_w$ angles are possible because the tetramer is also hydrogen bonded to the anion [$O_w\cdots O_{COO^-/COOH}$ distances 3.025(4) and 2.788(6) Å], and no acute H-O-H angles are actually present.

This tetramer, in turn, interacts through a net of hydrogen bonds, with the [*trans*-deccaH]$^-$ monoanion. The small water clusters act as "reinforcement" units along the anionic chain [$O_{COOH}\cdots O_{COO^-}$ = 2.471(2) Å; $O_w\cdots O_{COOH}$ = 2.987(5) Å], as it is shown in figure 10.

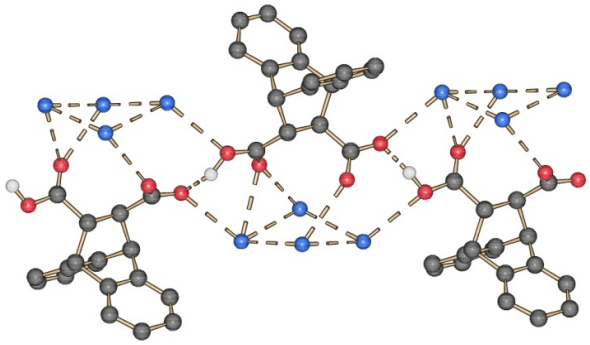

(a)

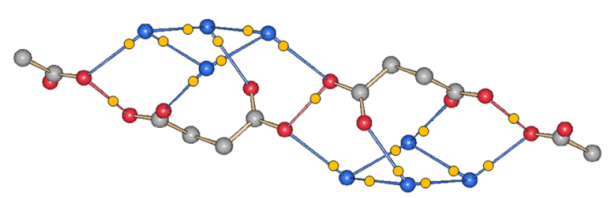

(b)

Fig.10. (a) Chains formed by the water tetramers and the (*trans*-deccaH)$^-$ anions in crystalline **6**. (b) Ribbon formed by water tetramers and (*trans*-deccaH)$^-$ anions in crystalline **6**. For sake of clarity only the HOOC-C-C-COO$^-$ fragments are shown for the anions. H_{CH} atoms omitted for clarity. Yellow spheres represent H_{water} and H_{COOH} atoms. Blue solid lines represent intermolecular H-bonds involving water molecules; red solid lines represent anion···anions H-bonds: here the H atom has been arbitrarily assigned to one of the COO groups.

As it can be seen in figure 11, these infinite chains are arranged to form almost hexagonal channels that run along the [1 0 1] direction, which are filled by stacks of $[(\eta^5\text{-}C_5Me_5)_2Co]^+$ cations. In projection the overall structure is closely reminiscent of that of compound (**4**).

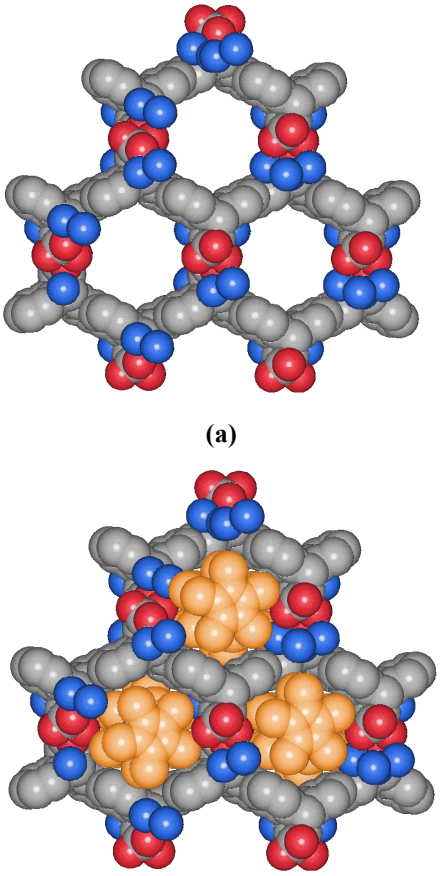

(a)

(b)

Fig.11. (a) Projection along the [1 0 1] direction of the channels formed by the anions (*trans*-deccaH)$^-$ and the water tetramers in solid **6**; (b) view along the same direction filled by cationic stacks. H atoms omitted for clarity.

The role of the water molecules may be that of enlarging, via formation hydrogen bonds formation, the size of the channels formed by the organic anions, thus allowing the bulky cations to fit inside. In the absence of water molecules the [*trans*-deccaH]$^-$ anions could not fold around the $[(\eta^5\text{-}C_5Me_5)_2Co]^+$ cations, as it observed in compound **4**.

4.2.4 - [(η^6-C_6H_6)$_2$Cr][(trans-deccaH)] (7). Crystalline **7**, the only derivative of bis-benzene chromium reported in this paper, provides a further example of how an hexagonal honeycomb type arrangement of the organic moieties *unsustained* by strong hydrogen bonds can be organized around the organometallic cations. The packing is shown in Figure 12 and ought to be compared with those shown above in figures 7 and 11. The intramolecular hydrogen bond within the [*trans*-deccaH]$^-$ monoanion is comparable to those observed in the other compounds of this series ($O_{COOH}\cdots O_{COO^-}$ 2.457(3) Å).

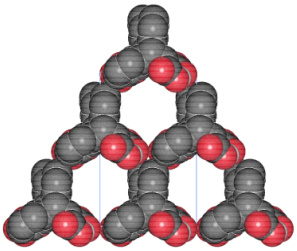

(a)

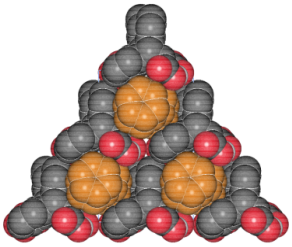

(b)

Fig.12. (a) Space-filling representation of the honey-comb framework formed by the [*trans*-deccaH]$^-$ anions, (b) space-filling representation of how the cationic piles fit inside the channels extending along the *c*-axis. H_{CH} atoms omitted for clarity.

5 Conclusions

In previous studies the group has reported several examples of organic-organometallic superstructures obtained with the idea that *confinement* of all strong donor/acceptor hydrogen bonding groups on the organic or inorganic networks would lead to spontaneous self-assembly of the anions in honeycomb or other porous structures that could accommodate the organometallic cations $[Co(\eta^5\text{-}C_5H_5)_2]^+$, $[Cr(\eta^6\text{-}C_6H_6)_2]^+$, $[Fe(\eta^5\text{-}C_5Me_5)_2]^+$ and $[Co(\eta^5\text{-}C_5Me_5)_2]^+$. The regular cylindrical shape of these cations appeared to play a role in directing the assembly of the anionic frameworks, also with the participation of C-H ···O interactions between the acceptor -COOH/COO^- sites on the networks and the C-H groups protruding from the complex surface.[11] In this section we have shown that, although the "hydrogen bonding confinement" strategy is essentially correct and can be extended to more complex dicarboxylic acids, such as *cis*-9,10-dihydroanthracene-9,10-α,β-succinic acid anhydride (*cis*-decca) and *trans*-9,10-dihydro-9,10- ethanoanthracene-11,12-dicarboxylic acid (*trans*-deccaH_2) leading to novel architectures, the hydrogen bond *is not* the key structure-directing interaction. In compounds **1**, **2**, **5**, where there is abundance of hydrogen bonding donors because of the 1:2 organometallic:organic stoichiometric ratios, the formation of interanionic hydrogen bonds is possible and the resulting structures show extended network patterns and self-assembly around the cations of the type observed before. In compounds **3**, **4**, **6** and **7**, where deprotonation leads to intramolecular hydrogen bonds, hence forbids inter-anionic hydrogen bonding, alternative solutions are adopted. In compounds **4** and **7** the three-stem star-like shape of the anions *takes the lead* and generates the observed close packing arrangement thanks to a perfect match in terms of size and shape with the small sandwich organometallic cations $[Co(\eta^5\text{-}C_5H_5)_2]^+$, and $[Cr(\eta^6\text{-}C_6H_6)_2]^+$ cations. Compounds **3** and **7**, on the other hand, provide a sort of proof of concept because the larger shape of the cations does not allow an equivalent efficient arrangement, hence the crystal structure of **5** adopts a columnar organization, while **7** drags in four water molecules as space filler to generate a honeycomb arrangement similar to that in **4** and **7**. The use of organometallic building blocks in the preparation of two-dimensional (2D) and three-dimensional (3D) framework materials has obvious potential, yet, in spite of the large efforts in crystal engineering, it remains an area that is relatively underdeveloped. The observation that the same topology can be attained by selecting molecular/ionic components on the basis of their shape, rather than of their supramolecular bonding capacity, might affect the way we look at the engineering of metal-organic frameworks. All in all, the series of compounds examined in this study shows how

difficult it still is to "make crystals by design", because of the complex interplay of different and not always converging factors/interactions such as hydrogen bonding, shape, charge balance, and space filler solvent molecules in the formation of stable crystalline aggregates. However, the analysis of differences between crystal structures obtained with structurally similar molecules may indicate ways to obtain polymorphs of a same compound, or ways to interconvert crystal forms by adding/removing solvent molecules. A study of this type is under way.

Experimental Section

The neutral compound $[(\eta^5\text{-}C_5H_5)_2Co]$, bought from Alfa-Aesar, and all reactants and reagents, purchased from Sigma-Aldrich, were used without further purification. Reagent grade solvents and bi-distilled water were used. ^{1}H-NMR spectra were recorded on a Varian Mercury400, chemical shifts of ^{1}H-NMR signals were expressed in part per million (δ_H) using internal standard TMS ($\delta_H = 0.00$).

*Synthesis of trans-deccaH_2***.** Dioxane (25 mL) was added to a mixture of fumaric acid (0.645 g, 5.6 mmol) and anthracene (3.0 g, 17 mmol). After refluxing for 3 days at 104 °C the solvent was removed by rotary evaporation under reduced pressure. A saturated solution (100 mL) of Na_2CO_3 was added and the mixture was stirred for half-day. The mixture was filtered (in order to remove the unreacted anthracene) and conc. HCl was added to the clear solution to pH = 1. The solid product was recovered by filtration of the hot solution. Yield = 90 %. m.p. = 251-252°C (lit. m.p. = 252.5°C). ^{1}H-NMR (400 MHz, DMSO-d_6, TMS) δ_H: 12.52 (s, 2H, COOH), 7.065-7.371 (m, 8H, aromatic CH), 4.707 (s, 2H, methine CH) and 3.549 (s, 2H, methine CH). See figure ES1 for the comparison between the experimental and simulated powder x-ray diffraction patterns.

*Synthesis of cis-decca***.** p-Xylene (30 mL) was added to a mixture of maleic anhydride (0.346 g; 5.3 mmol) and anthracene (0.62 g; 3.56 mmol). The mixture was refluxed at 135°C for 1 hour. The resulting solution was allowed to cool to room temperature, yielding a white powder that was removed by filtration and washed with few millilitres of ethyl acetate. Solid *cis*-decca was re-crystallized from hot ethyl acetate. Colourless prismatic crystals formed upon cooling the ethyl acetate solution. Yield = 80 %. m.p. = 262°C (lit. m.p. = 262-263°C). ^{1}H-NMR (400 MHz, $CDCl_3$-d_1, TMS) δ_H: 7.41 (m, 8H, aromatic CH), 4.87 (s, 2H, methine

CH) and 3.55 (s, 2H, methine CH). See figure ES1 for the comparison between the experimental and simulated powder x-ray diffraction patterns.

Synthesis of [(η^5-C_5H_5)$_2$Co][(cis-deccaH)(cis-deccaH$_2$)] (1). 30 mg (0.16 mmol) of [(η^5-C_5H_5)$_2$Co] were suspended in ca. 15 mL of nitromethane. Oxygen was bubbled into the suspension until a dark yellow solution was obtained. 44 mg (0.16 mmol) of trans-deccaH_2 were added to the solution, which was kept under stirring for two hours. The solution was then filtered, to remove unreacted material, and kept in the dark. Pale brown crystals suitable for X-ray diffraction were obtained by slow evaporation of the solvent at RT.

Synthesis of [(η^5-C_5H_5)$_2$Co][(cis-deccaH)(cis-deccaH$_2$)]·H_2O (2). 30 mg (0.16 mmol) of [(η^5-C_5H_5)$_2$Co] were suspended in ca. 10 mL of water. Oxygen was bubbled into the suspension until a bright yellow solution was obtained. 44 mg (0.16 mmol) of trans-deccaH_2 were added to the solution, which was kept under stirring for two hours, The solution was then filtered, to remove unreacted material, and kept in the dark. Recrystallization of the bright yellow powder from water yielded single crystals suitable for X-ray diffraction.

Synthesis of [(η^5-C_5Me_5)$_2$Co][cis-deccaH] (3). 36.5 mg (0.11 mmol) of [(η^5-C_5Me_5)$_2$Co] were suspended in ca. 20 mL of nitromethane. Oxygen was bubbled into the suspension until a dark yellow solution was obtained. 26.1 mg (0.11 mmol) of *cis*-decca were added to the solution, which was kept under stirring for two hours; the solution was then filtered, to remove unreacted material, and kept in the dark. Pale brown crystals suitable for X-ray diffraction were obtained by slow evaporation of the solvent at RT.

Synthesis of [(η^5-C_5H_5)$_2$Co][trans-deccaH] (4). 30 mg (0.16 mmol) of [(η^5-C_5H_5)$_2$Co] were suspended in ca. 15 mL of nitromethane and oxidized by bubbling oxygen into the suspension until a dark yellow solution was obtained. 47 mg (0.16 mmol) of trans-deccaH_2 were added to the solution, which was kept under stirring for two hours, the solution was filtered, to remove unreacted material, and kept in the dark. Pale brown crystals suitable for X-ray diffraction were obtained by slow evaporation of the solvent at RT.

Synthesis of [(η^5-C_5H_5)$_2$Co][(trans-deccaH)(trans-deccaH$_2$)] (5). The same procedure used for the synthesis of (**1**) was repeated here, but using 2 equivalents of *trans*-deccaH_2 (94 mg;

0.31 mmol). Yellow crystals suitable for X-ray diffraction were obtained by slow evaporation of the solvent at RT. Solid (**4**) can also be obtained directly in the solid state by manual grinding solid (**3**) for 10 minutes with 1 equivalent of *trans*-deccaH$_2$.

Synthesis of [(η^5-C_5Me_5)$_2$Co][trans-deccaH]·4H$_2$O (6). 40.7 mg (0.12 mmol) of [(η^5-C_5Me_5)$_2$Co] were suspended in ca. 15 mL of bidistilled water. The suspension was stirred until a bright yellow solution was obtained. 37 mg (0.13 mmol) of trans-deccaH2 were added to the solution, which was kept under stirring for two hours; the solution was then filtered, to remove unreacted material, and placed in the dark. Pale brown crystals suitable for X-ray diffraction were obtained by slow evaporation of water at RT.

Synthesis of [(η^6-C_6H_6)$_2$Cr][(trans-deccaH)] (7). 20 mg (0.10 mmol) of [(η^6-C_6H_6)$_2$Cr] were suspended in ca. 15 mL of nitromethane and oxidized by bubbling oxygen into the suspension until a dark yellow solution was obtained. 28 mg (0.10 mmol) of trans-deccaH$_2$ were added to the solution, which was kept under stirring for two hours; the solution was filtered, to remove unreacted material, and placed in the dark. Pale brown crystals suitable for X-ray diffraction were obtained by slow evaporation of the solvent at RT.

X-ray diffraction. Single-crystal data for compounds (**1**)—(**7**) were collected on an Oxford X'Calibur S CCD diffractometer equipped with a graphite monochromator (Mo-Kα radiation, λ = 0.71073Å) and operating at room temperature except for compounds **5**, which was collected at 150K. Crystal data and details of measurement for all compounds are listed in Table 1. All non-hydrogen atoms were refined anisotropically; H_{OH} atoms were either directly located or added in calculated positions; H_{CH} atoms for all compounds were added in calculated positions and refined riding on their respective carbon atoms. SHELX97[25a] was used for structure solution and refinement on F^2, PLATON[25b] and SCHAKAL99[25c] were used for hydrogen bonding analysis and molecular graphics, respectively.
X-ray powder data were collected on a Philips X'Pert automated diffractometer with Cu-Kα radiation. The program PowderCell[25d] was used for calculation of X-ray powder patterns on the basis of single crystal data. The identity between bulk materials and single crystals was always verified by comparing calculated and experimental powder diffraction patterns.

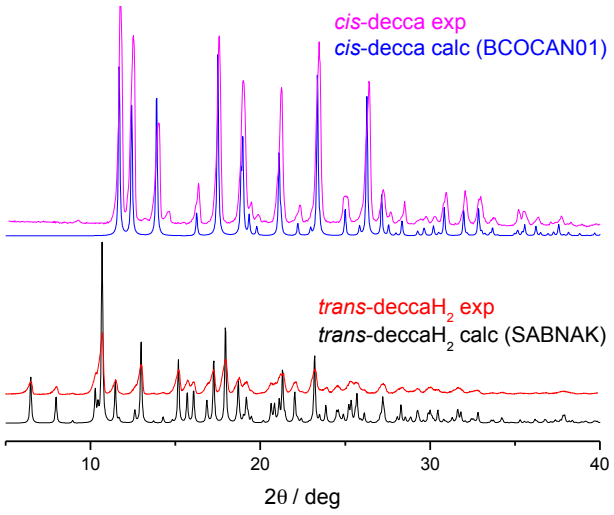

Figure ES1. Comparison of powder x-ray patterns for *trans*-deccaH$_2$ (black-line is the calculated and red-line is the experimental pattern) and *cis*-decca (blue-line is the calculated and magenta-line is the experimental pattern).

Table ES1a. Crystal data and details of measurements for compounds (**1**)—(**3**).

	1	**2**	**3**
Formula	$C_{46}H_{37}O_8Co$	$C_{46}H_{39}O_9Co$	$C_{76}H_{86}O_8\ Co_2$
Z	2	4	2
Z'	1	0.5	2
a (Å)	6.9519(2)	12.948	12.5536(6)
b (Å)	8.8643(4)	32.013	14.6337(7)
c (Å)	30.6884(9)	9.058	17.4280(8)
α (deg)	87.744(3)	90	88.839(4)
β (deg)	87.644(2)	90	89.410(4)
γ (deg)	77.553(3)	90	79.904(4)
fw	776.69	794.70	1245.31
V ($Å^3$)	1844.2 (1)	3754.6	3151.32(1)
D_{calc} (Mg/m^3)	1.399	1.406	1.312
μ (mm^{-1})	0.523	0.517	0.584
Cryst. System	Triclinic	Orthorhombic	Triclinic
Space group	P-1	Pnma	P-1
n° of collected reflns	40270	27427	25385
n° of indep. reflns	8892	3914	14115
R1[on F_0^2, I>2sigma(I)]	0.0543	0.1415	0.0909
wR2 (all data)	0.1091	0.4494	0.2633
T (K)	293	293	150

Table ES1b. Crystal data and details of measurements for compounds (**4**)—(**7**).

	4	**5**	**6**	**7**
Formula	$C_{28}H_{24}O_4Co$	$C_{46}H_{37}O_8Co$	$C_{38}H_{52}O_8Co$	$C_{30}H_{25}O_4Cr$
Z	4	4	4	4
Z'	1	1	1	1
a (Å)	15.9614(9)	9.446(2)	14.0376(7)	16.3726(9)
b (Å)	9.8616(5)	22.886(4)	19.4515(6)	9.9754(6)
c (Å)	14.7153(9)	17.238(3)	14.9838(7)	14.5407(8)
α (deg)	90	90	90	90
β (deg)	105.083(7)	100.653(18)	118.555(6)	104.215(6)
γ (deg)	90	90	90	90
fw	482.39	776.69	694.72	501.50
V ($Å^3$)	2236.5(2)	3662(1)	3593.7(3)	2302.1(2)
D_{calc} (Mg/m^3)	1.433	1.409	1.286	1.447
μ (mm^{-1})	0.801	0.527	0.528	0.534
Cryst. System	Monoclinic	Monoclinic	Monoclinic	Monoclinic
Space group	Cc	$P2_1/n$	C2/c	Cc
n° of collected reflns	5109	13743	10720	17557
n° of indep. reflns	3042	7207	4063	7472
R1[on F_0^2, I>2sigma(I)]	0.0412	0.0524	0.0643	0.0487
wR2 (all data)	0.0833	0.1011	0.1798	0.0941
T (K)	293	293	293	293

References

[1] (a) Desiraju, G. R., Ed., *Crystal Engineering: The Design of Organic Solids*, Elsevier: Amsterdam, 1989. (b) Blake, A. J.; Champness, N. R.; Hubberstey, P.; Li, W. S.; Withersby, M. A.; Schroder, M. *Coord. Chem. Rev.* **1999**, 183, 117-138. (c) Braga, D. *J. Chem. Soc. Dalton Trans.* **2000**, 3705-3713. (d) Moulton, B.; Zaworotko, M. J. *Chem. Rev.* **2001**, 101, 1629-1658. (e) Braga, D. *Chem. Commun.* **2003**, 2751-2754. (f) Braga, D.; Desiraju, G. R.; Miller, J.; Orpen, A. G.; Price, S. *CrystEngComm* **2002**, 4 500-509. (g) Hollingsworth, M. D. *Science* **2002**, 295, 2410-2413. (h) Hosseini, M. W. *CrystEngComm*, **2004**, 6, 318-322. (i) Brammer, L. *Chem. Soc. Rev.* **2004**, 33, 476-489. (j) Braga, D.; Brammer, L.; Champness, N. *CrystEngComm* **2005**, **7,** 1. (k) Desiraju, G. R. *Angew. Chem. Int. Ed.* **2007**, 46, 8342 – 8356 (l) Braga, D.; Grepioni, F.; Maini, L. *Chem. Commun.* **2010**, 46, 6232–6242.

[2] (a) Desiraju, G. R.; Steiner T., Eds., *The Weak Hydrogen Bond in Structural Chemistry and Biology*, Oxford University Press: Oxford, 1999. (b) Braga, D.; Grepioni, F.; Biradha, K., Pedireddi, V.R.; Desiraju, G. R. *J. Am. Chem. Soc.* **1995**, 117, 3156-3166. (c) Calhorda, M. .J. *Chem. Commun.* **2000**, 801-809. (d) Nangia, A. *J. Chem. Sci.* **2010**, 122, 295–310. (e) Thalladi, V. R.; Goud, B. S.; Hoy, V. J.; Allen, F. H.; Howard, J. A. K.; Desiraju, G. R. *Chem. Commun.* **1996**, 401-402. (f) Braga, D.; Brammer, L.; Champness, N. L. *CrystEngComm* **2005**, **7**, 1-19. (g) Desiraju, G. *Cryst. Growth Des.* **2011**, 11, 896–898.

[3] Reger, D. L.; Horger J.; Smith, M. D.; Long, G. J. *Chem. Commun.* **2009**, 6219-6221.

[4]. (a) Roswell, J. L.; Yaghi, O. M. *Angew. Chem. Int. Ed.* **2005**, 44, 4670-4679. (b) Collins, D.; Zhou, H. C. *J. Mater. Chem.* **2007**, 17, 3154-3160. (c) Kitagawa, S.; Matsuda, R. *Coord. Chem. Rev.* **2007**, 251, 2490-2509. (d) Dybtsev, D.; Chun, H.; Yoon, S. H., Kim, D.; Kim, K. *J. Am. Chem. Soc.* **2004**, 126, 5666-5667. (e) Dinca, M.; Long, J. *Angew. Chem., Int. Ed.* **2008**, 47, 6766-6779. (f) Belof, J.; Stern, A.; Eddaoudi, M.; Space, B. *J. Am. Chem. Soc.* **2007**, 129, 15202– 15210.

[5] (a) Chen, B.; Yang, Y.; Zapata, F.; Lin, G.; Qian, G.; Lobkovsky, E. *Adv. Mater.* **2007**, 19, 1693-1696. (b) Wong, K. L.; Law, G. L.; Yang, Y. Y.; Wong, W. T. *Adv. Mater.* **2006**, 18, 1051-1054. (c) Maspoch, D.; Ruiz-Molina, D.; Wurst, K.; Domingo, N.; Cavallini, M.; Biscarini, F.; Tejada, J.; Rovira, C.; Veciana, J. *Nat. Mater.* **2003**, 2, 190-195. (d) Halder, G.; Kepert, C.; Moubaraki, B.; Murray, K.; Cashion, J. *Science* **2002**, 298, 1762-1765.

[6] (a) Fujita, M.; Kwon, Y. J.; Washizu, S.; Ogura, K. *J. Am. Chem. Soc.* **1994**, 116, 1151-1152. (b) Seo, J.; Whang, D.; Lee, H.; Jun, S.; Oh, J.; Jeon, Y.; Kim, K. *Nature* **2000**, 404, 982-986. (c) Wu, C. D.; Hu, A.; Zhang, L.; Lin, W. *J. Am. Chem. Soc.* **2005**, 127, 8940-

8941. (d) Wu, C. D.; Lin, W. *Angew. Chem., Int. Ed.* **2007**, 46, 1075-1078. (e) Dybtsev, D.; Nuzhdin, A.; Chun, H.; Bryliakov, K.; Talsi, E. P.; Fedin, V. P.; Kim, K. *Angew. Chem., Int. Ed.* **2006**, 45, 916-920. (f) Cho, S. H.; Gadzikwa, T.; Afshari, M.; Nguyen, S.; Hupp, J. *Eur. J. Inorg. Chem.* **2007**, 31, 4863-4867. (g) Cho, S.H.; Ma, B.; Nguyen, S. T.; Hupp, J. T.; Albrecht-Schmitt, T. E. *Chem. Commun.* **2006**, 24, 2563-2565. (h) Alkordi, M.; Liu, Y.; Larsen, R.; Eubank, J.; Eddaoudi, M. *J. Am. Chem. Soc.* **2008**, 130, 12639-12641.

[7] (a) Pan, L.; Olson, D. H.; Ciemnolonski, L. R.; Heddy, R.; Li, J. *Angew. Chem., Int. Ed.* **2005**, 45, 616-619. (b) Chen, B.; Liang, C.; Yang, J.; Contreras, D.; Clancy, Y.; Lobkovsky, E.; Yaghi, O. M.; Dai, S. *Angew. Chem., Int. Ed.* **2006**, 45, 1390-1393. (c) Dybtsev, D.; Chun, H.; Yoon, S.; Kim, D.; Kim, K. *J. Am. Chem. Soc.* **2004**, 126, 32-33. (d) Custelcean, R.; Gorbunova, M. *J. Am. Chem. Soc.* **2005**, 127, 16362-16363. (e) Bourrelly, S.; Llewellyn, P.; Serre, C.; Millange, F.; Loiseau, T.; Ferey, G. *J. Am. Chem. Soc.* **2005**, 39, 13519-13521.

[8] Braga, D.; Grepioni, F.; Desiraju, G. R. *Chem. Rev.* **1998**, 98, 1375– 1405.

[9] Braga, D.; Giaffreda, S.; Grepioni, F.; Pettersen, A.; Maini, L.; Curzi, M.; Polito, M. *Dalton Trans.* **2006**, 1249– 1263.

[10] Braga, D.; Grepioni, F. *Coord. Chem. Rev.* **1999**, 183, 19.

[11] Braga, D.; Grepioni, F. *Acc. Chem. Res.* **2000**, 33, 601-608.

[12] (a) Braga, D.; Bazzi, C.; Grepioni, F.; Novoa, J. J. *New J. Chem.* **1999**, 23, 577-579. (b) Braga, D.; Grepioni, F.; Tagliavini, E.; Novoa, J. J.; Mota, F. *New. J. Chem.* **1998**, 22, 755-757. (c) Novoa, J. J.; Nobeli, I.; Grepioni, F.; Braga, D. *New J. Chem.* **2000**, 24, 5-8. (d) Braga, D.; Maini, L.; Grepioni, F.; Mota, F.; Rovira, C.; Novoa, J. J. *Chem. Eur. J.* **2000**, 6, 4536-4551. (e) Braga, D.; D'Oria, E.; Grepioni, F.; Mota, F.; Novoa, J. J.; Rovira, C. *Chem. Eur. J.* **2002**, 8, 1173-1180. (f) Braga, D.; Grepioni, F.; Novoa, J. J. *Chem. Commun.* **1998**, 1959-1960.

[13] (a) Braga, D.; Angeloni, A.; Grepioni, F.; Tagliavini, E. *Chem. Commun.* **1997**, 1447-1448. (b) Braga, D.; Angeloni, A.; Grepioni, F.; Tagliavini, E. *Organometallics* **1997**, 16, 5478-5485.

[14] Braga, D.; Eckert, M.; Fraccastoro, M.; Maini, L.; Grepioni, F.; Caneschi, A.; Sessoli, R. *New J. Chem.* **2002**, 26, 1280-1286.

[15] Braga, D.; Maini, L.; Prodi, L.; Caneschi, A.; Sessoli, R.; Grepioni, F. *Chem. Eur. J.* **2000**, 6, 1310-1317.

[16] Braga, D.; Angeloni, A.; Maini, L.; Götz, A.W.; Grepioni, F. *New J. Chem.* **1999**, 23, 17-24.

[17] Braga, D.; Angeloni, A.; Tagliavini, E.; Grepioni, F. *J. Chem. Soc. Dalton Trans.* **1998**, 1961-1968.

[18] (a) Grepioni, F.; Gladiali, S.; Scaccianoce, L.; Ribeiro, P.; Braga, D. *New. J. Chem.* **2001**, 25, 690-695.

[19] (a) Braga, D.; Giaffreda, S.; Grepioni, F.; Maini, L.; Polito, M. *Coord. Chem. Rev.* **2006**, 250, 1267– 1285. (b) Braga, D.; Maini, L.; Polito, M.; Tagliavini, E.; G. *Coord. Chem. Rev.* **2003**, 246, 53–71. (c) Braga, D.; Maini, L.; Polito, M.; Scaccianoce, L.; Cojazzi, G.; Grepioni, F. *Coord. Chem. Rev.* **2001**, 216-217, 225-248. (d) Braga, D.; Grepioni, F. *Coord. Chem. Rev.* **1999**, 183, 19– 41.

[20] (a) Bachman, W. E.; Scott, L. B. *J. Am. Chem. Soc.* **1948**, 70(4), 1458-1461; (b) Weber, E.; Csoregh, I.; Ahrendt, J.; Finge S.; Czugler, M. *J. Org. Chem.* **1988**, 53, 25, 5831-5839. (c) Diaz de Delgado, G.; Belkis Ramirez V, B.; Velàsquez, W.; Rodriguez, P. *Acta cryst*. **2002**, E58, o501-o503.

[21] Janiak, C. *J. Chem. Soc., Dalton Trans.* **2000**, 3885–3896 and references therein.

[22] (*a*) Infantes, L.; Motherwell, S. *CrystEngComm*, **2002**, 4, 454–461; (*b*) Infantes, L.; Chisholm, J.; Motherwell, S. *CrystEngComm*, **2003**, 5, 480–486; (*c*) Mascal, M.; Infantes, L.; Chisholm, J. *Angew. Chem., Int. Ed.*, **2006**, 45, 32–36.

[23] (a) Ludwig, R. *Angew. Chem., Int. Ed.*, **2001**, 40, 1808–1827; (b) Masella, M.; Gresh, N; Flament, J.-P. *J. Chem. Soc., Faraday Trans.*, **1998**, 94, 2745–2753.

[24] (a) Supriya, S.; Das, S. K. *CrystEngComm*, **2008**, 10, 1743-1746; (b) Chacko, K. K.; Saenger, W. *J. Am. Chem. Soc.*, **1981**, 103, 1708–1715; (c) Zabel, V.; Saenger, W.; Mason, S. A. *J. Am. Chem. Soc.*, **1986**, 108, 3664–3673; (d) Stephens, F. C.; Vagg, R. S. *Inorg. Chim. Acta*, **1982**, 57, 43–49; (e) Xu, J.; Radkov, E.; Ziegler, M.; Raymond, K. N. *Inorg. Chem.*, **2000**, 39, 4156–4164; (f) Favas, M. C.; Kepert, D. L.; Skelton, B. W.; White, A. H. *J. Chem. Soc., Dalton Trans.*, **1980**, 454–458; (g) Supriya, S.; Das, S. K., *New J. Chem.*, **2003**, 27, 1568–1574; (h) Long, L. S.; Wu, Y. R.; Huang, R. B.; Zheng, L. S. *Inorg. Chem.*, **2004**, 43, 3798–3800 (i) Fabelo, O.; Pasán, J.; Cañadillas-Delgado, L.; Delgado,F. S.; Labrador, A.; Lloret, F.; Julve, M.; Ruiz-Pérez, C. *CrystEngComm*, **2008**, 10, 1743-1746; (j) Zuhayra, M.; Kampen, W. U.; Henze, E.; Soti, Z.; Zsolnai, L.; Huttner, G.; Oberdorfer, F. *J. Am. Chem. Soc.* **2006**, 128, 424-425.

[25] (a) Sheldrick, G. M. SHELXL97, Program for Crystal Structure Determination; University of Go¨ ttingen: Göttingen, Germany, 1997. (b) Speck, A. L. PLATON; Acta Crystallogr., Sect. A **1990**, 46, C34. (c) Keller, E. SCHAKAL99, Graphical Representation of

Molecular Models; University of Freiburg: Freiburg, Germany, 1999. (d) Kraus, W.; Nolze, G. PowderCell; BAM: Berlin; subgroups developed by Müller, U.; Universität Gh Kassel: Kassel, Germany.

Chapter 3 - Design of a solid state [2+2] photodimerization using a supramolecular template

1 Introduction

The photochemical [2+2] cycloaddition constitutes a practical way to synthesize cyclobutane derivatives. In photochemical reactions intermediates may be formed which are not accessible under thermal conditions, thus leading to specific products that could not be obtained otherwise.[1]

Photochemical reactions can be performed, in principle, in the gas phase, in solution or in the solid state. For practical reasons most photochemical reactions are carried out in solution[2] and only in the last decades photochemical reactions in the solid state have been gaining attention.

The main advanteages of photechimal reactions in the solid state are the following advantages:

(i) they are environmental friendly (no solvents are needed) and

(ii) the selectivity of these reactions can be increased if the environment in which the reaction takes place acts as a constraint on reactant geometry, providing regio- and enantioselective access to molecular products in high yields.[3]

The best known example of [2+2] photocycloaddition occurring in the solid state is dimerization of cinnamic acid, which gives many isomers in solution, while different polymorphs of cinnamic acid yield two different photoproducts upon UV irradiation.[4]

The first X-ray diffraction study on the [2+2] photodimerization was carried out by Schmidt in the 1960s.[5] His studies suggested that crystalline cinnamic acid (and its derivatives) photochemically reacts producing a cyclobutane derivative (scheme 1). The key regulating the reaction of crystalline cinnamic acids is the presence of a supramolecular arrangement of the molecules in the crystal able to give a topological control on the cyclization, because of the olefinic double bonds are locked in appropriate distance and adequate orientation by crystal packing. Schmidt postulated the geometric parameters required for the reaction in the solid-states reactions. This reaction is enabled if in the crystal the double bonds are arranged approximately parallel and at a separation less than 4.2 Å.

Schmidt also observed that the photodimerization takes place only in the case of the *trans*-isomer of the cinnamic acid.[6] The demonstration of the occurrence of the solid-state photodimerization in olefins was afterwards performed by Thomas and co-workers through single crystal X-ray diffraction studies.[7]

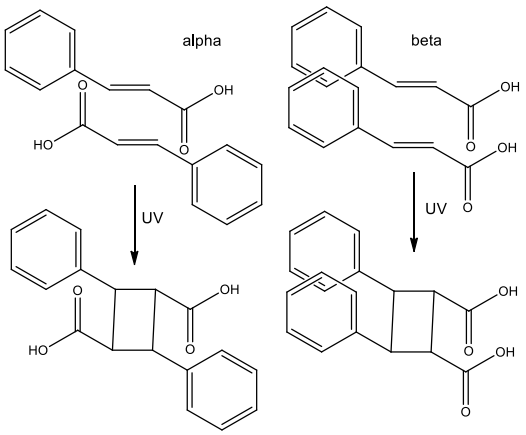

Scheme 1. Representation of the cinnamic acid photodimerization in the solid state studied by Schmidt. The reaction yields the *trans* (starting from polymorph α) or the *cis* isomer (starting from polymorph β) of the truxillic acid, depending on the starting mutual orientation of the cinnamic acid molecules.

Since the work of Schmidt, which delineated a "topological principle" for [2+2] photoreactions in the solid state, chemists have devised many methods to satisfy this condition.

Intermolecular photoreactions performed in the solid state offer a greater degree of control over the product distribution than the corresponding reactions carried out in the liquid state. In the liquid state the reactive molecules adopt several mutual orientations, as they are in constant motion. For this reason, it is impossible to predict the success of an intermolecular photoreaction in this phase, and several possible photoproducts are often formed in the liquid state.

Solid state photodimerization allows us to control, to some extent, the reaction outcome. The crystalline state provides a fixed relative orientation and proximity of reactant molecules, and ensures that unwanted products are formed.

Modern approaches focus on topological reaction control and may be classified into three general cathegories,[8] based on methods that employ:

(i) Intramolecular substitution, also denoted as supramolecular steering group approach. In this approach the substituents are covalently attached to reactants to "steer" molecules, after crystallization, in an appropriate arrangement for reaction. Electrostatic,[9] donor-acceptor[10] and hydrogen bond[11] interactions have been successfully used for steering the synthesis of molecular solids.

(ii) Auxiliary components. In this approach an auxiliary component is employed to align olefins that are to undergo the photoreaction. The auxiliary component is typically in the form of a molecular cavity, as in the case of cyclodextrins compounds.[12] The method relies on the fact that the host accommodates the guest within a tubular framework that photodimerizes upon UV irradiation.

(iii) Linear templates. This approach utilizes rigid molecules to assemble and preorganize, *via* relatively strong and directional interactions, two suitably functionalized olefins in a geometry that is appropriate for the photoreaction. To this end it is possible to use interactions, between the reactants and the template, such as hydrogen bonds,[13] metal coordination,[14] halogen-nitrogen interactions,[15] etc.

Scheme 2 shows two possible photoproducts obtained from a reactive molecule in the liquid state and how the steering group approach or the template can help narrowing the distance between the two π-systems to ensure reactive proximity or further narrowing the distance to enhance yield of photodimerization.

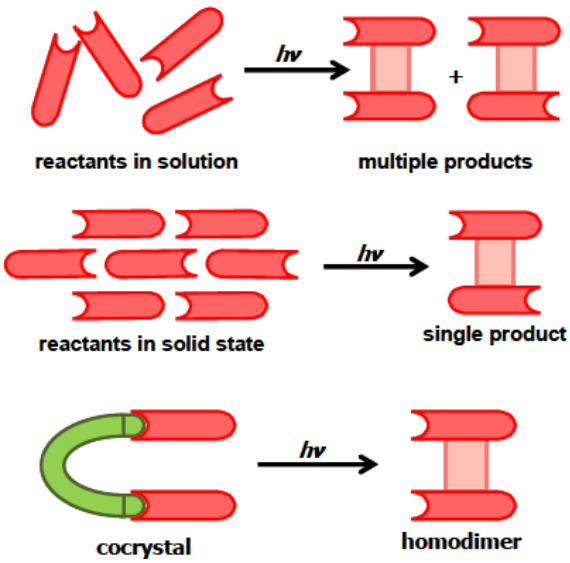

Sheme 2. The major product of a photodimerization depends on the state in which the reaction is performed. Solid state reactions provide greater control than liquid state reactions, and templated reactions can enhance yield or alter the type of major product.

2 Aim of the work: photodimerization of trans-1,2-Bis(4-pyridyl)ethylene

This part of work describes a strategy to achieve topological control over the solid-state photodimerization process of *trans*-1,2-Bis(4-pyridyl)ethylene (BpE), by using co-crystal and salt formation in a linear template approach.

The dimerization of BpE molecules can potentially yield a tetrakis(4-pyridyl)cyclobutane (tpcb) derivative with four possible regioisomers: *rctt*, *rtct*, *rcct* and *rccc*, as shown in figure 1. Of these the most favorable *rctt*-tpcb isomer has been isolated in the majority of cases reported in the literature.[16]

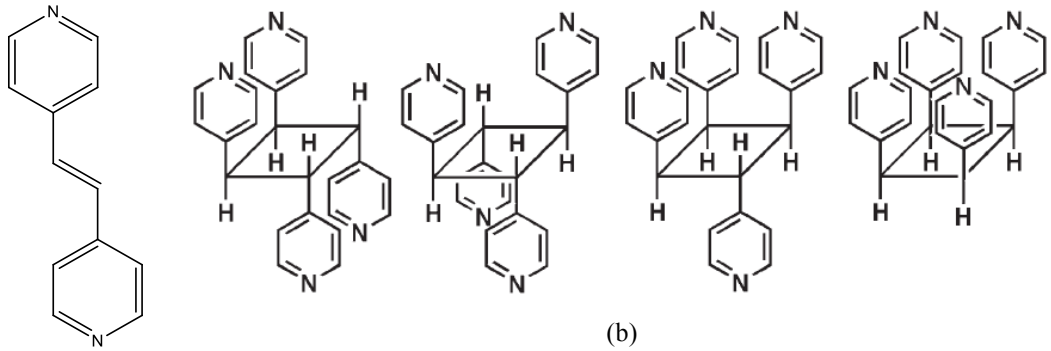

Fig.1. (a) *trans*-1,2-Bis(4-pyridyl)ethylene (BpE) and (b) sketches of the possible regioisomers of tpcb, from left to right: *rctt*, *rtct*, *rcct* and *rccc*. Here *rctt*, for example, means regio cis,trans,trans and the geometrical isomers are described with reference to a single pyridyl group, in a clockwise manner.

The experiment design can be divided in three steps: (i) identification of a suitable template for [2+2] photodimerization of BpE; (ii) synthesis of crystalline materials (co-crystals and molecular salts) and crystal structure determination in order to establish if the supramolecular aggregates are good candidates for the solid-state photoreaction; (iii) UV-irradiation of the crystalline materials in order to achieve the [2+2] cycloaddition, identification of the outcome of the UV-irradiation and isolation of the photoproduct.

3 Choice of a suitable supramolecular template

The 1,2,3,4-cyclobutane-tetra-carboxylic acid[17] ($CBTCH_4$) was selected as a potential linear-template for the photodimerization of BpE because: (i) it is a rigid molecule with four hydrogen bond donor groups lying, in pairs, approximately parallel and at a distance of *ca.* 3.6 Å and (ii) with pyridyl derivatives it gives the neutral or charge assisted supramolecular synthon[18] [O—H…N or O…H—N^+] (see scheme 3).

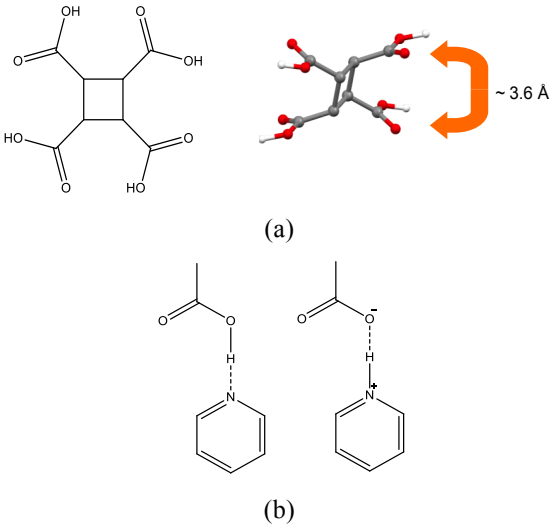

Scheme 3. (a) The $CBTCH_4$ chosen as a potential linear template for photodimerization of BpE and its crystal structure showing the distance between the hydrogen bond donors and (b) the O—H···N supramolecular synthon between the pyridil N-atom of the reactant and the carboxylic, this interaction can be either neutral or charge assisted depending on whether there is proton transfer.

Identification of a suitable template for [2+2] photodimerization of [BpE] could be carried out by using the concept of structural similarity[19] *i.e.* the design of comparable three-dimensional dimensional crystal packing arrangements from building blocks that have very similar molecular structures such as Bpy (linear and flat) and BpA (same number of C-atoms) or markedly different ones, such as DABCO (plumpy, spherical), see scheme 4.

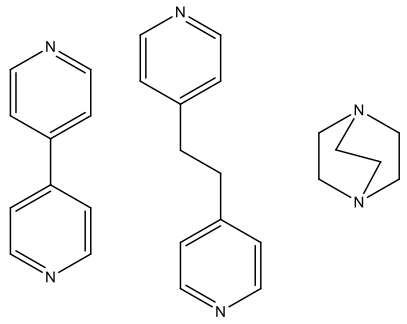

Scheme 4. Molecules used to evaluate the templating ability of the $CBTCH_4$ toward BpE; from left to right: 4,4'-bypyridine (BPy), 1,2-Bis(4-pyridyl)ethane (BpA) and 1,4-diazabiclyclo[2.2.2.]octane (DABCO).

Crystal structures of co-crystalline pairs [Bpy]/[$CBTCH_4$], [BpA]/[$CBTCH_4$] and [DABCO]/[$CBTCH_4$] were not present in the Cambridge Structural Database;[20] the preliminary synthesis of these co-crystalline materials was therefore necessary in order to evaluate the potential templating capability of the $CBTCH_4$.

4 Structural description and characterization of the co-crystals and salts used to evaluate the template capability

*4.1 - [BPy]$_2$·[CBTCH$_4$] (**1**)*. In (**1**) each carboxylic function is linked via neutral hydrogen bond ($O_{OH}\cdots N$ = 2.606 – 2685(1) Å] to a Bpy nitrogen atom, leading to formation of a supramolecular polymer made up of an alternation of two stacked [Bpy] and one [CBTCH$_4$] molecule, as shown in figure 2. Separation distance between stacked Bpy molecules is 3.953(2) Å. P-XRD, performed on ground crystals of (**1**), confirms that the bulk material obtained *via* crystallization from the ethanolic solution corresponds to (**1**)**.**

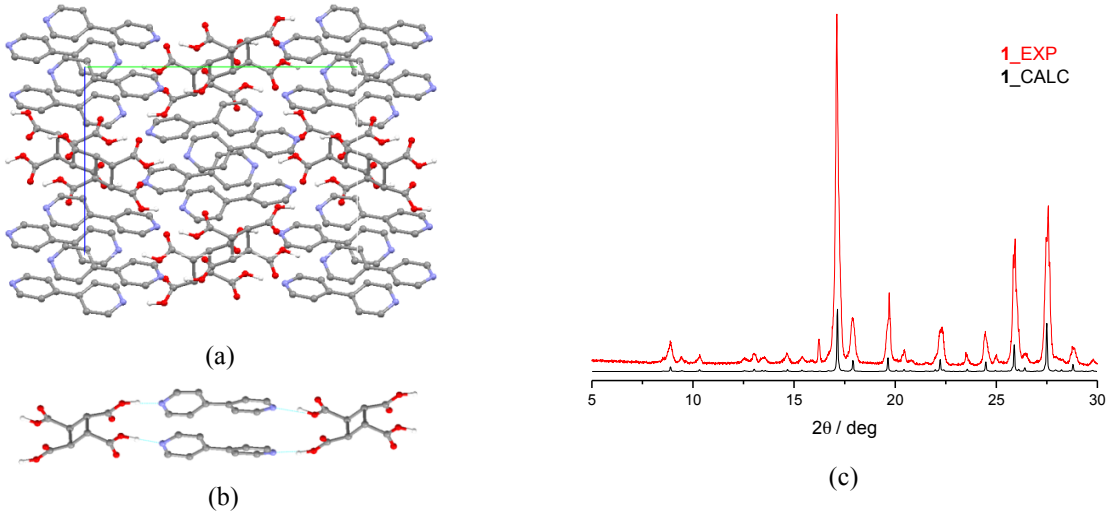

Fig. 2. (a) Crystal packing of (**1**) viwed along the *a*-axis, (b) supramolecular polymer held by hydrogen bonds present in (**1**); H_{CH} atoms omitted for clarity. (c) Powder X-ray diffraction patterns of (**1**): (red) experimental and (black) simulated on the baisi of the single crystal structure.

4.2 - [BpA]$_2$·[CBTCH$_4$] (2). In (**2**) each carboxylic function is linked *via* neutral hydrogen bonds [O···N = 2.624(7) Å] to a BpA nitrogen atom, resulting in chains formed by an alternation of two BpE and one CBTCH$_4$ molecule, see figure 3. P-XRD on ground crystals of (**2**), confirms that the bulk material obtained *via* slow evaporation of the dimethysulfoxyde solution corresponds to (**2**), see figure 3.

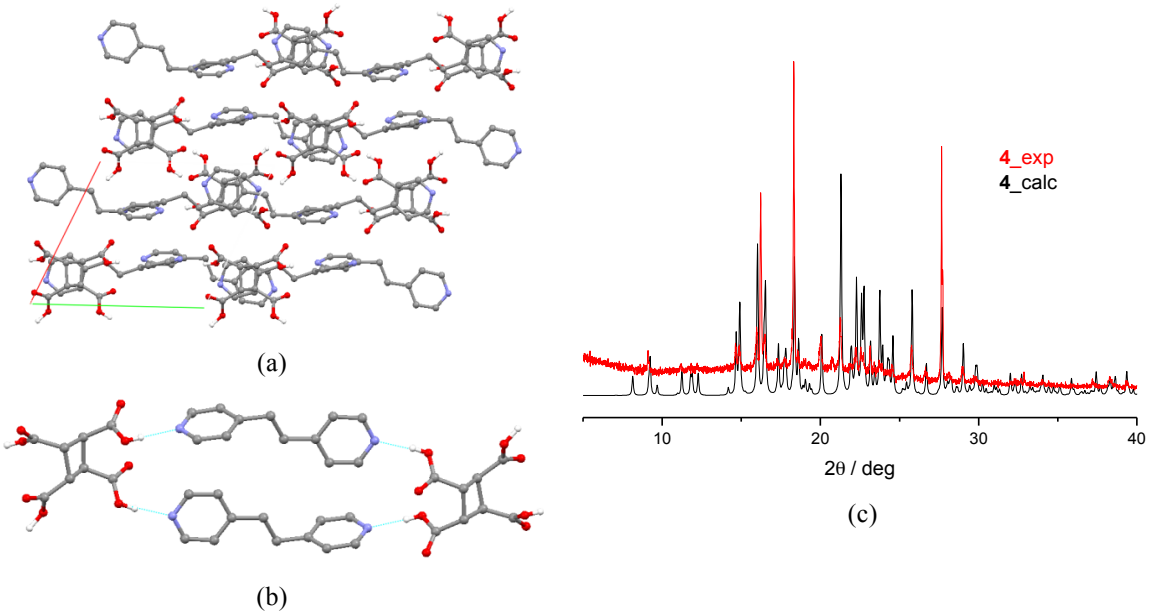

(a)

(b)

(c)

Fig. 3. (a) Crystal packing of (**2**) viewed along the *c*-axis and (b) supramolecular polymer held by hydrogen bonds; H_{CH} atoms omitted for clarity. (c) Powder X-ray diffraction patterns of (**2**): experimental (red-line) and simulated from single crystal structure (black-line).

4.3 - [BPyaH$_2$]·[CBTCH$_2$]·2H$_2$O (3). Crystal structure of (**3**) is notably different compared to those of (**1**) and (**2**). First of all, (**3**) is a hydrated salt, secondly it is characterized by the presence of layers in which the $[CBTCH_2]^{2-}$ anions interact with water molecules in order to form a 2D network parallel to the *ab*-plane [$O_{OH}\cdots O_w$ = 2.604(9) Å; $O^-\cdots O_w$ = 2.772(8) Å]. These planes are connected via charge assisted hydrogen bonds between the $[BPyeH_2]^{2+}$ and $[CBTCH_2]^{2-}$ units [$N\cdots O^-$ = 2.618(4) Å].

P-XRD confirms that the bulk material obtained *via* crystallization from ethanol-water (1:1) solution corresponds to **3** (figure 4).

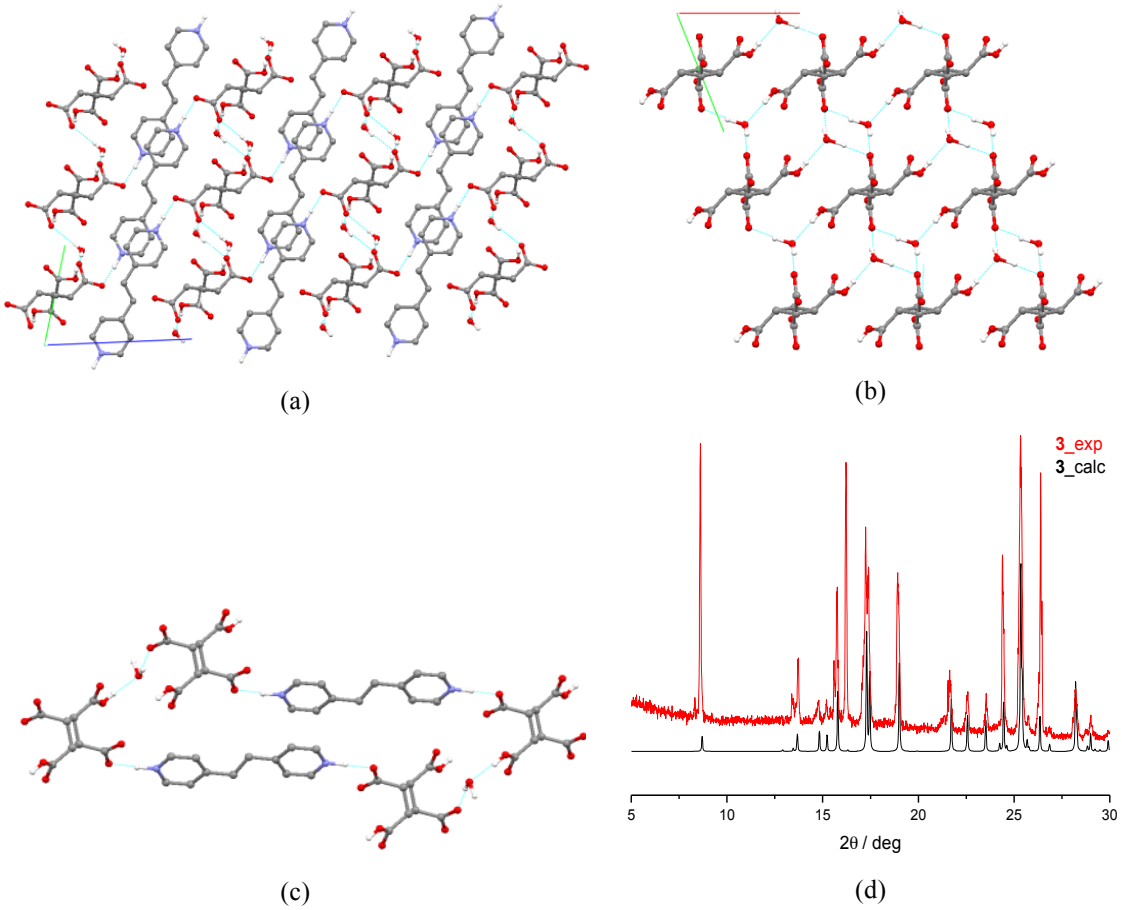

Fig.4. (a) Crystal packing of (**3**) viewed along the *a*-axis, (b) 2-D hydrogen bonding network formed by water molecules and anions in crystalline (**3**) and (c) hydrogen bonding interactions between anions and cations in crystalline (**3**); H_{CH} atoms omitted for clarity. (d) Powder X-ray diffraction patterns of (**3**): experimental (red-line) and simulated from single crystal structure (black-line).

TGA measurements indicate a weight loss of ~ 8 % (36.17 g mol^{-1}) in the range 90-150°C that corresponds to 2 moles of water molecules (35.98 g mol^{-1}); at ca. 200°C a degradation process occurs; the DSC trace on heating (1st cycle) shows a single endothermic peak (onset

at 94.5 °C, peak at 104.3°C and ΔH = 212.2 J g^{-1}); this is the same water evaporation process observed in TGA, see figure 5.

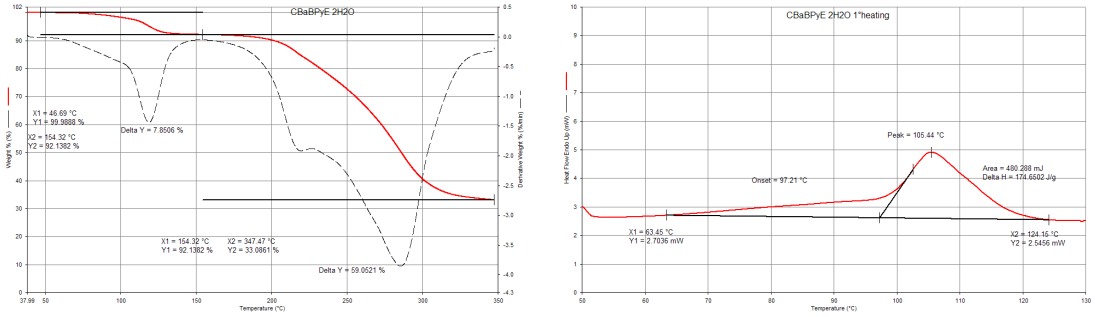

(a) (b)

Fig.5. (a) TGA and (b) DSC traces for the salt (**3**).

Variable temperature PXRD were particularly useful to follow the dehydration process; heating a polycrystalline sample of (**3**) at 135°C yields a new phase ((**3**)_anhydrous) that does not revert when the sample is cooled to 25°C (also after mechanical mixing and standing in air), see figure 6.

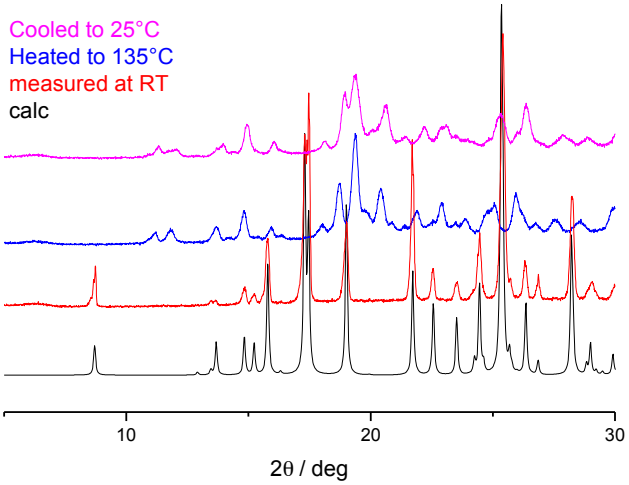

Fig.6. VTPXRD patterns for (**3**): calculated on the basis of single-crystal structure (black-line), experimental at RT (red-line), recorded after heating at 135°C (blue line) and after cooling at 25°C (magenta line).

4.4. - [DABCOH$_2$]·[CBTCH$_2$] (4). Crystal structure of (**4**) is characterized by the presence of layers parallel to the *ab*-plane. The ionic moieties within each layer are held together by a net of charge-assisted hydrogen bonds between carboxylic and carboxylate groups from the $[CBTCH_2]^{2-}$ anions [$O_{OH}\cdots O^-$ = 2.55(2)1 Å] and between the carboxylate and the $[DABCOH_2]^{2+}$ units [$O^-\cdots N$ = 2.646(2) Å], see figure 7. No relevant interaction between layers is present. P-XRD confirms that the bulk material obtained via slow evaporation of the solution corresponds to (**4**).

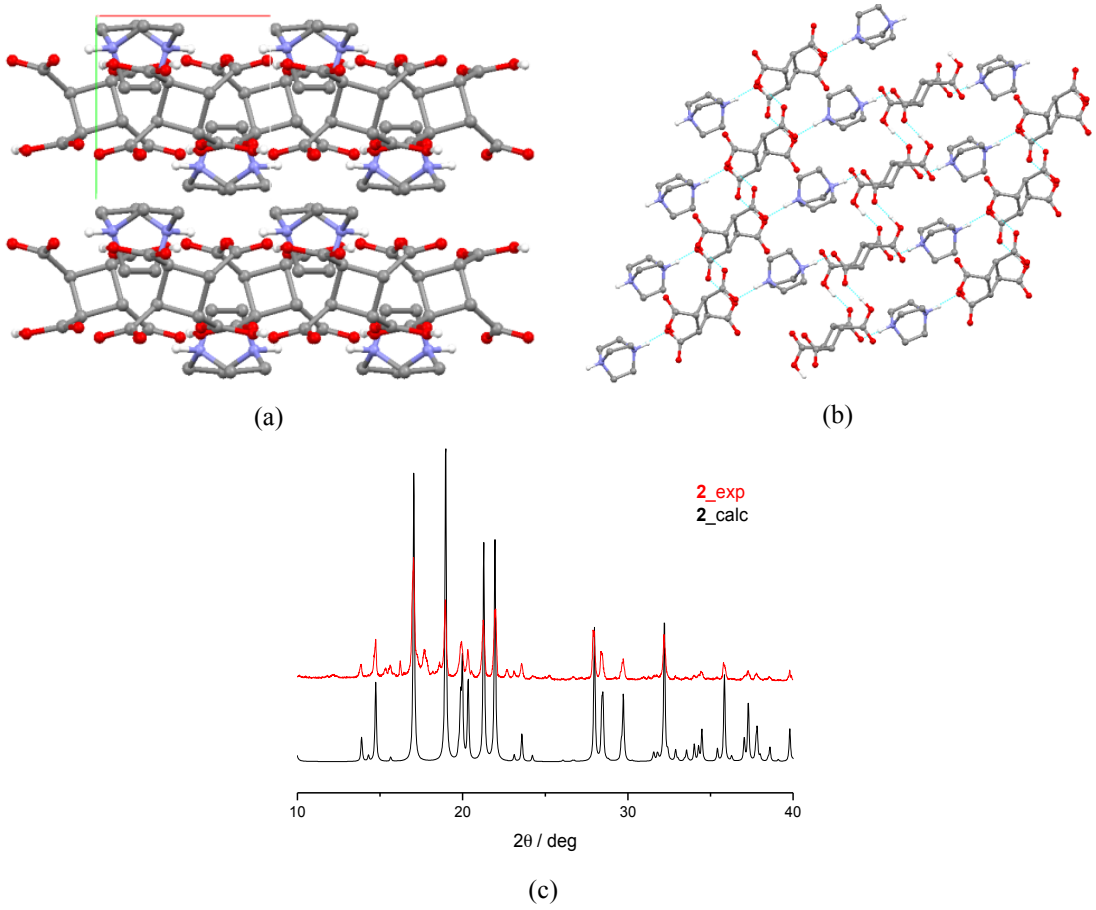

Fig. 7. (a) Crystal packing of (**4**) viewed down the *c*-axis and (b) 2-D hydrogen bonding network formed by cations and anions in crystalline (**4**); H_{CH} atoms omitted for clarity. (c) Powder X-ray diffraction patterns of (**4**): experimental (red-line) and simulated from single crystal structure (black-line).

After evaluation of the templating capability of the [$CBTCH_4$], we assumed that:

(i) a molecular salt of [BpE] with [$CBTCH_4$] would have similar supramolecular arrangements to the corresponding [BpA] and [DABCO] salts, thus yielding to photostable crystals.

(ii) a co-crystal of [BpE] with [$CBTCH_4$], would have similar supramolecular arrangements to the corresponding [Bpy] and [BpA] co-crystals; what is more, such co-crystal would be photoactive.

5 Synthesis and characterization of photoreactive crystalline materials

Depending on the nature of the solvent used for the crystallization experiments, it was be possible to get three different crystal phases for the couple [BpE]/[$CBTCH_4$]: the hydrated salts [$BpEH_2$]·[$CBTCH_2$]·$2H_2O$ (**5**), from ethanol/water 1:1 mixture; the co-crystal [$BpE]_2$·[$CBTCH_4$] (**6**) from dimethyl-formamide and the anhydrous salt [BpEH]·[$CBTCH_3$] (**7**) from ethanol; only the last two satisfy the topochemical postulate by Schimdt[7] and they are potentially photoreactive.

*5.1 [$BpEH_2$]·[$CBTCH_2$]·2H_2O (**5**)*. In (**5**), the $[CBTCH_2]^{2-}$ anions form hydrogen bonding interactions with the water molecules [$O^- \cdots O_W$ = 2.620(3); $O_{OH} \cdots O_W$ = 2.776(3) Å] in order to form a 2D network parallel to the *ab*-plane. These planes are connected via charge assisted hydrogen bonds between the $[BPyeH_2]^{2+}$ and $[CBTCH_2]^{2-}$ units [$N \cdots O^-$ = 2.618(4) Å]. The olefinic double bonds are at a separation distance of 6.072(5) Å that does not allow the photodimerization.

There is no match between the diffraction patterns recorded on the bulk material obtained and the calculated on the basis of crystal structure of (**5**), see figure 8.

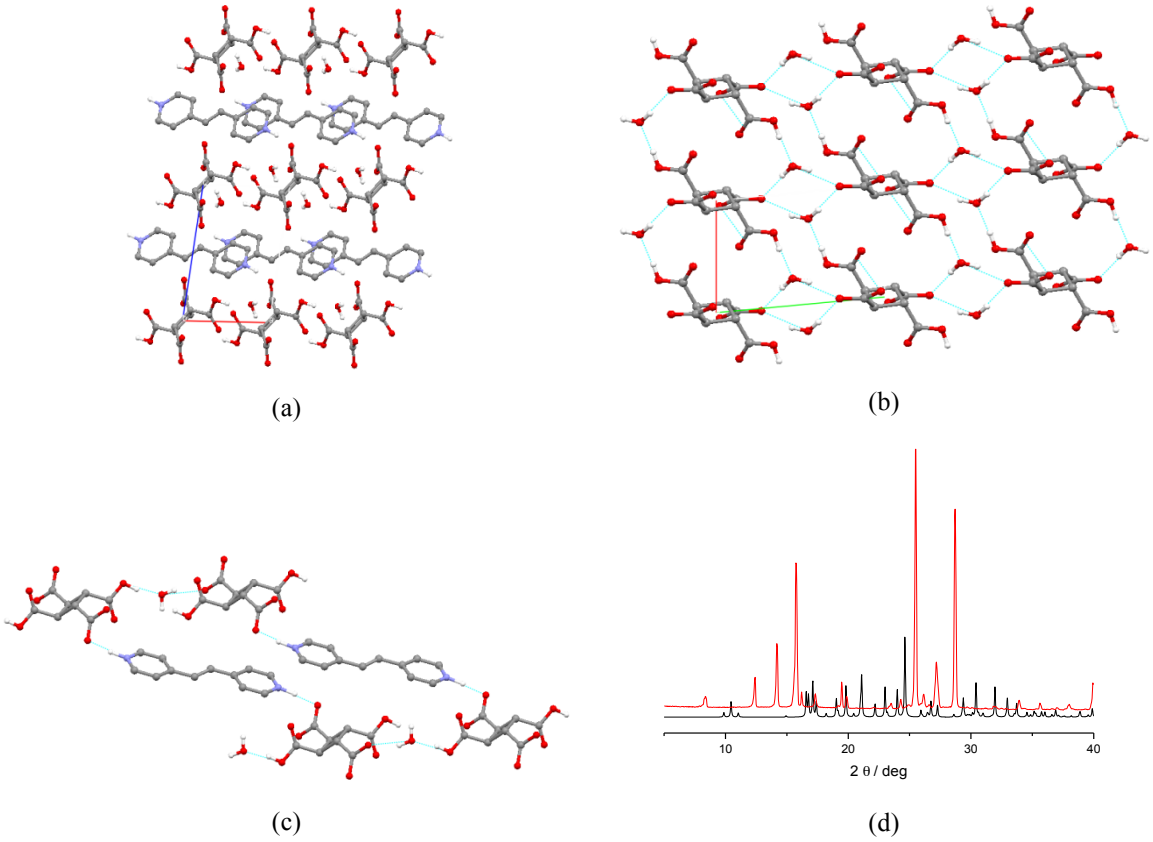

Fig.8. (a) Crystal packing of the hydrated salt [$BpEH_2$]·[$CBTCH_2$]·2H_2O (**5**) viewed along the *b*-axis, (b) 2-D hydrogen bonding network formed by water molecules and anions in crystalline (**5**) viewed down the *c*-axis and (c) detail showing the hydrogen bonding interactions between anions and cations in crystalline (**5**). H_{CH} atoms omitted for clarity.

*5.2 - [BpE]$_2$·[CBTCH$_4$] (**6**)*. As expected, the structure of the [Bpy]$_2$·[CBTCH$_4$] (**1**), [BpA]$_2$·[CBTCH$_4$] (**2**) and [BpE]$_2$·[CBTCH$_4$] (**6**) co-crystals are very similar. In solid **6**, therefore, the acid CBTCH$_4$ works as a linear template, namely there is a direct interaction between template and reactants, resulting in the formation of mono-dimensional supramolecular chains that contain the two olefins properly arranged to undergo the photoreaction (see figure 9).

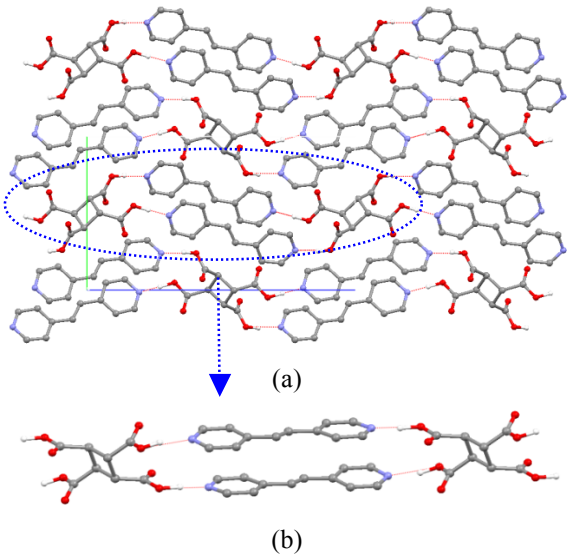

Fig.9. (a) Crystal packing of the co-crystal [BpE]$_2$·[CBTCH$_4$] (**6**) viewed along the *a*-axis;. (b) Detail showing the supramolecular polymer held by hydrogen bonds [$O_{OH}\cdots N$ = 2.655 (2) – 2.607(1) Å]. Note that the olefins are well aligned to undergo photodimerization (separation distance is 3.285(4) Å). H_{CH} omitted for clarity.

*5.3 - [BpEH]·[CBTCH$_3$] (**7**)*. In the salt (**7**) the acid, losing a proton, acts in a less common fashion, i.e. there is no direct interaction between the template and the reactant.

The crystalline structure of (**7**) consists in a 2D network of mono-deprotonated [CBTCH$_3$]$^-$ anions, interacting each other through charge assisted and neutral hydrogen bonds [$O^-\cdots O_{CO}$ = 2.544(4) Å and $O_{OH}\cdots O_{CO}$ = 2.606(4) Å]. These sheets are separated by chains of BpEH$^+$ held together by charge assisted hydrogen bonds between pyridine rings [$N\cdots N$ = 2.864(6) Å] (see figure 9). The chains are stacked in two different fashions with two separation distances of 6.060(2) Å and 3.767(1) Å, respectively, of which only the latter is expected to allow photodimerization. This kind of arrangement is quite uncommon in other related organic salts: a database analysis reveals that a similar type of motif exists only in another crystal structure.[21]

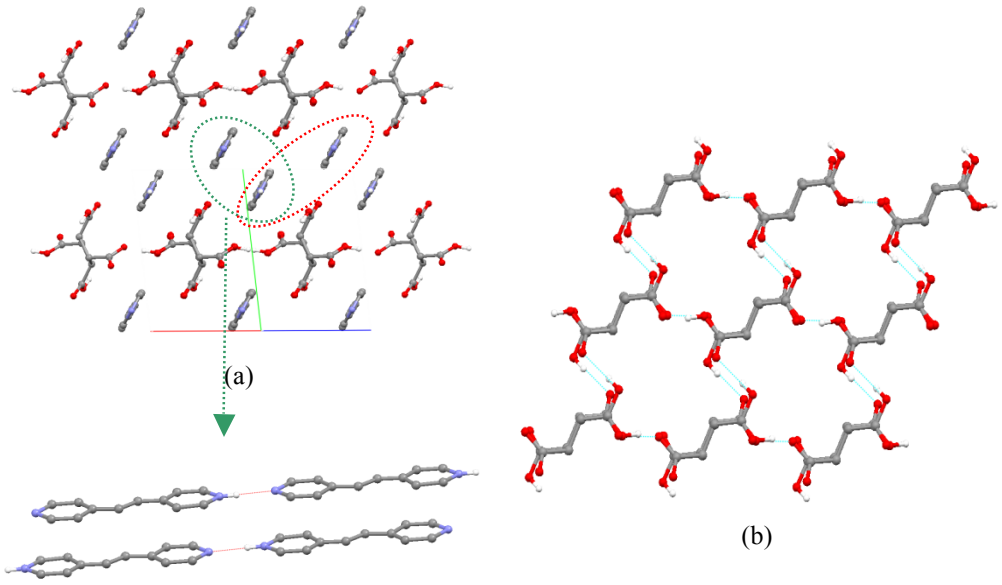

Fig.10. (a) Crystal packing of the anhydrous salt [BpEH]·[$CBTCH_3$] (**7**) viewed along the [-1 0 1] direction; note that the olefins are stacked in two fashions, the unfavourable arrangement (dotted red) and the favourable one to photodimerization (dotted green) *(rings are not in place in figure 10)*, (b) 2-D hydrogen bonding anionic-water network in crystalline viewed down the *c*-axis (**7**) and (c) Detail showing the hydrogen bond interactions present in the favourable stack of $BpEH^+$ chains. H_{CH} omitted for clarity.

As shown in figure 11, PXRD analysis of the ground crystals revealed that both crystalline (**6**) and (**7**) are consistent with the respective structures.

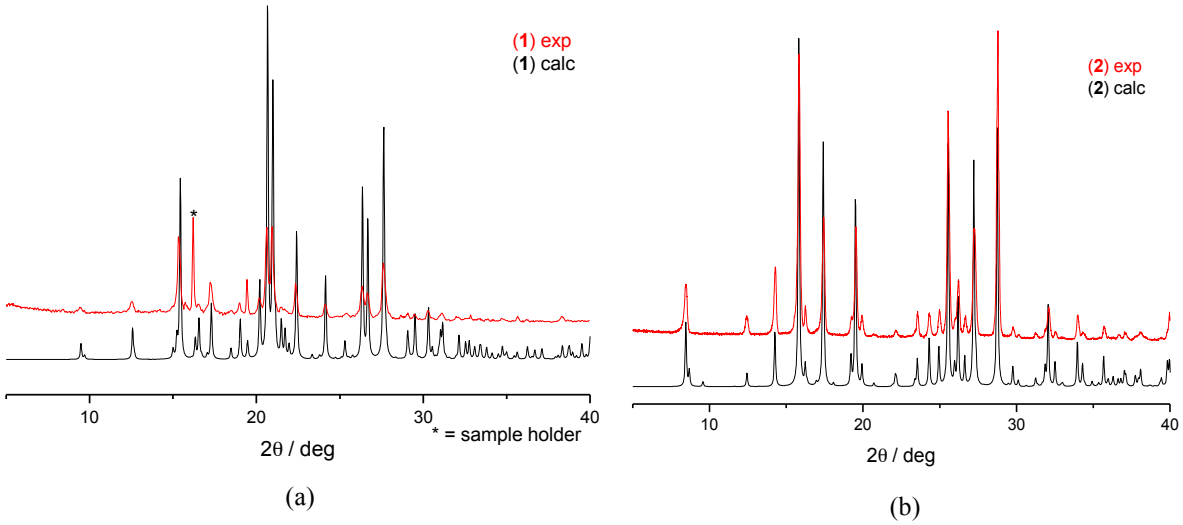

Fig.11. Comparison between the simulated (black) and experimental (red) powder diffraction patterns for (a) the co-crystal [$BpE]_2$·[$CBTCH_4$] (**6**) and (b) the salt [BpEH]·[$CBTCH_3$] (**7**).

6 Solid state photoreaction

6.1 - Irradiation experiments. Upon irradiation, single crystals and polycrystalline samples of (**6**) and (**7**) lose their crystallinity, because during irradiation each C-atom of the C=C bond of the olefin undergoes a change in position to form the cyclobutane ring. Such movement is invariably accompanied by the accumulation of strain and stress in the solid.[22] This accumulation can, and most often does, result in collapse of the single crystal lattice or amorphization.

6.2 - Identification of the product: rctt-tetrakis(4-pyridil)cyclobutane. As determined by ^{1}H-NMR analysis, irradiation of polycrystalline powders (**6**) and (**7**) result in the stereospecific formation of *rctt*-tetrakis(4-pyridyl)cyclobutane (tpcb). The identity of the photoproduct is confirmed by the emergence of cyclobutane protons at 4.6 ppm (singlet in DMSD-d_6), see figure 12.

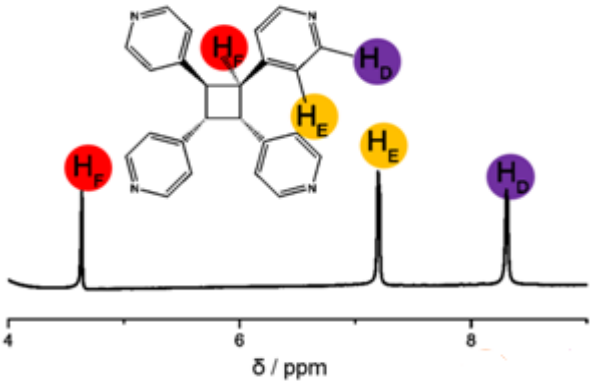

(a)

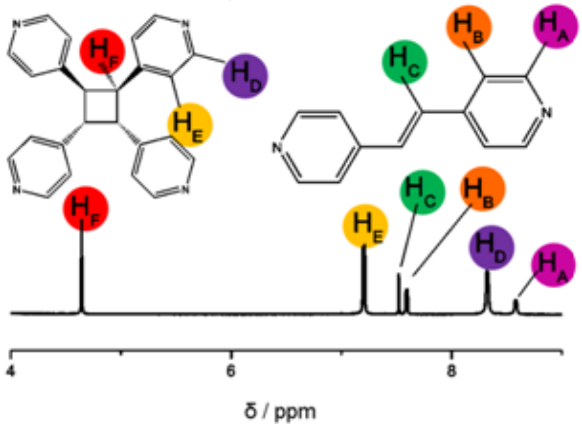

(b)

Fig.12. ^{1}H-NMR spectra in DMSD-d_6: (**a**) the co-crystal [BpE]·[$CBTCH_4$] (**6**) after irradiation for 24 h and (**b**) the salt [BpEH]·[$CBTCH_3$] (**7**) after irradiation for 72 h (**c**). For the latter the solid-state photoreaction reaches a steady state. Courtesy of Dr. M. Baroncini.

6.3 - Isolation of the rctt-tetrakis(4-pyridil)cyclobutane. The photoproduct *rctt*-tetrakis(4-pyridil)cyclobutane (tpcb) can be isolated *via* basic extraction (washing the irradiated solid with a saturated K_2CO_3 solution) and re-crystallized from acetone. Powder pattern of the ground crystals is in good agreement with the simulated pattern from the known crystal structure,[23] see figure 13.

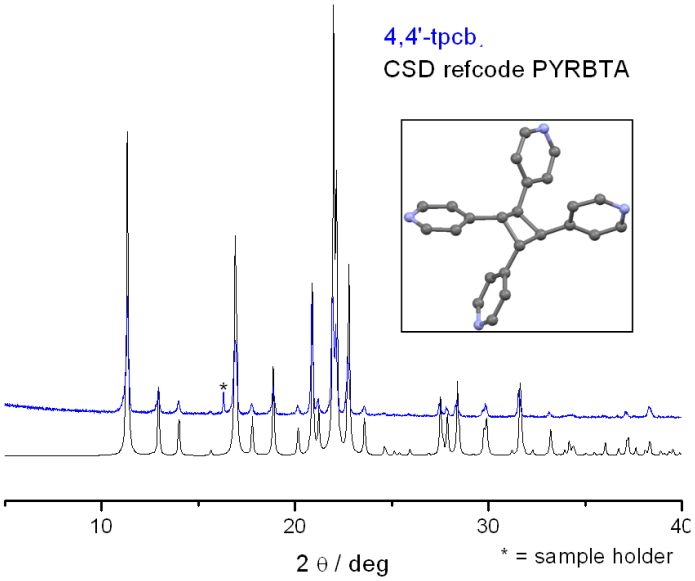

Fig.13. Powder X-ray diffraction patterns for the photoproduct tpcb: experimental (blue-line) and simulated from single crystal structure (black-line). Inset: molecular structure of crystalline 4,4'-tpcb reported in the literature (CSD refcode PYRBTA); H_{CH} atoms omitted for clarity.

7 Co-crystal of rctt-tetrakis(4-pyridil)cyclobutane. A porous hydrogen bonded network

*7.1 - [4,4'-tpcb][CBTCH$_4$]·EtOH (**8**)*. Re-crystallization of the photoproduct *rctt*-tetrakis(4-pyridil)cyclobutane (tpcb) together with the template affords the solvated co-crystal (**8**).

Th crystal structure of [4,4'-tpcb][CBTCH$_4$]·EtOH consists in a highly porous, 3D hydrogen bonded network [O···N = 2.583(8) – 2.591(3) Å] containing disordered solvent molecules (ethanol is disordered over two position) inside the mono-dimensional channels running parallel to the [1 0 0] direction, see figure 14. Channel opening is of *ca.* 7-9 Å and PLATON-squeeze calculations indicate a potentially accessible void volume of 573 Å^3 (30.8% of the unit cell volume of 1873.7 Å^3).

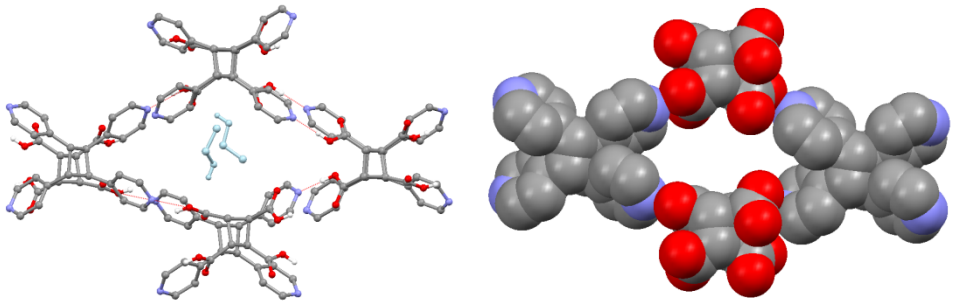

(a) (b)

Fig.14. Mono-dimensional channels present in crystalline [4,4'-tpcb][CBTCH$_4$]·EtOH, ethanol (pale blue) is disordered over two position (a) and space-filling representation showing the channel (b). H_{CH} omitted for clarity. View along the *a*-axis.

A TGA/FTIR measurement (figure 15) indicates that the stoichiometry is [4,4'-tpcb][CBTCH$_4$]·EtOH.

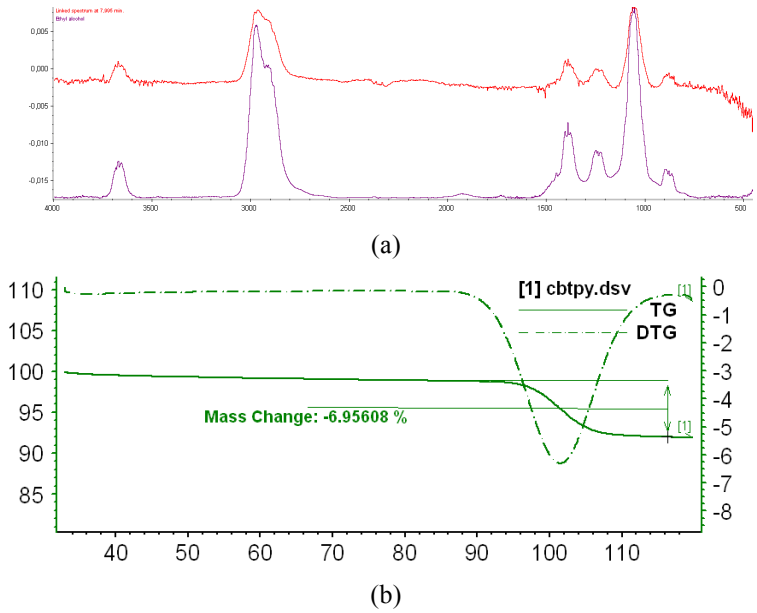

(a)

(b)

Fig.15. (**a**) FTIR spectra obtained from the gases evolved from TGA experiment (**b**) performed on [4,4'-tpcb][CBTCH$_4$]·EtOH .

As evidenced by a comparison between diffraction patterns (figure 16), ground crystals correspond to [4,4'-tpcb][CBTCH$_4$]·EtOH (**8**). Further grinding (*ca.* 10 minutes) produces changes in the powder pattern, probably due to formation of the de-solvated phase; this is in line with what observed upon TGA/FTIR measurement (figure 15) and can be confirmed by VT-PXRD experiments (figure 17) and hot-stage microscopy (figure 18). After kneading

with 2 drops of ethanol, this phase reverts to the original [4,4'-tpcb][$CBTCH_4$]·EtOH (**8**). Solvent removal-uptake, from crystal channels, triggers reversible structural transformations.

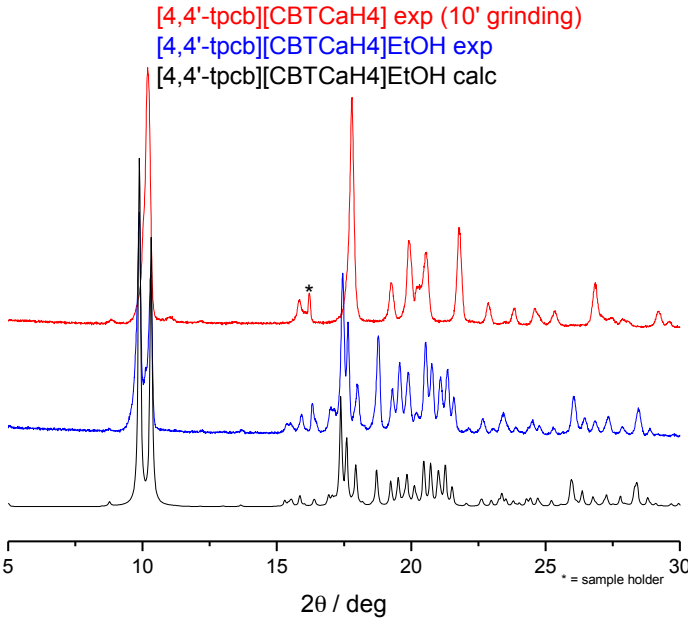

Fig.16. Comparison of experimental (blue) and simulated (black) patterns for [4,4'-tpcb][$CBTCH_4$]·EtOH (**8**). De-solvated phase (red) can be obtained from further grinding.

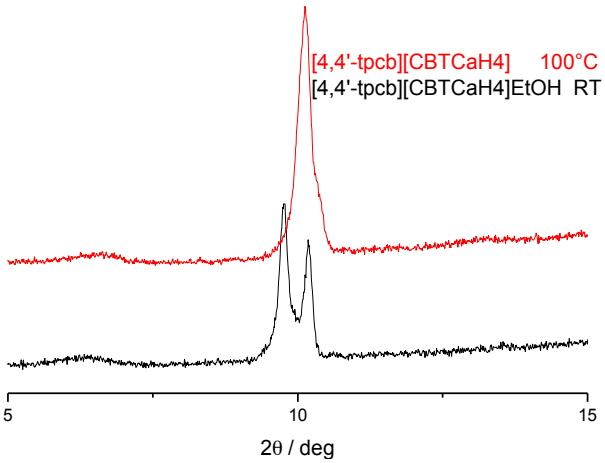

Fig.17. Detail of the VT-PXRD showing how crystalline [4,4'-tpcb][$CBTCH_4$]·EtOH (**8**) (black) converts to the de-solvated phase (red) upon heating from RT to 100°C.

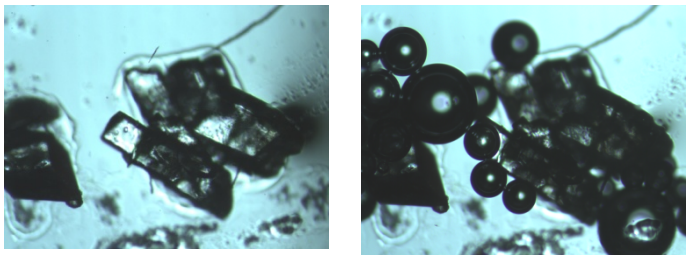

(**a**) (b)

Fig.18. Hot Stage Microscopy images taken on crystals of [4,4'-tpcb][$CBTCH_4$]·EtOH (**8**), on heating from RT (a) to 105°C (b): note the formation of bubbles at high temperature, due to solvent (ethanol) extrusion from the crystalline channels.

8 Conclusions

Crystalline materials containing the tetra-carboxyllic acid [$CBTCH_4$] and a series of organic bases have been synthesized and characterized, this gave us the following co-crystals and salts: [$Bpy]_2$·[$CBTCH_4$] (**1**), [$BpA]_2$·[$CBTCH_4$] (**2**), [$BpAH_2$]·[$CBTCH_2$]·$2H_2O$ (**3**) and [$DABCOH_2$]·[$CBTCH_2$] (**4**), their structural analysis allowed to rationalize how the hydrogen bond motifs vary depending on the shape of the base and how they affect the arrangemnet of the base within the crystal packing. After evaluation of the ability of [$CBTCH_4$] as a templating unit, crystalline materials containing the reactant [BpE] have been obtained. In the molecular hydrated salt [$BpEH_2$]·[$CBTCH_2$]·$2H_2O$ (**5**) olefins are misaligned, leading to a photostable material. In the co-crystal [$BpE]_2$·[$CBTCH_4$] (**6**), on the contrary, [$CBTCH_4$] acts effectively as a linear template, organizing the dinitrogen bases in a π-stacked fashion via hydrogen bonds, thus forming mono-dimensional supramolecular networks; in the salt [BpEH]·[$CBTCH_3$] (**7**) the monodeprotonated acid form hydrogen bonding interactions only with the other anions, leaving the monoprotonated $BpEH^+$ cations to self-assemble in pairs of infinite rows in the solid. In both last cases the preorganization of two BpE molecules for solid-state cycloaddition leads exclusively to *rctt*-tetrakis(4-pyridyl)cyclobutane. In the co-crystal (**6**) the photoreaction is nearly quantitative, while in the molecular salt (**7**) a steady-state is reached, probably due to positional disorder of the stacked $BpEH^+$ cationic chains. Further the photoproduct *rctt*-tetrakis(4-pyridil)cyclobutane (tpcb) together with the template [$CBTCH_4$[can be used to synthesize the porous crystalline material [4,4'-tpcb][$CBTCH_4$]·EtOH (**8**) that shows reversible release-uptake of solvent molecules.

Experimental section

Starting materials: 1,2,3,4-cyclobutane-tetra-carboxylic acid [$CBTCH_4$], 4-4'-bipyridine [Bpy], 1,2-Bis(4-pyridyl)ethane [BpA], 1,4-diazabiclyclo[2.2.2.]octane [DABCO] and *trans*-1,2-Bis(4-pyridyl)ethylene [BpE] were purchased from Sigma-Aldrich and used without further purification with exception of [BpE] that was purified prior to use,[24] all solvents from Sigma-Aldrich and used without further purification.

Table 1 summarizes chemical information on the compounds described in this study.

(**1**) $[Bpy]_2 \cdot [CBTCH_4]$. 4-4'-bipyridine (43.0 mg, 0.28 mmol) and 1,2,3,4-tetracarboxylic-cyclobutane acid (31.1mg, 0.14 mmol) were mixed in a stoichiometric ratio 2:1 and boiled in ethanol (*ca.* 8mL); colourless crystals (prisms) grew from the resulting solution in *ca.* 2 days.

(**2**) $[BpA]_2 \cdot [CBTCH_4]$. 1,2-Bis(4-pyridyl)ethane (24.5 mg, 0.133 mmol) and 1,2,3,4-cyclobutanetetracarboxylic acid (0.0309g, 0.133 mmol) were mixed and boiled in ethanol/water (*ca.* 8 mL); colourless crystals (needles) grew from the resulting solution in *ca.* half-day.

(**3**) $[BpAH_2] \cdot [CBTCH_2] \cdot 2H_2O$. 1,2-Bis(4-pyridyl)ethane (71.7 mg, 0.39 mmol) and 1,2,3,4-cyclobutanetetracarboxylic acid (45.2 mg, 0.39 mmol) were mixed and boiled in *ca.* 8 mL dimethylsulfoxyde; colourless crystals (prisms) grew from the solution after 3 weeks.

(**4**) $[DABCOH_2] \cdot [CBTCH_2]$. 1,2,3,4-cyclobutanetetracarboxylic acid (27 mg, 0.12 mmol) and 1,4-diazabiclyclo[2.2.2.]octane (13 mg, 0.116 mmol) were mixed and boiled in ethanol / water (1 : 1) *ca.* 8 mL until a clear solution was obtained; colourless crystals (prisms) grew by slow evaporation in few days.

(**5**) $[BpEH_2] \cdot [CBTCH_2] \cdot 2H_2O$. 1,2-Bis(4-pyridyl)ethylene (18.9 g, 0.104 mmol) and 1,2,3,4-cyclobutanetetracarboxylic acid (24.2 g, 0.104 mmol) were mixed and boiled for few minutes in ethanol / water (1:1) *ca.* 8 mL; colourless crystals (small needles) grew from the resulting solution in few days.

(**6**) $[BpE]_2 \cdot [CBTCH_4]$: 1,2-Bis(4-pyridyl)ethylene (19.2 mg; 0.11 mmol)and 1,2,3,4-tetracarboxylic-cyclobutane (24.1 mg; 0.10 mmol) were dissolved in *ca.* 8 mL of dimethylformamide and boiled for few minutes. Single crystals (blocks) of (**1**) were obtained by slow evaporation at RT.

(**7**) $[BpEH] \cdot [CBTCH_3]$: Bis(4-pyridyl)ethylene (19.8 mg; 0.11 mmol) and 1,2,3,4-tetracarboxylic-cyclobutane (25.0 mg; 0.11 mmol) 1,2- were suspended in *ca.* 8 mL of ethanol and heated up to reach a clear solution. Single crystals (needles) of (**2**) grew when the resulting solution was left to cool RT.

(**8**) [BpEH]·[$CBTCH_3$]: Bis(4-pyridyl)ethylene (39.8 mg; 0.11 mmol) and 1,2,3,4-tetracarboxylic-cyclobutane (25.2 mg; 0.11 mmol) 1,2- were suspended in *ca.* 8 mL of ethanol and heated up to reach a clear solution. Single crystals (needles) of (**8**) grew when the resulting solution was left to cool RT.

Table 1. Chemical information about the compounds part of this study.

$[Bpy]_2$·[$CBTCH_4$]	**1**	co-crystal
$[BpA]_2$·[$CBTCH_4$]	**2**	co-crystal
[$BpAH_2$]·[$CBTCH_2$]·$2H_2O$	**3**	salt
[$DABCOH_2$]·[$CBTCH_2$]	**4**	salt
[$BpAH_2$]·[$CBTCH_2$]·$2H_2O$	**5**	salt
$[BpE]_2$·[$CBTCH_4$]	**6**	co-crystal
[BpEH]·[$CBTCH_3$]	**7**	Salt
[4,4'-tpcb][$CBTCH_4$]·EtOH	**8**	co-crystal

Single-crystal data for compounds (**1**), (**2**), (**3**), (**4**), (**5**), (**6**), (**7**) and (**8**) were collected on an Oxford X'Calibur S CCD diffractometer equipped with a graphite monochromator (Mo-Kα radiation, λ = 0.71073Å) and operating at room temperature. Data collection and refinement details are listed in Table 2.

All non-hydrogen atoms were refined anisotropically; H_{OH} atoms were either directly located or, when possible, added in calculated positions; H_{CH} atoms for all compounds were added in calculated positions and refined riding on their respective carbon atoms. SHELX97[25a] was used for structure solution and refinement on F^2, PLATON[25b] and Mercury25[c] were used for hydrogen bonding analysis and molecular graphics, respectively.

Powder data were collected on a Philips X'Pert automated diffractometer with Cu-Kα radiation. The program PowderCell[25d] was used for calculation of X-ray powder patterns on the basis of single crystal data. The identity between the bulk materials obtained and the structures obtained by single crystals was verified by comparing calculated and observed powder diffraction patterns.

Thermogravimetric analysis (TGA) were performed with a Perkin-Elmer TGA-7. Each sample, contained in a platinum crucible, was heated in a nitrogen flow (20 cm^3 min^{-1}) at a rate of 5°C min^{-1}, up to decomposition. Samples weights were in the range 5–10 mg.

Differential scanning calorimetry (DSC) Calorimetric measurements were performed with a Perkin-Elmer DSC-7 equipped with a PII intracooler. Temperature and enthalpy calibrations

were performed using high-purity standards (n-decane, benzene and indium). Heating of the aluminium open pans containing the samples (3–5 mg) was carried out at 5°C min^{-1} in the temperature range 40–300 °C.

Ca. 400 mg of co-crystal (**6**) or salt (**7**) were finely ground and distributed in a thin layer on an agate mortar and irradiated at 365 nm using a UV-handlamp (*Vilber Lourmat*, VL-4.LC). Small portions of irradiated solid were taken out at interval of 24 hours for ^{1}H-NMR analysis. In order to reach fast conversion, crystalline powders were gently re-mixed every 2 hours.

Hot Stage experiments were carried out using a Linkam TMS94 device connected to a Linkam LTS350 platinum plate. Images were collected with the imaging software Cell, from an Olympus BX41 stereomicroscope.

^{1}H-NMR spectra were recorded on a Varian Mercury400, chemical shifts of ^{1}H-NMR signals were expressed in part per million (δ_H) using internal standard TMS (δ_H = 0.00). DMSO-d_6 bought from Cambridge Isotope Lab.

Table 2a. Crystal data and structures refinements for compounds (**1**)-(**4**).

	1	**2**	**3**	**4**
Formula	$C_{28}H_{24}N_4O_8$	$C_{32}H_{32}O_8N_4$	$C_{20}H_{24}N_2O_{10}$	$C_{14}H_{20}N_2O8$
fw	544.51	600.61	452.41	344.32
a (Å)	12.0032(1)	10.7205(1)	7.1418(8)	6.3207(3)
b (Å)	17.1249(1)	12.2741(1)	7.6788(9)	6.3733(4)
c (Å)	13.1443(1)	12.7037(1)	10.5822(9)	18.1531(9)
α (deg)	90	79.037(9)	73.720(9)	90
β (deg)	111.529(1)	88.207(1)	81.906(8)	98.261(4)
γ (deg)	90	64.414(12)	67.038(1)	90
V ($Å^3$)	2513.4(3)	1477.7(3)	512.60(9)	723.69(7)
Z	4	2	2	4
D_{calc} (Mg/m^3)	1.365	1.350	1.466	1.580
μ (mm^{-1})	0.101	0.098	0.119	0.131
Cryst. System	Monoclinic	Triclinic	Triclinic	Monoclinic
Space group	$P2_1/n$	P-1	P-1	P2/n
n° of collected reflns	10271	9785	4154	2988
n° of indep. reflns	5294	5811	2295	1617
R1[on F_0^2, I>2sigma(I)]	0.0517	0.1053	0.0454	0.0462
wR2 (all data)	0.1120	0.3013	0.1132	0.1125

Table 2b. Crystal data and structures refinements for compounds (**5**)-(**8**).

	5	**6**	**7**	**8**
Formula	$C_{20}H_{22}O_{10}N_2$	$C_{32}H_{28}N_4O_8$	$C_{20}H_{18}N_2O_8$	$C_{34}H_{34}N_4O_9$
fw	450.39	596.19	414,37	642,66
a (Å)	6.0716(6)	7.0584(4)	12.1830(4)	10.4956(9)
b (Å)	9.4102(11)	10.8433(6)	7.9320(5)	11.1647(8)
c (Å)	10.0122(12)	18.2878(10)	11.3062(1)	18.1760(16)
α (deg)	64.523(12)	90	86.206(2)	86.743(7)
β (deg)	78.80(1)	94.893(5)	68.453(3)	76.427(7)
γ (deg)	80.197(9)	90	64.399(2)	64.585(8)
V ($Å^3$)	504.146(3)	1394.58(4)	910.53(7)	1867.68
Z	2	4	2	2
D_{calc} (Mg/m^3)	1.424	1.421	1.511	1.481
μ (mm^{-1})	0.114	0.104	0.119	0.116
Cryst. System	Triclinic	Monoclinic	Triclinic	Triclinic
Space group	P-1	P21/c	P-1	P-1
n° of collected reflns	3402	14623	12781	15943
n° of indep. reflns	2082	3300	4168	8493
R1[on F_0^2, I>2sigma(I)]	0.067	0.0386	0.0911	0.1387
wR2 (all data)	0.148	0.0902	0.3101	0.4378

References

[1] R.B. Woodward, Roald Hoffmann, *J. Am. Chem. Soc.*; 1965; **87**(2); 395-397.

[2] M. B. Smith and J. March in *March's Advanced Organic Chemistry: Reactions, Mechanisms and Structure*, 2007, Wiley, Hoboken, NJ.

[3] (a) G. Kaupp, *Top. Curr. Chem.*, 2005, **254**, 95–183 (b) K. Tanaka and F. Toda, *Chem. Rev.*, 2000, **100**, 1025–1074.

[4] (a) C. N. Riiber, *Chem. Ber.*, 1902, **35**, 2411–2415 (b) C. N. Riiber, *Chem. Ber.*, 1913, **46**, 335–338.

[5] K. Osaki, G. M. J. Schmidt, *Isr. J. Chem.*, 1972, 10, 189-193.

[6] G. M. J. Schmidt, *Pure App. Chem.*, 1986, 647-678.

[7) H. Nakanishi, W. jones, J. M. Thomas, *Chem. Phys. Lett.*, 1980, **71**, 44-48.

[8] (a) Macgillivray, cap 19, pp355-362 in *Strength From Weakness: Structural Consequences of Weak Interactions in Molecules, Supermolecules and Crystals,* edited by A. Domenicano and I. Hargittai (b) S. Anderson, H. L. Anderson, In *Templated Organic Synthesis*; Diederich, F.; Stang, P. J., Eds.: Wiley-VCH: New York, pp. 1–38, 2000.

[9] G.W. Coates, A. R. Dunn, L.M. Henling, J.W. Ziller, E.B. Lobkovsky and R.H. Grubbs, *J. Am. Chem. Soc.*, 1998, 120, 3641-3649.

[10] (a) C. V. K. Sharma, K. Panneerselvam, L. Shimoni, H. Katz, H. L. Carrell, G. R. Desiraju, *Chem. Mater.* 1994, **6**, 1282-1292 (b) Y. Maekawa, S. Kato and M. Hasegawa, *J. Am. Chem. Soc.,* 1991, **113***,* 3867-3872.

[11] K. S. Feldman and R. F. Campbell, *J. Org. Chem.* 1995, **60**, 1924–1925.

[12] (a) T. J. Brett, J. M. Alexander, J. L. Clark, C. R. Ross Gerard, S. Harbison and J. J. Stezowski, *Chem. Commun.*, 1999, 1275–1276. (b) K. Tanaka, F. Toda, E. Mochizuki, N. Yasui, Y. Kai, I. Miyahara and K. Hirotsu, *Angew. Chem. Int. Ed.*, 1999, **38**, 23.

[13] (a) L. R. MacGillivray, J. L. Reed and J. A. Reepmeester, *J. Am. Chem. Soc.*, 2000, **122**, 7817 (b) L. R. MacGillivray, G. S. Papaefstathiou, T. Friscic, T. D. Hamilton, D. K. Bucar, Q. Chu, D. B. Varshney and I. G. Georgiev, *Acc. Chem. Res.*, 2008, **41**, 280–291, and references therein; (c) L. R. MacGillivray, *J. Org. Chem.*, 2008, **73**, 3311–3317 (d) L. R. MacGillivray, G. S. Papaefstathiou, T. Friscic, D. B. Varshney and T. D. Hamilton, *Top. Curr. Chem.*, 2005, **248**, 201–221 (e) X. Gao, T. Friscic, L. R. MacGillivray, *Angew. Chem. Int. Ed.* 2004, **43***,* 232-236 (f) G. S. Papaefstathiou, A. J. Kipp, L. R. MacGillivray, *Chem. Commun.*, 2001, 2462-2463.

[14] (a) N. L. Toh, M. Nagarathinam and J. J. Vittal, *Angew. Chem., Int. Ed.*, 2005, **44**, 2237–2241 (b) I. G. Georgiev and L. R. MacGillivray, *Chem. Soc. Rev.*, 2007, **36**, 1239–1248 (c) A. Ajamian and J. L. Gleason, *Angew. Chem.*, Int. Ed., 2004, **43**, 3754–3760 (d) P. G. Cozzi, *Chem. Soc. Rev.*, 2004, **33**, 410–421; (e) B. C. G. Soderberg, Coord. *Chem. Rev.*, 2004, **248**, 1085–1158; (f) J. J. Becker and M. R. Gagne, *Acc. Chem. Res.*, 2004, **37**, 798–804. (g) R. Robson, *Inorg. Nucl. Chem. Lett.*, 1970, **6**, 125–128; (h) H. Okawa, *Bull. Chem. Soc. Jpn.*, 1970, **43**, 3019–3021. (j) D. Visinescu, M. Andruh, A. Muller, M. Schmidtmann and Y. Journaux, *Inorg. Chem. Commun.*, 2002, **5**, 42–45; (k) M. Pascu, M. Andruh, A. Muller and M. Schmidtmann, *Polyhedron*, 2004, **23**, 673–678. (i) G. S. Papaefstathiou, Z. Zhong, L. Geng and L. R. MacGillivray, *J. Am. Chem. Soc.*, 2004, **126**, 9158–9159.

[15] T. Caronna, R. Liantonio, T. A. Logothetis, P. Metrangolo, T. Pilati and G. Resnati, *J. Am. Chem. Soc.*, 2004, **126**, 4500–4501.

[16] M. Nagarathinam, A. Malik, P. Peedikakkal and J. Vittal, *Chem. Commun.*, 2008, 5277–5288 and references cited therein.

[17] D.Braga, O.Benedi, L.Maini, F.Grepioni, Private Communication at CSD, 2003.

[18] (a) Gautam R. Desiraju, *Angew. Chem., Int. Ed.*, 1995, **34**, 17 (b) A. Nangia and G. R. Desiraju,*Topics in Current Chemistry*, 1998, **198**, 57-95.

[19] J. Xiao, M. Yang, J. W. Lauher and F. W. Fowler, *Angew.Chem*., *Int*. *Ed*. 2000, **39**, 2132–2135 (b) N. Shan and W. Jones, *Tetrahedron Letters, 2003,* **44**, 3687–3689.

[20] CCDC, The Cambridge Structural Database, *ConQuest* 1.13, Cambridge, UK, 2011.

[21] Naito N. T., Inabe T., Bull Chemical Soc Jpn, 2003, 76, 3, 1351-1362, CCSD refcode BAYBIN.

[22] (a) T. Frišcic and L. R. MacGillivray, *Z. Kristallogr.*, 2005, **220**, 351–363 (b) G. J. Halder and C. J. Kepert, *Aust. J. Chem.*, 2006, **59**, 597–604.

[23] J. Vansant, S. tropet, G. Smeets, J. P. Declercq, G. Germain and M. van Meerssche, *J. Org. Chem.*, 1980, **45**, 1656-1573, CCSD refcode PYRBTA.

[24] Yellow powder, mp 148-153C. Recrystallization from a ethanol-water (1:1) gives a white powder, mp 151-152°C, lit 152°C.

[25] (a) G. M. Sheldrick, SHELX97, *Program for Crystal Structure Determination*; University of Gottingen: Gottingen, Germany, 1997. (b) A. L. Speck, PLATON; *Acta Crystallogr., Sect. A*, 1990, 46, C34; (c) C. F. Macrae, I. J. Bruno, J. A. Chisholm, P. R. Edgington, P. McCabe, E. Pidcock, L. Rodriguez-Monge, R. Taylor, J. van de Streek and P.

A. Wood, *J. Appl. Cryst.*, 2008, **41**, 466-470 (d) PowderCell programmed by W. Kraus and G. Nolze (BAM Berlin) subgroups derived by Ulrich Muller (Gh Kassel).

Chapter 4 - Design of Low Molecular Weight Gelators and Metallogelators

1 Introduction

Gels (from the latin *gelu* — freezing, cold, ice or *gelatus* — frozen, immobile) are a class of materials consisting of a solid three-dimensional network that spans the volume of a liquid medium and ensnares it through surface tension effects. Gels are defined as a substantially diluted cross-linked system, which exhibits no flow when in the steady-state.[1]

Both by weight and volume gels are mostly fluid in composition and thus exhibit densities similar to those of their constituent liquids.

Gels have become commonplace in everyday life.[2] Supramolecular gels are those held together by non covalent interactions such as hydrogen bonds and metal-ligand interactions. As pointed out by Flory already in 1974[3] and recalled by Dastidar in his recent review[4] "gels are materials that are easier to recognize than to define". Crystallization of a gelator compound is not an easy job, especially when crystallization takes place from the very gelling solvent. The examples available in the literature are very few, in particular when small coordination compounds are involved.[5] Steed, Clarke and coworkers have very recently published an exhaustive review on metal- and anion-binding supramolecular gels.[6] Of particular interest are supergelator systems, because they are effective in gel formation at very low concentration, i.e. below 1% w/v).[2]

Gels find applications in almost all areas of materials chemistry,[7] and are nowadays been approached with the objective of finding materials suitable for crystallization of new crystal phases.[8] The quest for new crystal forms of molecular species has come to the forefront of solid state chemistry investigations because of the number of potential applications of the different physico-chemical properties of different crystal forms of a same species (polymorphs, co-crystals, hydrates, solvates, salts etc.).[8, 9]

1.1 Classification of gels

Gels can be classified in different ways based upon their origin constitution, type of cross-linking and medium (scheme 1).[10]

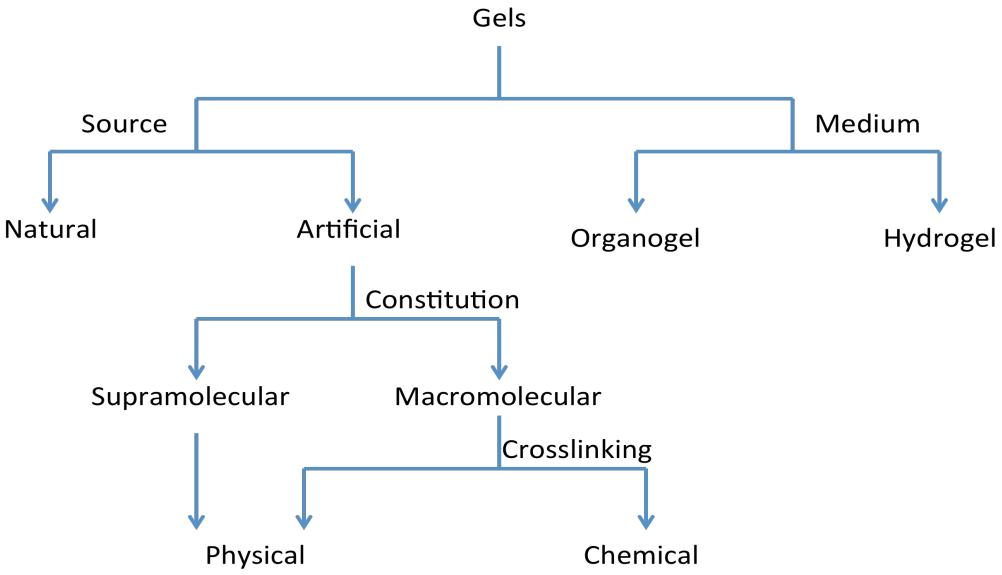

Scheme 1. Classification of gels. Gels can be organized according to multiple characteristics: source of the gel (natural/artificial), gel medium (organic/aqueous/aero/xero), constitution of the gel (macromolecular/supramolecular), and type of crosslinking (physical/chemical).

Depending upon source, gels can be classified into natural gels and artificial or synthetic gels. Gels derived from synthetic compounds can be subdivided into macromolecular (polymer) and molecular gels based on their constitution.

Macromolecular gels can be formed either by chemical cross-linking or physical interactions. When gels are formed by strong chemical bonds, they cannot be redissolved and their formation is thermally irreversible, whereas gels formed by weak noncovalent interactions (physical interaction) can be converted back to sols, i.e. their formation is reversible. Depending upon the solvents, gels can be classified into organogels and hydrogels. If the gel is formed with organic solvents it is called organogel, if it is formed with water it is called hydrogel. Depending upon the drying process, xerogels or aerogels can be obtained. Materials in which the typical pore structure and network are largely maintained when the pure liquid of a gel is replaced by air are called *aerogels*. Aerogels are highly porous solid materials with extremely low densities, open pores, and high specific surface areas. These result in interesting physical properties, such as extremely low thermal conductivity and low sound velocity, combined with high optical transparency. A *xerogel* is formed by

conventional drying of wet gels, i.e. by increasing the temperature or decreasing the pressure with concomitant large shrinkage (and eventually collapse) of the initially uniform gel body. Shrinkage upon drying of a wet gel body is showed in scheme 2.

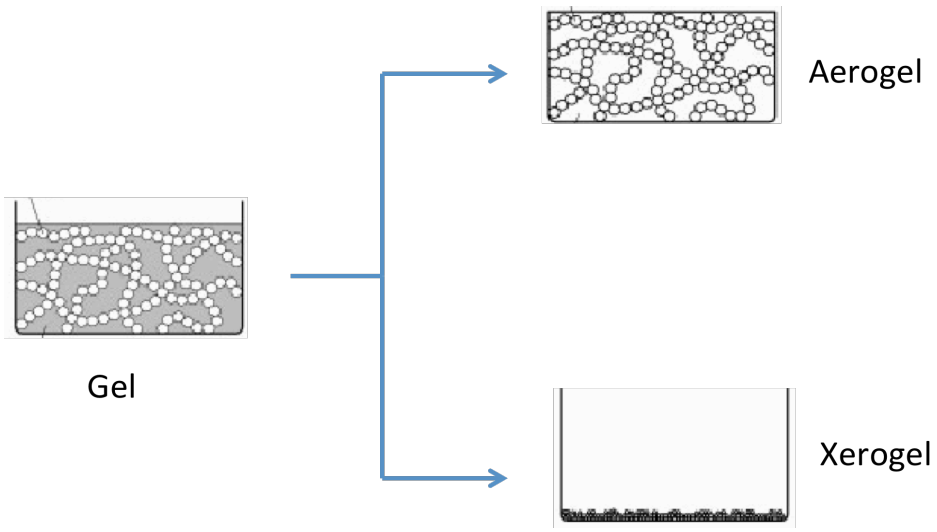

Scheme 2. Shrinkage upon drying of a wet gel to give an aerogel and a xerogel.

Organogels have in common with other gel systems that the gelling agent forms a continuous three- dimensional entangled network in the solvent, thereby preventing the flow of liquid. Gels derived from low molecular mass compounds are called supramolecular gels. Although the formation of organogels from small organic molecules is an excellent example of supramolecular self-assembly process, most organogelators have been found serendipitously rather than by design, and many aspects of organogels are still poorly understood. In recent years *low molecular mass gelators* (LMWGs) have attracted considerable interest due to molecules of great structural diversity. Their discovery and development are particularly important, as potential applications can be envisaged in almost all areas of materials chemistry.[7]

1.2 Low Molecular Weight Gelators (LMWGs) and Metallo Gelators (MGs)

A subclass of materials able to form physical gels is represented by Low Molecular Weight Gelators (LMWGs), also referred as Low Molecular-Mass Organic Gelators (LMOGs).

LMWGs consist of organic compounds; generally they can be defined as chemical species with a molecular weight of less than 2000 Da, which show gelation behavior in organic and/or aqueous solvents. In one-component systems a compound can be present in solution and at the same time it can form a gel with the solvent, whereas in true two-component

systems an individual component can be present in an isotropic solution, and only on addition of the second component a gel actually forms. In the case of one-component systems, gelator molecules interact with each other to form gel networks via non covalent interactions, such as π- π stacking, hydrogen bonding, van der Waals interaction etc., whereas, in the case of two-component gelators, one compound forms a complex with a different compound through donor-acceptor interaction, hydrogen bonding interaction, etc. If one of the two components is a metal salt these systems can be defined as Metallo Gelators (MGs).

1.3 Gelation mechanism and formation of supramolecular gels

The formation of gels from small organic molecules or complexes is an excellent example of a hierarchical supramolecular self-assembly process.[2,7] The aggregation of gelator molecules is driven by multiple, weak interactions such as hydrogen bonding interactions, π- π stacking, metal coordination,[2] van der Waals interactions.[2] The phenomenon of gelation is presumably due to formation of nano- to micrometer-sized fibers becoming entangled and trapping solvent via surface tension.

To understand the mechanism of gel formation, a gel can be broken down into a primary, secondary, and tertiary structure, much like a protein (Figure 1).[11,12]

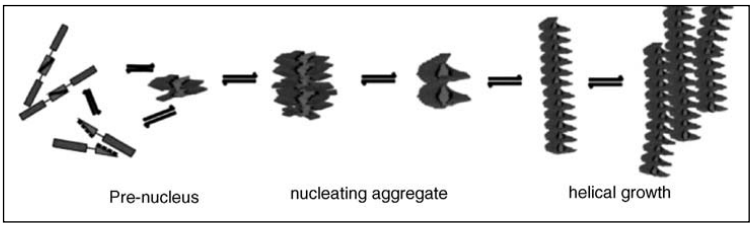

(a)

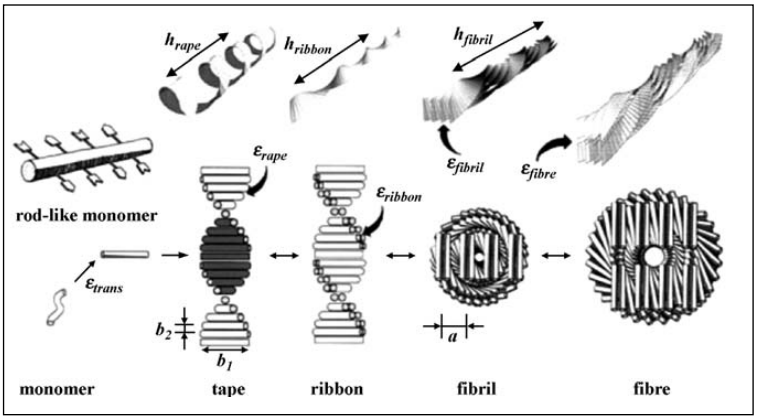

(b)

Fig.1. Hierarchical self-assembly process of gel-phase materials. As illustrated for synthetic systems developed by (a) Meijer's group[13] and (b) Aggeli and coworkers.[14]

The primary structure (angstrom to nanometer scale) is determined by the molecular level recognition events that promote anisotropic aggregation in one or two dimensions of the gelator molecules. Assembly of small organic molecules in solvents into fibrous structures poses interesting challenges in the fields of molecular recognition and self-assembly. To achieve gelation, there must be a balance between the tendency of the molecules to dissolve and to aggregate.

The secondary structure (nano- to micrometer scale) is defined as the morphology of the aggregates, that is micelles, vesicles, fibers, ribbons or sheets, and is directly influenced by the molecular structure. The transition from molecular to primary and secondary structure has been explained by several methods.[12] Boden and co-workers have modeled the hierarchical self-assembly of rod-like chiral molecules, such as peptides in a β-strand conformation, into ribbons and fibers.[14]

Finally, the tertiary structure of a gel (micro- to millimeter scale) involves the interaction of individual aggregates and ultimately determines whether a gel is formed or, instead, fibers (or other aggregates) precipitate from solution rather than trapping it. Transition from secondary to tertiary structure is determined by the type of interactions at work among the fibers. The type of cross-linking often determines the rheological properties of the gel.

Gels derived from small molecules are usually prepared by heating the compounds in the appropriate solvent and cooling the resulting saturated solution to room temperature. When the hot solution is cooled, molecules start to condense and three are the possible outcomes: (i) a highly ordered aggregation giving rise to crystals, (ii) a random aggregation resulting in an amorphous precipitate and (iii) an aggregation process intermediate between these two that gives rise to a gel.

There is clearly a relationship between gelation and crystallization, as in both cases a solid-like component assembles in a liquid-like phase as a consequence of multiple noncovalent interactions. However, in gelation, the solid-like network remains solvated and hence does not fully phase separate. As such, gelation can be considered to be a compromise between solubilization and phase separation. Furthermore, in a gelation process – unlike in crystallization – aggregation usually occurs in three dimensions; in gels the growth of the supramolecular polymer is usually one dimensional.

Perhaps one of the key advantages of this kind of materials is their reversibility. Upon an appropriate stimulus, molecular gels undergo a gel-to-sol transition, due to disruption of the supramolecular interactions that hold the gel-structure together; the solutions revert to the gel

state upon cooling; thus making the whole hierarchical self-assembly process completely reversible.

For example, raising the temperature has a profound effect on the assembly process, due to the entropic term ($\Delta G = \Delta H - T\Delta S$), and promotes disassembly of the gel into the less ordered sol-state.[2]

Molecular gel formation is also concentration dependent; at low concentration the interaction between molecules is unable to yield supramolecular polymers. The critical gelation concentration (CGC) is the lowest possible gelator concentration needed to form a stable gel. Typically, molecular gels contain <2% w/v gelator. Molecules which achieve gelation at concentrations <1% w/v are sometimes described as *supergelators*.[2]

There are two simple parameters which are widely used to define and explore the gel–sol phase boundary (i.e. the conversion of the material from a gel to a sol and *vice versa*) macroscopic properties of molecular gels:

(1) *Critical gelation concentration* or (CGC) – the minimum concentration of gelator required to form a sample-spanning self-supporting gel at a given temperature (usually RT).

(2) *Gel–sol transition temperature* (T_{gel}) – the gel-sol transition temperature is the required temperature below which the flow of the gel no longer is discernible over long periods.

1.4 Design of LMWGs

Gelation processes are highly dependent on the choice of solvent. For the purposes of this discussion we broadly classify gels as either organogels or hydrogels, where organogels form in organic solvents, whereas hydrogels form in water or aqueous solvents. The driving forces for gelation in these two classes of solvent are markedly different, as will be discussed below. The design of a gelator from first principles is a difficult and challenging task. More often than not, gelators are discovered serendipitously. However, there is now sufficient literature available to suggest the following broad guidelines about whether or not a molecule may be expected to gelate:

1. The molecule must be partly soluble in the solvent of choice (but not too much, otherwise it will dissolve).
2. The molecule must be partly insoluble in the solvent of choice (but not too insoluble otherwise it will precipitate).
3. The molecule must have the potential to form multiple noncovalent interactions with itself. Typically, although not exclusively, these might be hydrogen bonds and/or π–π interactions for organogels and hydrophobic and/or donor–acceptor interactions for hydrogels.
4. Van der Waals interactions are usually present to support the gelation process and, in very rare cases, gelation can occur solely through these very weak interactions.
5. These noncovalent interactions should should be directional (a degree of asymmetry is often advantageous).

Both the amide and urea groups possess a hydrogen bond donor (N—H) and a hydrogen bond acceptor (C=O), therefore they are good candidates for the formation of intermolecular hydrogen bonded networks.[15] Amide and urea groups are used frequently to introduce hydrogen bonding interactions and create LMWGs.[16]

2 Synthesis and characterization of molecules with potential behavior of LMWGs or MGs

The aim of this work is the synthesis of a set of molecules (see scheme 3) which might behave, potentially at least, as Low Molecular Weight Gelators (LMWGs) or Metallo Gelators (MGs).[2] This is done by keeping in mind that the design of a gelator from first principles is a difficult and challenging task and, more often than not, gelators are discovered serendipitously.

Commons featuresto this set of molecules, which makes them good candidates for the formation of metal complexes with transition metal cations, are as follows: (i) they are low weight molecules, (ii)

they possess di-substituted urea groups capable of forming hydrogen bond interactions with themselves and other species (anions and/or solvent molecules) and (iii) they possess at least a nitrogen atom in an accessible position.

The synthesis of this class of compounds is quite simple and relies on the formation of di-substituted urea starting from the reaction between an aril-isocyanate and a primary amine (either aromatic or aliphatic).[20] All compounds were characterized by single-crystal X-ray diffraction (see experimental section table 1a and 1b for crystallographic details).

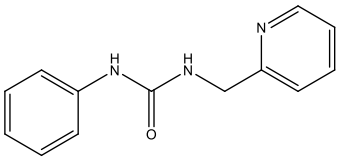

(a) [PPmU]

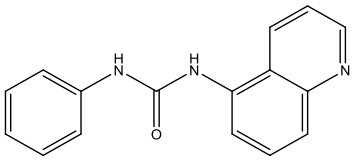

(b) [PQ5U]

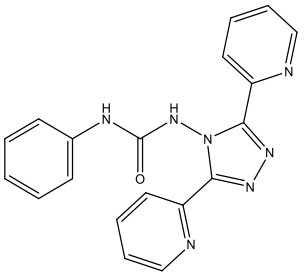

(c) [PDDPTU]

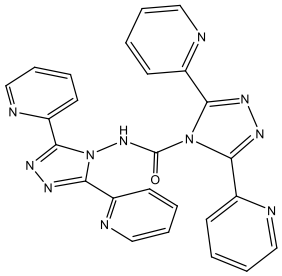

(d) [DDDPTU]

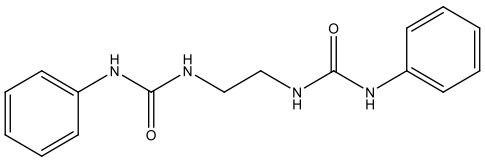

(e) [UEBP]

Scheme 3. Molecular structure of the synthesized set of compounds: (a) 1-phenyl-3-(pyridin-2-ylmethyl)urea [PPmU], (b) 1-phenyl-3-(quinolin-5-yl)urea [PQ5U] (c) 1-phenyl-3-(3,5-di(pyridin-2-yl)-4H-1,2,4-triazol-4-yl)urea [PDDPTU], (d) di-3-(3,5-di(pyridin-2-yl)-4H-1,2,4-triazol-4-yl)urea [DDDPTU] and (e) Urea, N,N''-1,2-ethanediylbis(N'-phenyl-) [UEBP].

2.1 - 1-phenyl-3-(pyridin-2-ylmethyl)urea [PPmU]. Compound [PPmU] crystallizes in the orthorhombic space group $Pca2_1$ with four molecules in the asymmetric unit (Z' = 4). The structure features the common urea-urea interaction that leads to formation of the well known urea tape motif (or urea head-to-tail tape), $R_2^1(6)$ in graph set notation;[18] see figure 2, the bifurcated N-H···O [N···O = 2.875(9) - 2.969(9) Å] impose an infinite strand-like structure to the molecule and no other supramolecular interactions are present in the crystal structure.

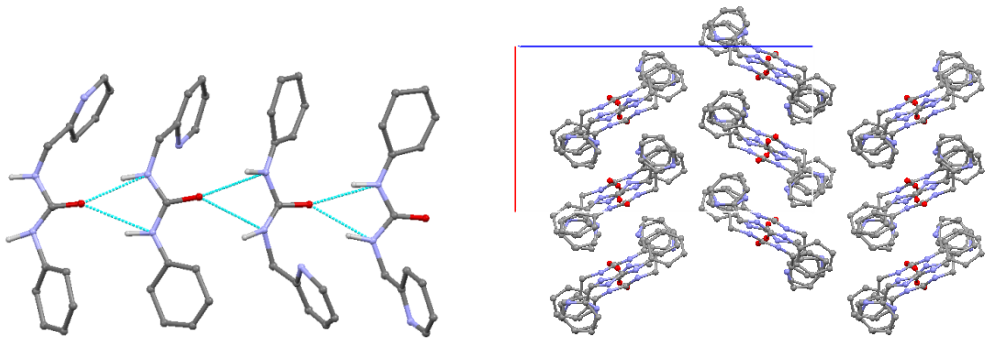

(a) (b)

Fig.2. (a) Urea tape motif present in the crystal structure of PPmU and (b) crystal packing of PPmU viewed along the *b*-axis. H_{CH} omitted for clarity.

2.2 - 1-phenyl-3-(quinolin-5-yl)urea [PQ5U].[17] Compound [PQ5U] crystallizes in the monoclinic space group Pc with one molecule in the asymmetric unit (Z' = 1). The structure features the common urea–urea interaction that leads to the formation of a urea tape motif, as shown in figure 3. The bifurcated hydrogen bondings are the only weak interactions present between molecules [N···O = 2.814(2) - 2.930(1) Å]. These interactions are responsible for the infinite strand-like crystal structure. A comparison between the XRPD pattern measured on complex PQ5U and that simulated on the basis of the single crystal structure confirms the exact nature of the polycrystalline sample (see figure 4).

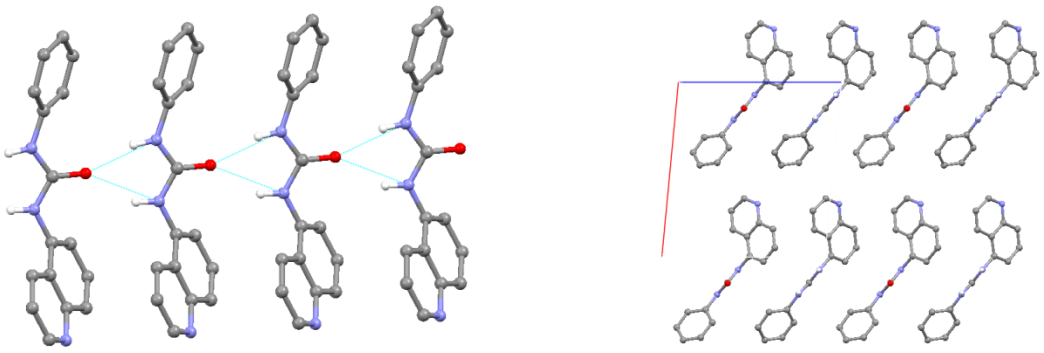

(a) (b)

Fig.3. (a) Urea tape motif present in the crystal structure of PQ5U and (b) crystal packing of PQ5U viewed along the *b*-axis. H_{CH} omitted for clarity.

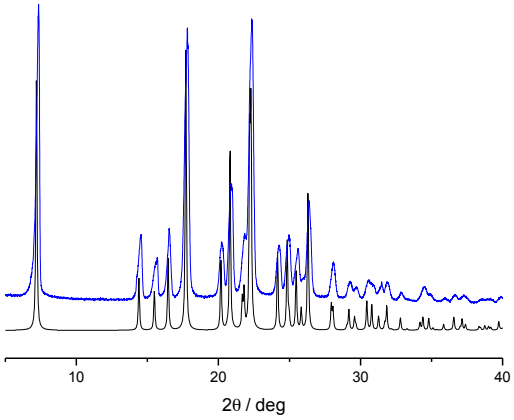

Fig.4. Comparison between the experimental XRPD obtained from polycrystalline PQ5U (blue-line) and that calculated on the basis of single-crystal data (black-line).

2.3 - 1-phenyl-3-(3,5-di(pyridin-2-yl)-4H-1,2,4-triazol-4-yl)urea [PDDPTU]. For this compound re-crystallization from hot methanol affords needle-shaped crystals that slowly convert to block-shaped crystals if left soaking in the mother liquor (figure 5). The respective crystal structures have been determined and identified as two different polymorphs denoted as form I and form II, respectively.

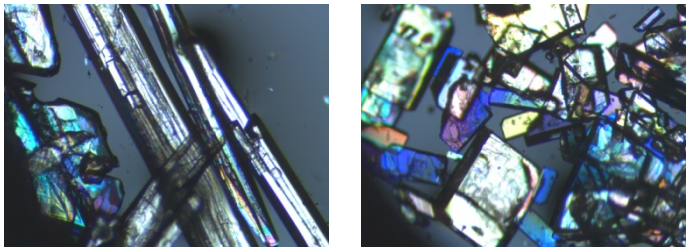

(a) (b)

Fig.5. Pictures taken on crystals of PDDPTU: (a) before (form I) and (b) after conversion to form II.

Polymorph I crystallizes in the monoclinic space group $P2_1/c$ with one molecule in the asymmetric unit (Z' = 1). Unlike the previously described compounds, the structure does not contain the common urea tape motif, because of the steric hindrance of the 3,5-di-pyridyl-4H-1,2,4-triazole moiety.
Molecules form an infinite supramolecular chain in which the units are held together by hydrogen bonding interactions between the urea and the nitrogen atoms from the bulky group 3,5-di-pyridyl-4H-1,2,4-triazole, resulting in a $R_2^2(9)$ motif in graph set notation[18] [N···N = 2.968(2)-3.011(2) Å], an extra (weak) π-stacking interaction between triazole and pyridine rings belonging to symmetry related molecules (centoid···centroid = 3.703(1) Å; centroid···plane = 3.350(3) – 3.511(8) Å), see figure 6.

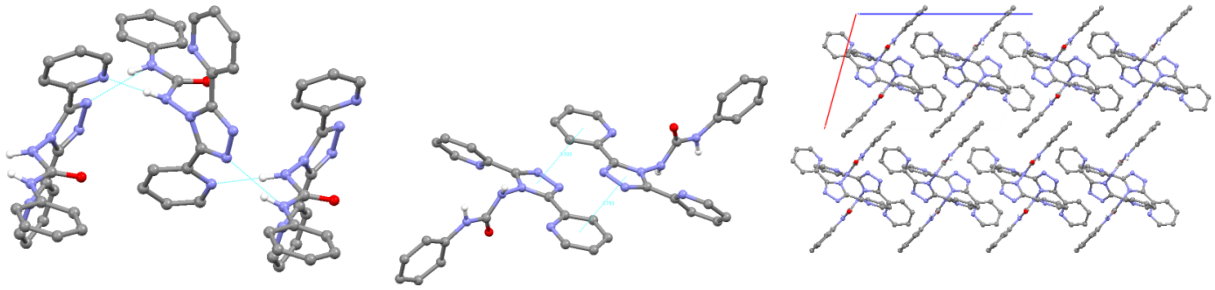

(a) (b) (c)

Fig.6. (a) The $R_2^2(9)$ motif present in crystal structure of PDDPTU (b) the weak π-stacking interaction between pyridine and triazole rings in I and (c) crystal packing of PDDPTU viewed down the *b*-axis. H_{CH} omitted for clarity.

A comparison between the XRPD patterns measured on polycrystalline sample of PDDPTU form I and that simulated on the basis of the single crystal structure confirm the exact nature of the polycrystalline sample (see figure 7).

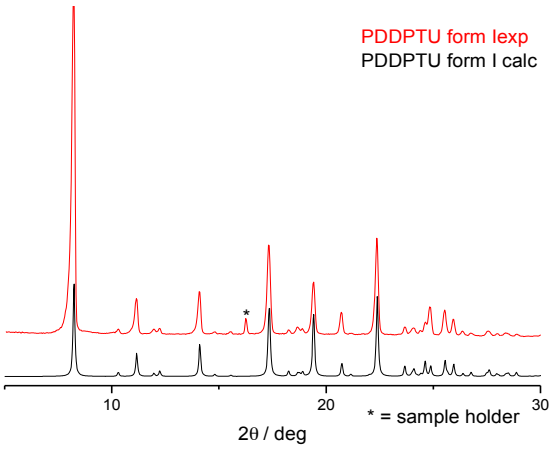

Fig.7. Comparison between the experimental XRPD obtained from polycrystalline PDDPTU (red-line) and that calculated on the basis of the single-crystal structure (black-line).

Polymorph II crystallizes in the monoclinic space group $P2_1$ with only one molecule in the asymmetric unit (Z' = 1). Crystal packing consists of infinite chains formed by intermolecular hydrogen bonding interactions between the urea group and the 3,5-di-pyridyl-4H-1,2,4-triazole moiety from a symmetry related molecule to give, even in this case, the $R_2^2(9)$ motif, [N···N = 3.150(4) - 2.992(5) Å], see figure 8.

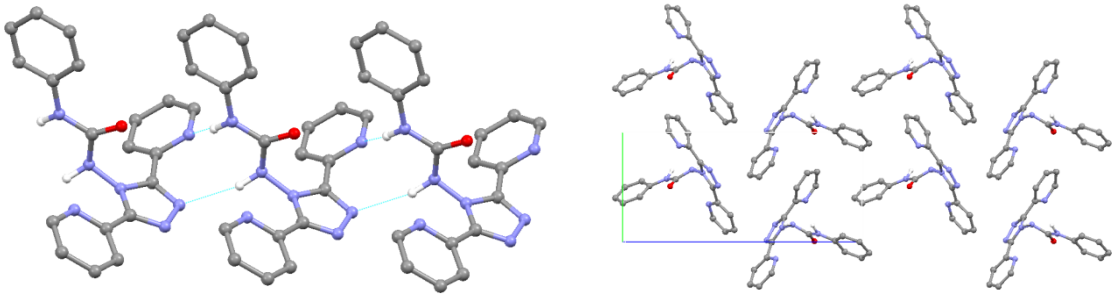

(a) (b)

Fig.8. (a) The $R_2^2(9)$ motif present in crystalline PDDPTU form II and (b) crystal packing of PDDPTU viewed down the *a*-axis. H_{CH} omitted for clarity.

A comparison between the XRPD patterns measured on a polycrystalline sample of PDDPTU form II and that simulated on the basis of the single crystal structure confirm the exact nature of the polycrystalline sample (see figure 9).

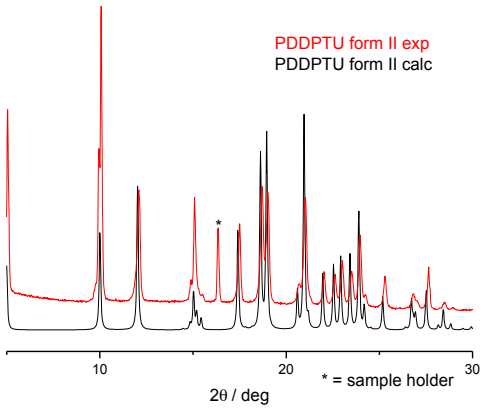

Fig.9. Comparison between the experimental XRPD obtained from polycrystalline PDDPTU form II (red-line) and that calculated on the basis of the single-crystal structure (black-line).

Crystalline PDDPTU form I and form II show very similar molecular conformations. As it can be seen in figure 10 the main difference is due to the phenyl-urea "tail". In form I and II the phenyl rings are almost coplanar with the urea group (torsion angle are between 3.80°-4.55° and 9.94°- 10.60° for form I and II, respectively), the bulky 3,5-di-pyridyl-4H-1,2,4-triazole moiety show larger dihedral angle with the urea (torsion angle are 121.26° and 132.96° for form I and II, respectively).

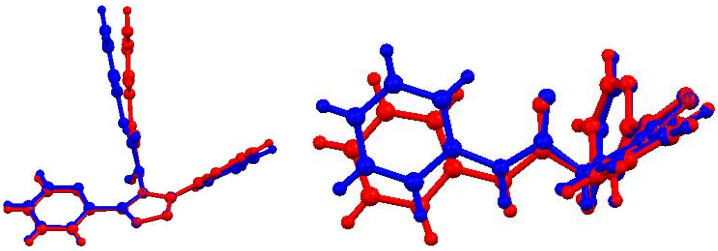

Fig.10. The conformations of two polymorphs (form I in red and form II in blue) are compared, with the two triazole ring superimposed. The main difference in conformation is in the orientation of the phenyl-urea tail.

Small amounts of solid were dissolved (boiling if necessary) in various solvents, filtered and left to re-crystallize. Polycrystalline material or single-crystals, when obtained, were subjected to SC and PXRD analysis. Results are summarized in table 2. Re-crystallization from hot acetonitrile results in a mixture of the two phases, although the crystal habit is that of form I (colourless needles).

Table1. Polymorph screening for compound PDDPTU.

Solvent	**SC-XRD**	**P-XRD**
Methanol	Form I + Form II (week-end)	Form II
Acetone	Form II	Form II
Acetonitrile	Form I	Form I + Form II [a]
Chloroform	Form II	Form II
Dichloromethane [b]	amorphous phase	Form I
p-Xylene	insoluble (RT/HT)	
Water	insoluble (RT/HT)	

a = See conversion via kneading (mechano-chemical conversion); b = as synthesized.

Form I and form II undergo a degradation process when heated at temperatures above ~ 200°C. The DSC trace on heating, in the range 40-190°C, does not show any process for both crystal forms, see figure 11.

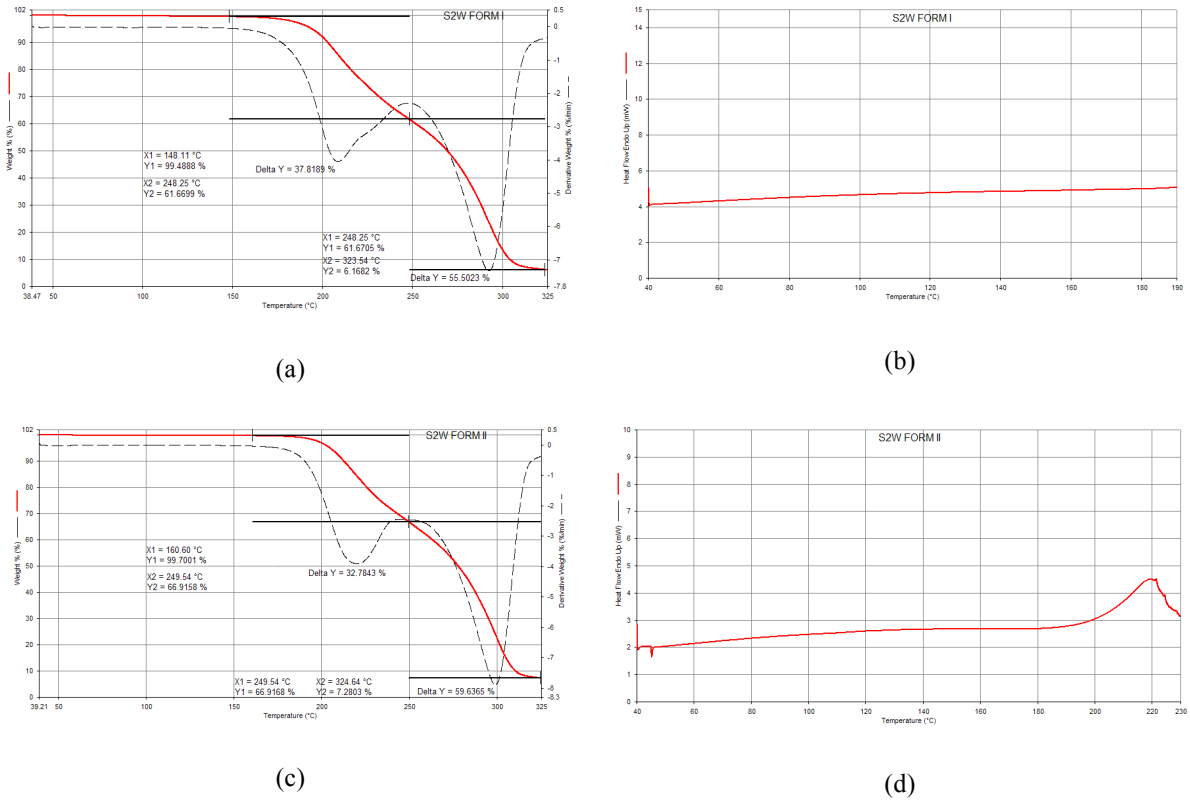

Fig.11. Thermograms (TGA and DSC traces) (a), (b) for PDDPTU form I and (c), (d) PDDPTU form II.

In order to investigate the relationship between the two polymorphs, variable temperature XRPD experiments were also performed, as shwon in figure 12. The system seems to be monotropic,[19] since I and II do not convert into each other on heating and/or cooling.

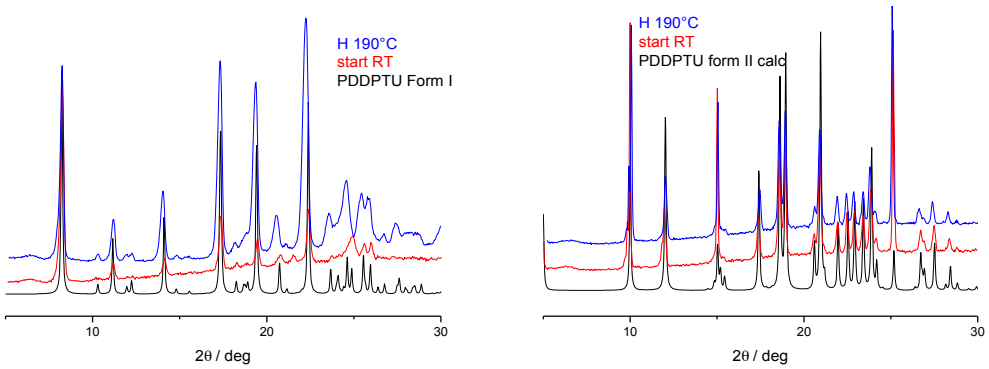

Fig.12. Variable temperature powder X-ray diffraction patterns. (a) PDDPTU form I and (b) PDDPTU form II. Both polymorphs do not convert into each other below decomposition temperature.

Conversion of form I in form II can be easily obtained in the presence of a catalytic amount of solvent, but it stops suddenly as soon as the solvent evaporates, see figure 13. In order to continue the conversion process, more solvent needs to be added.

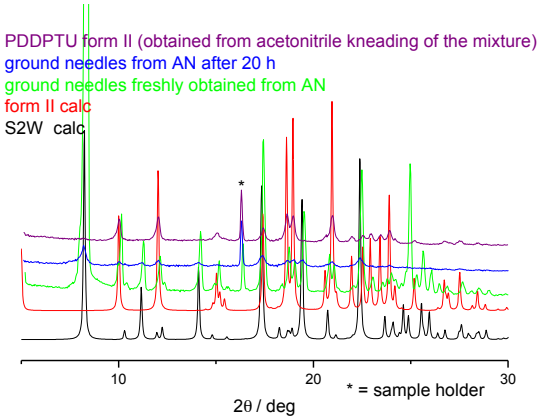

Fig.13. Kneading experiments: conversion from form I to form II stops when acetonitrile evaporates, but addition of a second drop of solvent, followed by kneading, resumes the conversion process.

2.4 - di-3-(3,5-di(pyridin-2-yl)-4H-1,2,4-triazol-4-yl)urea [DDDPTU]. Compound DDDPTU crystallizes as a dihydrate in the monoclinic space group C2/c; the asymmetric unit contains one molecule of DDDPTU and two of water (Z' = 1). The presence of the two bulky groups 3,5-di-pyridyl-4H-1,2,4-triazolyl- hinders formation of the urea-tape: urea groups form a net of hydrogen bonds by interacting with one water molecule [N···O = 2.828(3) Å], which, in turn, is linked via a second water molecule[O···O = 2.762(2) Å], to a nitrogen atom from the triazolyl- group [N···O = 2.845(3) - 2.873(3) Å] (see figure 14).

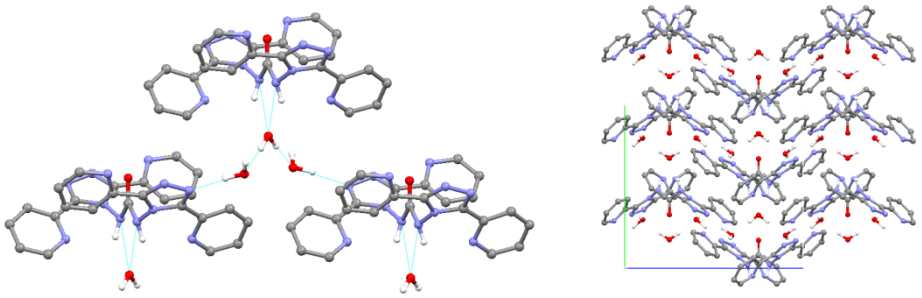

(a) (b)

Fig.14. (a) Hydrogen bonding interactions crystalline DDDPTU and (b) crystal packing of DDDPTU viewed down the *a*-axis. H_{CH} atoms omitted for clarity.

2.5 - Urea, N,N''-1,2-ethanediylbis(N'-phenyl-) [UEBP]. For this compound two polymorphs, called form I and form II, were obtained and characterized. UEBP form I crystallizes in the orthorhombic space group Pbca, while UEBP form II crystallizes in the monoclinic space group $P2_1/n$. Both forms display the typical urea-tape motif with $R_2^1(6)$ rings [O···N 2.838(2), 2.919(2) and 2.823(3), 3.069(3) Å for forms I and II, respectively] (see figure 15), but while in form I each molecule interacts with four adjacent molecules, thus generating a 2-D hydrogen bonded network (see figure 16), in form II each molecule is involved in interactions with two adjacent molecules, thus generating a 1-D network (see figure 17)

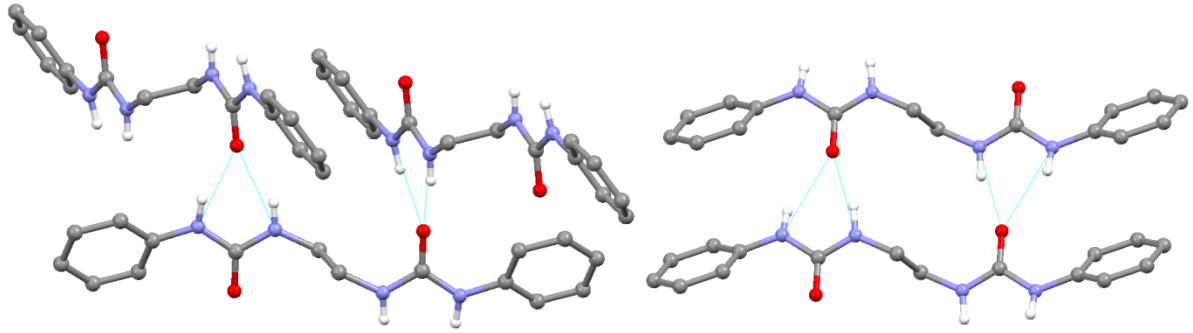

(a) (b)

Fig.15. Urea tape motif in crystalline UEBP: (a) form I and (b) form II. H_{CH} atoms omitted for clarity.

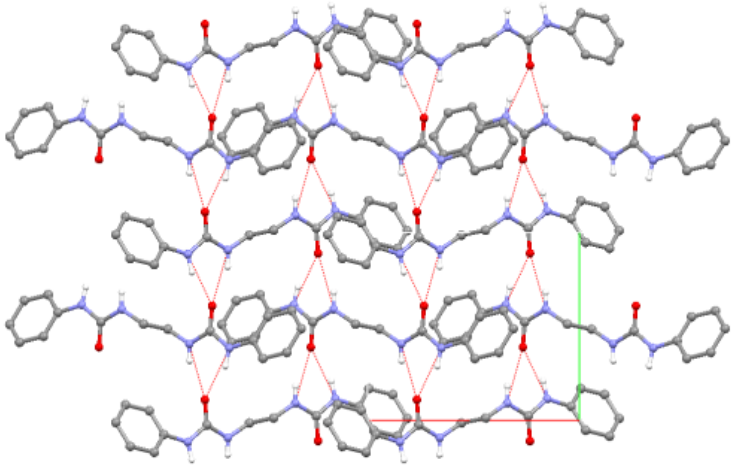

Fig.16. (a) The 2-D hydrogen bonding network in crystalline UEBP form I, viewed down the *c*-axis. H_{CH} omitted for clarity.

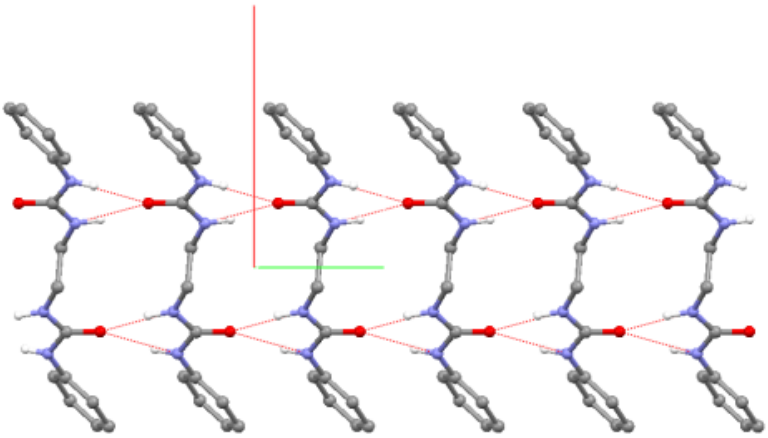

Fig.17 The 1D hydrogen bonded tape observed in form II, viewed down the c-axis H_{CH} omitted for clarity.

The polycrystalline sample of as synthesized UEBP is characterized by low crystallinity and differs from the obtained crystal structures. Heating the as synthesized phase results in the formation of UEBP form I (see figure 18).

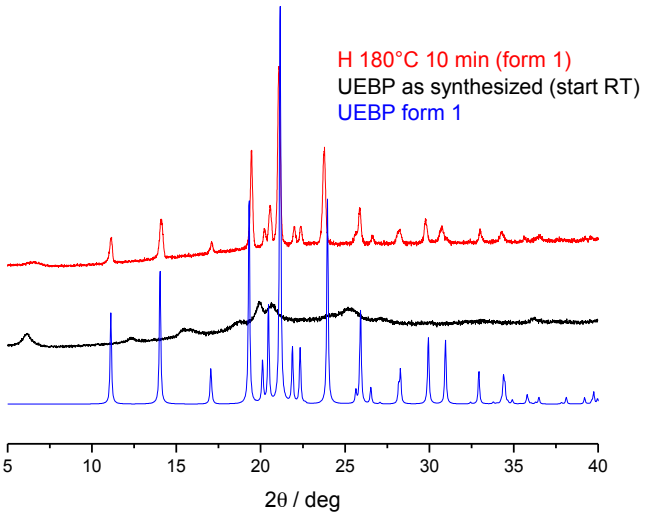

Fig.18. Variable temperature X-ray powder diffraction patterns for the as synthesized UEBP. Note how the as synthesized polycrystalline material converts to form I upon heating.

3 Gelation tests

Compounds PPmU, PDDPTU, DDDPTU and UEBP were all tested for gelation properties; upon heating, followed by slow cooling to room temperature, solutions of the pure compounds all yielded the starting materials. PQ5U behaves differently. The ligand in itself is *not* a gelator, and it is only slightly soluble in polar solvents such as MeOH, EtOH, i-PrOH and CH_3CN; suspensions are turned into clear solutions upon heating, and slow cooling to room temperature yields the starting solid. Upon addition of $AgNO_3$ to PQ5U solutions, though, supramolecular interactions build up between ligand, silver cations and nitrate anions, and thermo-reversible organo-gels are formed.

Gelation is obtained (Figure 19) only when the $AgNO_3$:PQ5U molar ratio is in the range from 1:2 to 1:1. Gel formation is not observed if other transition metals (e.g. zinc or cobalt) or different anions are employed (acetate, tetrafluoroborate). Table 2 lists the gelation properties of the system $AgNO_3$:PQ5U in different organic solvents.

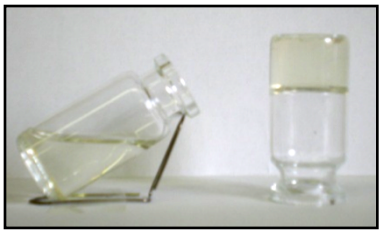

Fig.19 The clear sol (on the left) and the "tube inversion test" showing gel formation (on the right).

Table 2. Results of the gelation experiments, in different solvents, for $AgNO_3$:PQ5U stoichiometric ratios of 1:2 and 1:1 (S = clear solutions; I = insolubility; G = gel formation).

Solvent	Result	Solvent	Result
EtOH	G	THF	I
MeOH	G	1-butanol	G
i-PrOH	G	1-hexanol	S
CH_3CN	G	toluene	I
(-)ethyl-lactate	G	ethyl acetate	I
acetone	I	nitromethane	S
DMF	X[a]	dioxane	I
dichloromethane	I	ethanol amine	S
ethylene glycol	S	t-butanol	S
cyclohexane	I		

[a] decomposition product.

3.1 Gel characterization

Upon heating, gel-to-sol transition is observed, due to disruption of the supramolecular interactions that hold the gel-structure together; the solutions revert to the gel state upon cooling.

In order to evaluate the thermal stability of the gel, a plot of the gel-sol dissociation temperature (T_{gel}) in EtOH versus the gelator concentration was constructed (see the experimental section for details) by using the "dropping ball" method.[2b] Figure 20 clearly indicates that T_{gel} increases with the gelator concentration.[21] The gel-sol-gel interconversion is fully reversible over ten to fifteen cycles of heating and cooling. This means that the assembly of the gelator molecules arises from cooperative non-covalent interactions between the PQ5U molecules, the silver and nitrate ions, and these interactions are broken upon heating the gel.

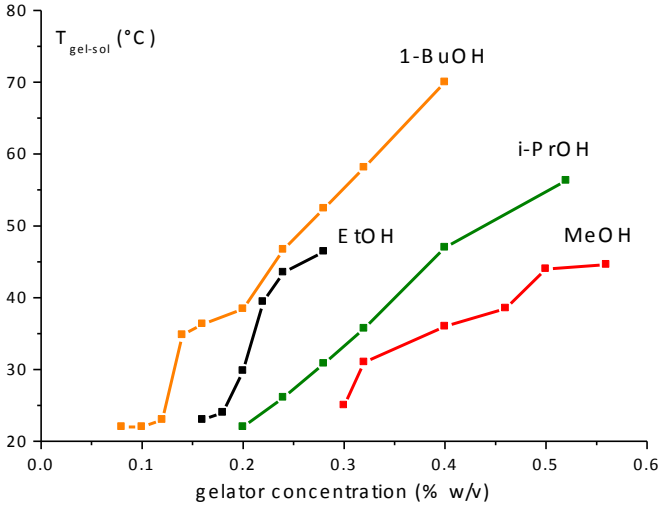

Fig.20. Effect of the concentration[12] (expressed in % w/v) on the gel-sol transition temperature in different solvents for an $AgNO_3$:PQ5U molar ratio of 1:2. The gel–sol transition for CH_3CN is at room temperature, irrespective of the gelator concentration. For this reason the corresponding plot was not included

XRPD patterns of fresh gels, obtained directly in the sample holder, were measured for the gels obtained from MeOH, i-PrOH, CH_3CN and EtOH (Figure 21). All samples show a broad peak at 2θ between 3 and 4 deg, which corresponds to a *d* spacing of ~2.5 nm; for gels obtained from ethanol and acetonitrile this peak is sharper then those obtained from methanol and i-propanol. If the gels are dried in open vials xerogels are formed: XRPD patterns of the air-dried samples (xerogels) were also recorded (see Figure 21): as it can be seen, the low angle peak is maintained for all samples, but more and different peaks are observed at higher angle. The same patterns can be observed if $AgNO_3$ and

PQ5U are ground together in the stoichiometric ratio 1:2 in the presence of a small quantity of solvent (kneading).

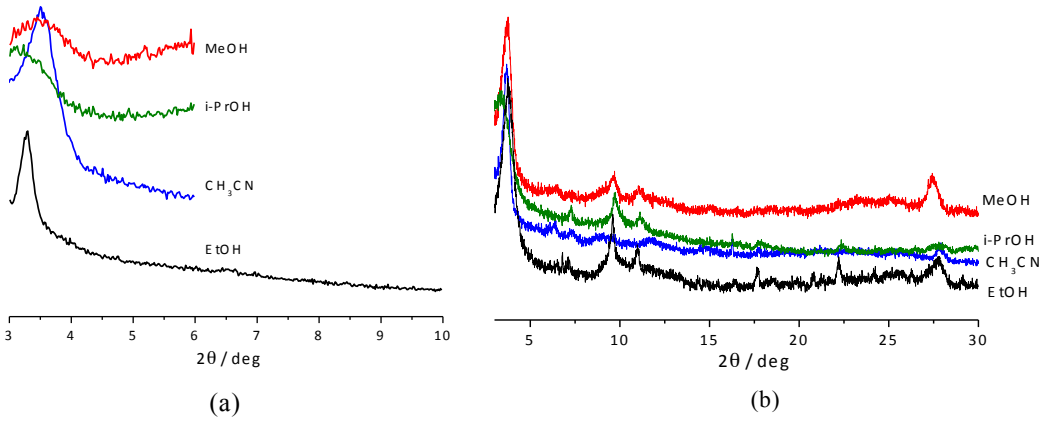

Fig.21. (a) XRPD patterns of fresh gels ($AgNO_3$:PQ5U = 1:2) obtained from acetonitrile, methanol, i-propanol and ethanol. (b) XRPD patterns of the xerogels ($AgNO_3$:PQ5U = 1:2) obtained from EtOH, MeOH, CH_3CN and i-PrOH.

SEM images (see Figure 22), of the xerogel obtained by air-drying the ethanol containing gel, reveals the presence of a 3D network of branched and entangled fibres, which must be effective in trapping the solvent molecules in the gel phase.

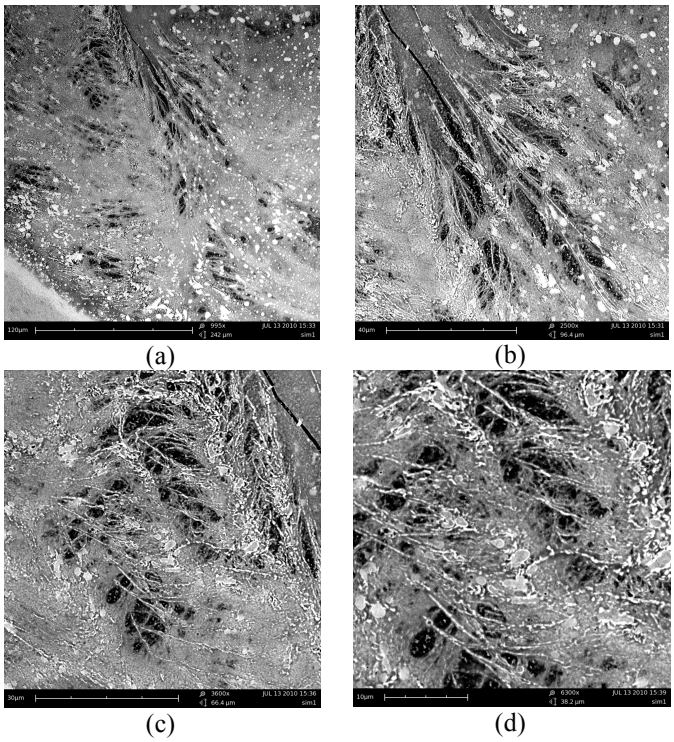

Fig.22. SEM images at various magnifications of the xerogels obtained by drying in the air the 1:2 $AgNO_3$:PQ5U gel from EtOH. (a) 995x (b) 2500x (c) 3600x and (d) 6300x The fibrous nature of the xerogel can be appreciated. The white spots indicate the presence of silver(I). Courtesy of Prof. G. Falini.

UV-vis absorption spectra of the PQ5U free ligand shows two bands in the region 200-400 nm, a sharp and strong band at 245 nm (ε = 40000 $M^{-1}cm^{-1}$) and another broad and weaker at 316 nm (ε =72000 $M^{-1}cm^{-1}$). PQ5U displays also a broad emission band, with a maximum at λ = 438 nm (λ_{ex} = 316 nm), see figure 5. Additions of silver nitrate (titration) do not affect the electronic absorption spectra (*i.e.* no isosbestic point); differently, emission is progressively quenched, see inset in figure 23.

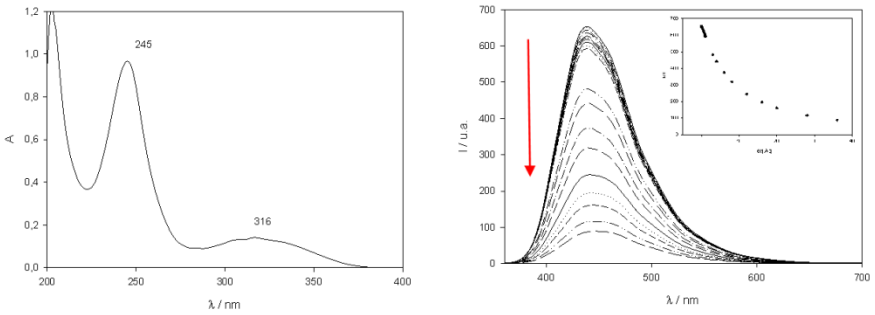

(a) (b)

Fig.23. (a) UV-VIS spectra of the PQ5U free ligand (conc. = 25 µM in ethanol). (b) Emission spectra registered during the titration, at room temperature, of PQ5U (1 µM in ethanol) with $AgNO_3$ (1.0 mM in ethanol); inset, plot of Ia.u. at 438 nm *vs.* Ag^+ equivalents added, Logβ = 4.37 for $[Ag(PQ5U)]^+$. Courtesy of Dr. M. Sgarzi.

Figure 24 shows the pictures of gel under daylight and UV and also the emission spectra in gel state. Upon gelation a structured and red-shifted band at λ = 471 nm appears (compare fig.5b and 6c). Position and shape are substantially independent on the stoichiometric ratio and average lifetimes are τ = 1.81 ns and τ = 2.86 ns, for the gels $AgNO_3$ / PQ5U 1: 1 and 1: 2, respectively.

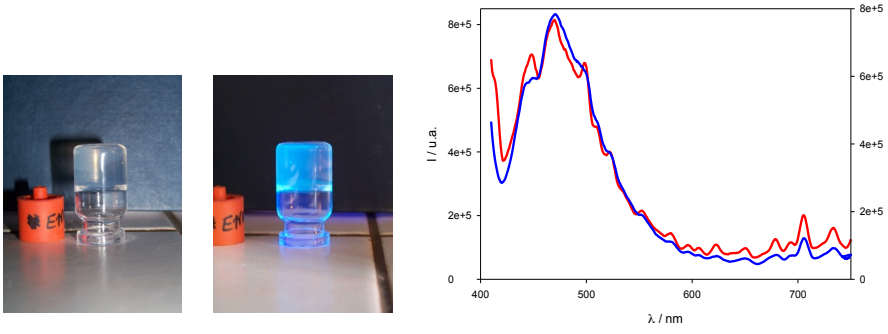

(a) (b) (c)

Fig.24. Pictures of the gel in ethanol under: (a) daylight and (b) UV (λ_{ex} = 365 nm) and (c) emission spectra (λ_{ex} = 316 nm) of the $AgNO_3$/PQ5U system 1:1 (red line) and 1:2 (blue line) in gel state (conc. = 0.13% w/v in ethanol) at room temperature. Courtesy of Dr. M. Sgarzi.

ESI-MS confirmed (figure 25) formation of the complexes $[Ag(PQ5U)_2]^+$ and $[Ag(PQ5U)(CH_3CN)]^+$ by revealing the corresponding peaks at m/z 635.0 and 410.9, as well as the signal associated with the protonated ligand $[PQ5U{\cdot}H]^+$ at 264.0; the peak at m/z 189.9 can be ascribed to the solvated cation $[Ag{\cdot}CH_3CN]^+$.

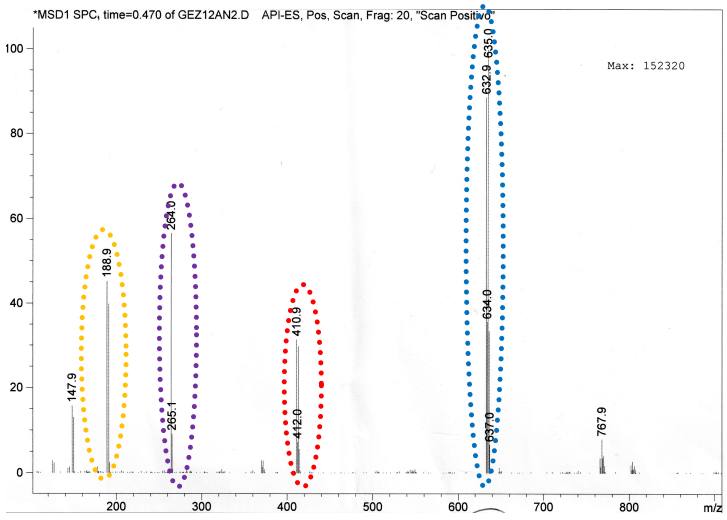

Fig.25. ESI-MS on diluted gel of acetonitrile. m/z : 635.0 $[Ag(PQ5U)_2]^+$ dotted blue; 410.9 $[Ag(PQ5U)(CH_3CN)]^+$ dotted red; 264.0 $[PQ5U{\cdot}H]^+$ dotted purple; 189.9 $[Ag{\cdot}CH_3CN]^+$ dotted yellow.

4 Crystal structures of the gelator

4.1 Polymorphs from gels

Vials containing gels obtained in CH_3CN, EtOH, i-PrOH and MeOH were sealed and left standing at room temperature. After a few days the gels contained in the vials had separated into clear solutions and crystalline materials deposited on the bottom of the vial (figure 26a). When the vials are left open in the air at room temperature, a xerogel is formed, which (depending on the laboratory temperature and humidity) may sometimes show the presence of tiny crystals grown on the fibrous material (see figure 26b).

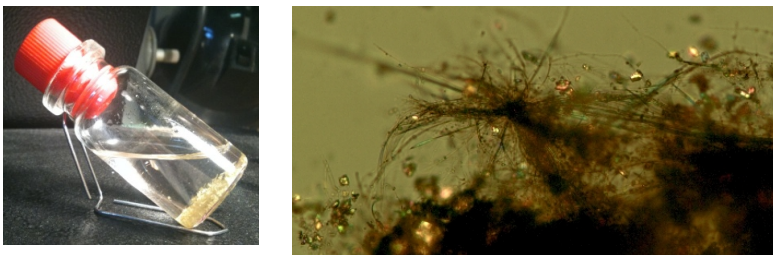

(a) (b)

Fig.26. (a) Crystallization of Form IV as obtained by drying in a sealed vial the 1 : 2 $AgNO_3$: PQ5U gel from MeOH. (b) picture taken with a polarizing microscope of the xerogel dried in the open air, note the presence of very small crystals.

Crystallizing a gelator complex system is normally a difficult task,[6,17,22] and more so if crystallization is attempted from the gelling solvent. If our gels are dried in sealed vials, phase separation takes place, resulting in clear solution and single crystals. Interestingly and, to the best of our knowledge, unprecedentedly, different crystal forms are obtained from different gelling solvents. We report here the polymorphs of the complex of formula $[Ag(PQ5U)_2]NO_3$ (see figure 27) obtained from CH_3CN, Form I, EtOH, Form II, i-PrOH, Form III and MeOH, Form IV which were characterized by single-crystal X-ray diffraction (see experimental section table 1d for crystallographic details).

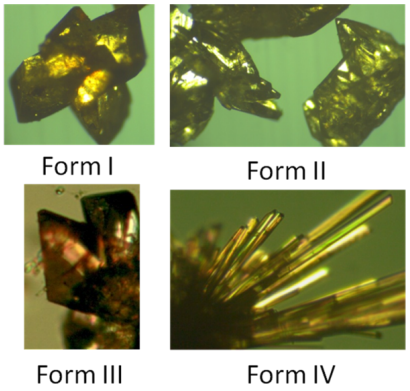

Fig.27. Images of the single crystals for the four polymorphs of the complex $[Ag(PQ5U)_2]NO_3$, as obtained from CH_3CN, Form I, EtOH, Form II, i-PrOH, Form III and MeOH, Form IV.

4.2 Structural description of the polymorphs of the complex $[Ag(PQ5U)_2]NO_3$

In terms of gross structural features the $[Ag(PQ5U)_2]^+$ units for Forms I–III are very similar, consisting of linearly coordinated ligand–Ag^+ systems, while Form IV contains a nitrate anion participating in the coordination sphere of the Ag^+ cation to which it is directly bound.

Figure 28 shows the first coordination sphere around the Ag^+ ion, which is completed by an O_{urea} atom and a silver cation in Form I, by two O_{urea} atoms in Forms II and III and by a nitrate anion and two C–H groups of adjacent ligands in Form IV and V. Coordination geometries around Ag^+ for all polymorphs (distances and angles) are listed in table 3.

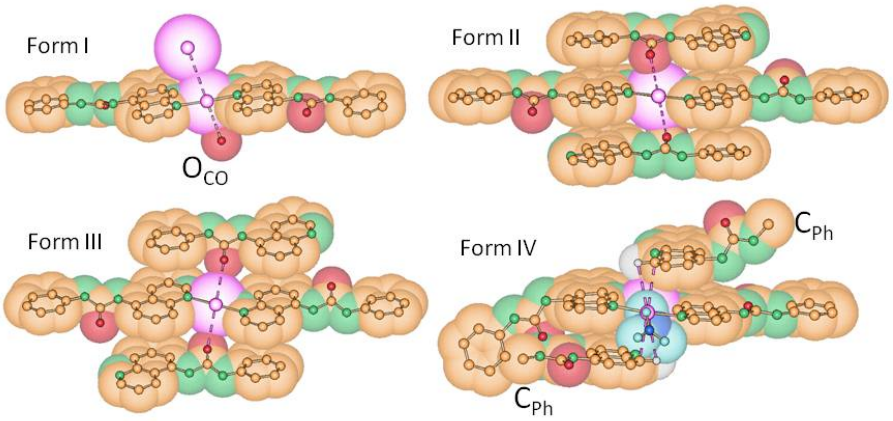

Fig.28. The first coordination sphere around the Ag^+ ion in Forms I to IV. In Form IV and V the NO_3^- anion directly interacts with the silver cation, and two (C-H)···Ag^+ interactions can also be observed. [Portions of the PQ5U ligands in Forms I and IV and V and most H atoms omitted for clarity].

Table 3. Coordination geometry around the silver ion for Forms I, II, III and IV.

	I	**II**	**III**	**IV**
Distances (Å)				
N—Ag	2.110(3) - 2.122(2)	2.135(3)	2.140(6)	2.188(2) - 2.200(2)
O_{urea}—Ag	2.867(3)	2.866(2)	3.131(4)	-
$O_{nitrate}$—Ag	-	-	-	2.685(2)
Angles (deg)				
N—Ag—N	176.4(1)	180.0(1)	180.0(2)	169.98(8)
O_{urea}—Ag—O_{urea}	-	180.0(6)	180	-
$O_{nitrate}$—Ag—N	-	-	-	86.47(2) - 102.39(2)

Since the relative ligand conformation in **Forms I** to **III** (*transoid*) and that in **Form IV** (*cisoid*) is different, one might be tempted to consider this latter compound as a different isomer of the complex. However, we reckon that these examples lend further support to the idea that the difference between molecular isomers and "crystal isomers", e.g. polymorphs,[23,24] can be semantic and depends on the compromise between minimization of crystal energy and of molecular energy.

Markedly differences can be detected in the interaction between the nitrate and urea group, see figure 29. Hydrogen bond ring motifs in urea-nitrate are as follow: in form I and II the nitrates act as a bridge between two $[Ag(PQ5U)_2]^+$ units *via* hydrogen bonding interaction with the urea forming an extended network, in polymorph I can be observed either synthons $R_2^1(6)$ and $R_2^2(8)$, while in form II only the $R_2^2(8)$ motif is present. In form III the nitrate (disordered over two positions) still interacts with the urea through the $R_2^2(8)$ synthon, but it does not act as bridge between the $[Ag(PQ5U)_2]^+$

units. Polymorph IV organizes itself forming dimers held together by intermolecular hydrogen bonds among the urea groups that displays the typical $R_2^1(6)$ motif, even though no tapes are present. The dimers are connected by hydrogen bonding interactions, $R_2^2(8)$ motif, between the nitrate and the urea. Hydrogen bond distances for urea-nitrate and urea-urea interaction, for all polymorphs, are listed in table 4; in scheme 4 are summarized the hydrogen ring motifs.

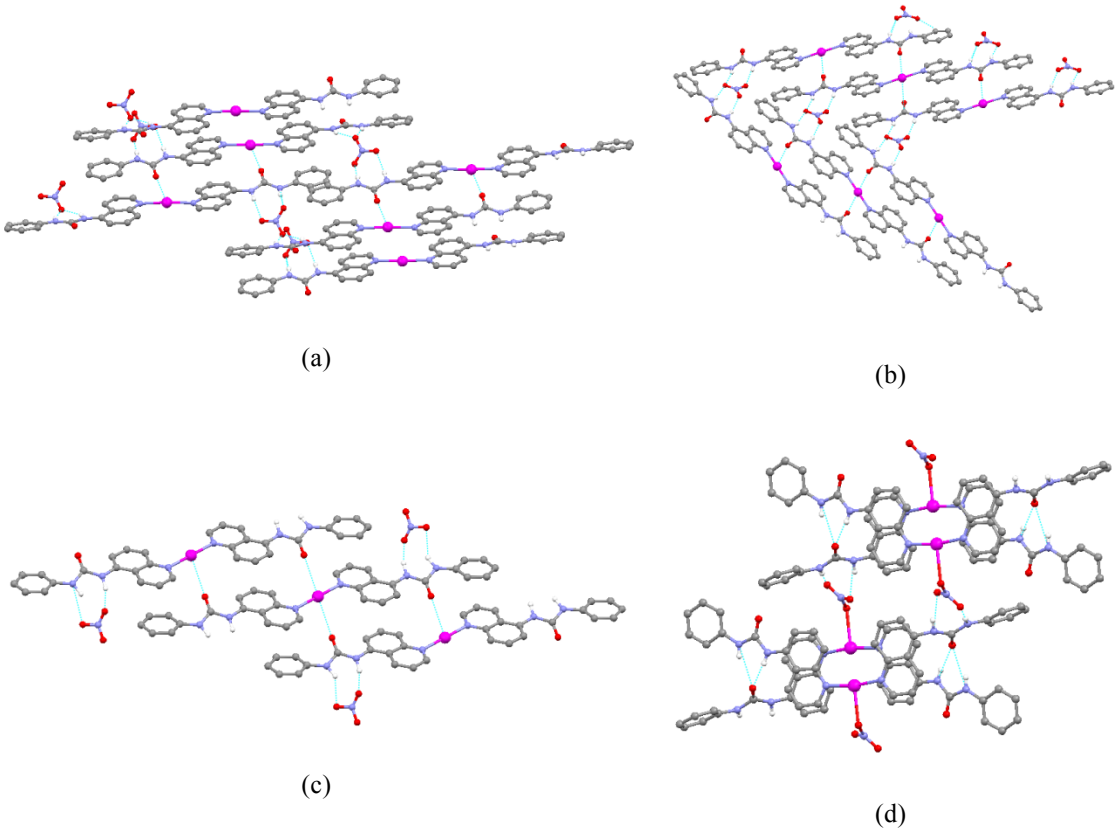

Fig.29. Silver ion coordination environment and urea-nitrate N—H···O hydrogen bond motifs in $[Ag(PQ5U)_2]NO_3$ polymorphs: a) $R_2^1(6)$ and $R_2^2(8)$ in form I, b) $R_2^2(8)$ in form II, c) $R_2^2(8)$ in form III, d) the urea-urea $R_2^1(6)$ and the urea-nitrate $R_2^2(8)$ in form IV. H_{CH} atoms omitted for clarity.

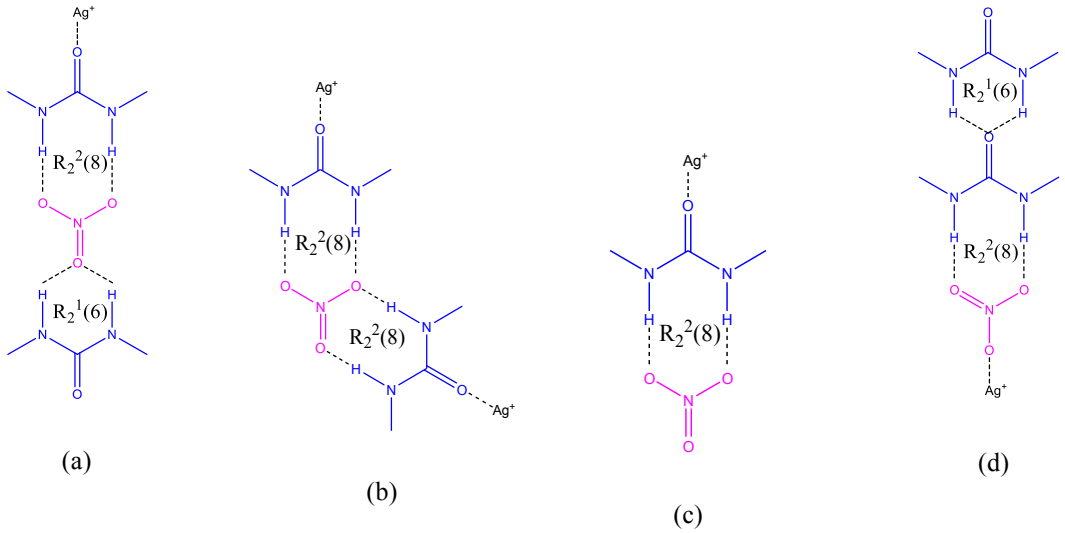

Scheme 4. Hydrogen bonding ring motifs in urea-nitrate and urea-silver interactions observed in: (a) Form I, (b) form II, (c) form III and (d) form IV.

Table 4. N—(H)···O hydrogen bond distances (donor-acceptor) for urea-nitrate and urea-urea interactions observed in Forms I, II, III and IV.

	Ring motif	I	II	III	IV
Urea-nitrate	$R_2^2(8)$	3.006(7)-3.119(7)	2.869(4)-3.283(3)	2.967(8)-3.01(1)	2.883(3)-3.034(4)
	$R_2^1(6)$	2.385(6)-2.939(6)	-	-	-
Urea-Urea	$R_2^1(6)$	-	-	-	2.944(3)-.3044(4)

5 Isomers of the Ligand PQ5U

In paragraph 2 we have shown that, in the presence of $AgNO_3$, the compound 1-phenyl-3-(quinolin-5-yl)urea (PQ5U)[17] behaves as a supergelator of alcohols (such as MeOH, EtOH, *n*-PrOH, *i*-PrOH and *n*-BuOH) and acetonitrile;[22] this prompted us to explore this class of compounds; to this end we decided to synthesize a series of isomers of the ligand PQ5U, namely the 1-(isoquinolin-5-yl)-3-phenylurea [PiQ5U] and the 1-phenyl-3-(quinolin-6-yl)urea [PQ6U] and the ligand 1,3-di(quinolin-5-yl)urea [DQ5U], see scheme 5, with the aim to: (i) establish if coordination compounds of these ligands are able to form molecular gels in alcohols and/or in other solvents and (ii) investigate the relationship between structure and gelation properties of these molecules/complexes.

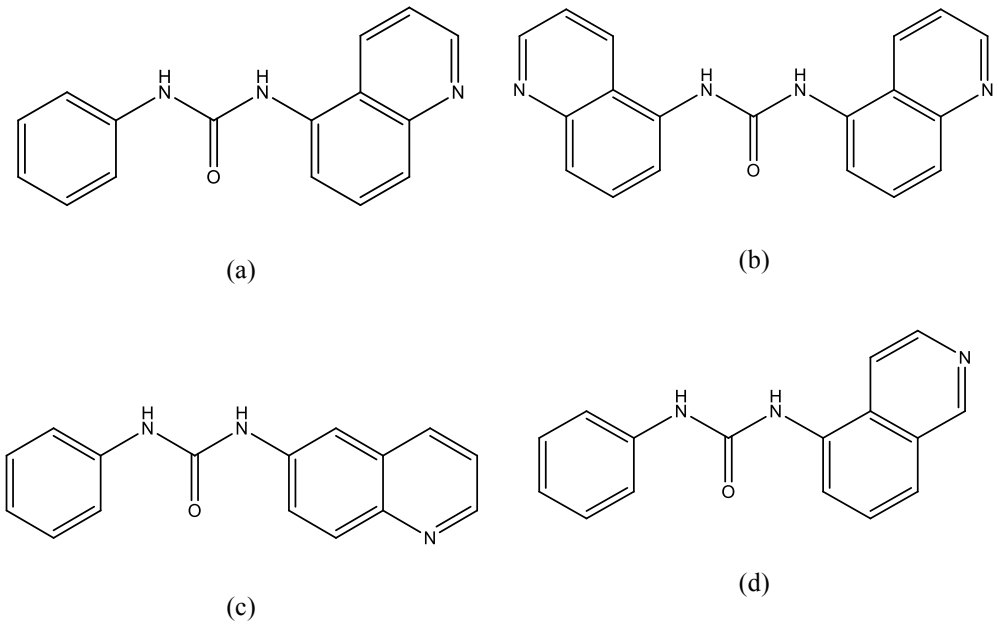

Scheme 5. (a) the ligand 1-phenyl-3-(quinolin-5-yl)urea [PQ5U], previously studied for its ability of forming gels in presence of $AgNO_3$ and the ligands taken into accounts in the present study: (b) the 1,3-di(quinolin-5-yl)urea [DQ5U], (c) 1,3-di(quinolin-6-yl)urea [PQ6U] and (d) the 1-(isoquinolin-5-yl)-3-phenylurea [PiQ5U]. Note that while [PQ6U] and [PiQ5U] are isomers of [PQ5U], the ligand [DQ5U] may be considered a sort of [PQ5U] "doubled".

5.1 - 1-phenyl-3-(isoquinolin-5-yl)urea [PiQ5U]. Compound [PiQ5U] crystallizes in the monoclinic space group $P2_1/c$. The structure features the common urea-urea interaction that leads to formation of the well known urea tape motif [$R_2^1(6)$ in graph set notation][18] or urea head-to-tail tape (see figure 30); the bifurcated N-H···O hydrogen bonds (N···O = 2.805(4) - 2.919(4) Å) impose an infinite strand-like structure to the molecule and no other significant supramolecular interactions are present in the crystal structure.

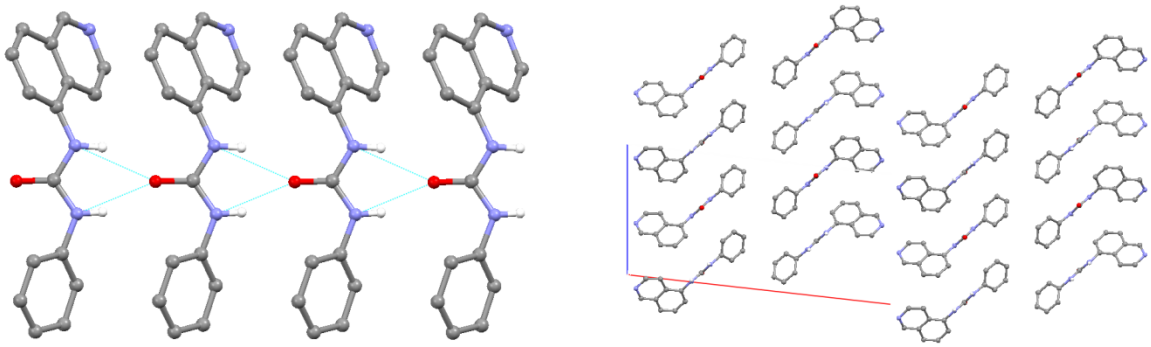

(a) (b)

Fig.30. (a) Urea tape motif present in crystal structure of PiQ5U and (b) crystal packing of PiQ5U viewed along the *b*-axis. H_{CH} atoms omitted for clarity.

A comparison between XRPD patterns measured on complex PiQ5U and simulated on the basis of single crystal data confirms the nature of the polycrystalline sample (see figure 31).

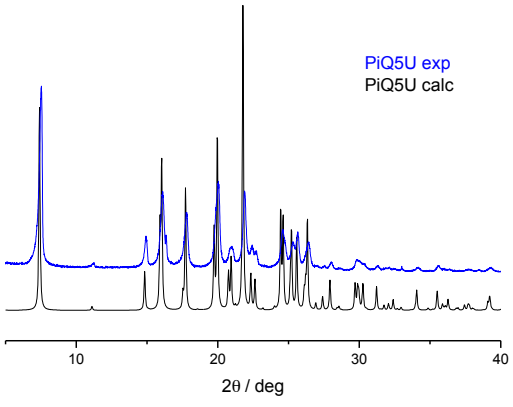

Fig.31. Comparison between diffraction patterns for PiQ5U, calculated on the basis of single crystal data (black-line), and experimental (RT, blue-line).

5.2 - 1,3-di(quinolin-6-yl)urea [PQ6U]. Compound [PQ6U] crystallizes in the monoclinic space group $P2_1/n$. The structure is characterized by the common urea tape motif; as shown in figure 32, [N···O = 2.871(7) - 2.907(7) Å].

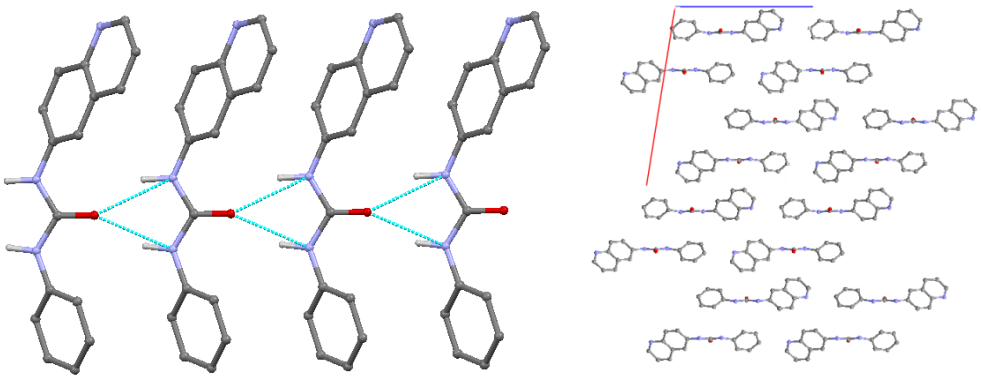

(a) (b)

Fig.32. (a) Urea tape motif present in crystalline PQ6U and (b) crystal packing of PQ6U viewed along the *b*-axis. H_{CH} not shown for clarity.

Crystal structure of [PQ6U] was determined from powder data, see figure 34 and experimental section for details.

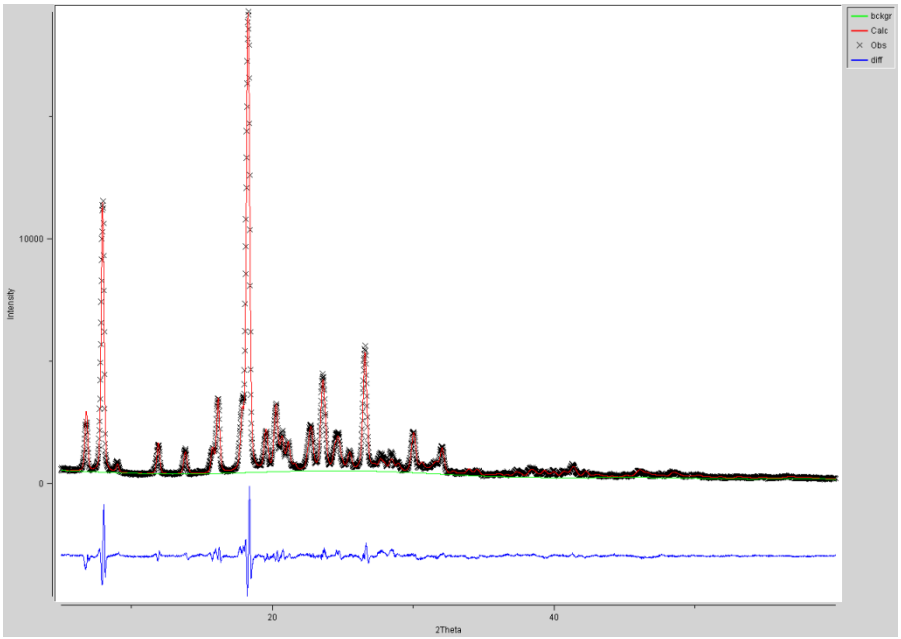

Fig.34. Experimental (black crosses), calculated (red curve), background (red curve) and difference (blue line) powder patterns for PQ6U. the x-axis is in degrees of 2θ. Peak positions are marked in black.

5.3 - 1,3-di(quinolin-5-yl)urea [DQ5U]. In the crystal structure of DQ5U are present intermolecular N-H···O interaction occur (N···O = 2.858(4) Å) leading to infinite tapes containing the head-to-tail urea-tape motif. Weak π-stacking interaction (ID = 3.695 Å; CD = 3.363 Å; offset = 1.53 Å) between the quinoline moieties, belonging to the same chain, help to stabilize the structure. The chains run parallel to the *a*-axis and no specific interactions are observed between adjacent chains, see figure 35.

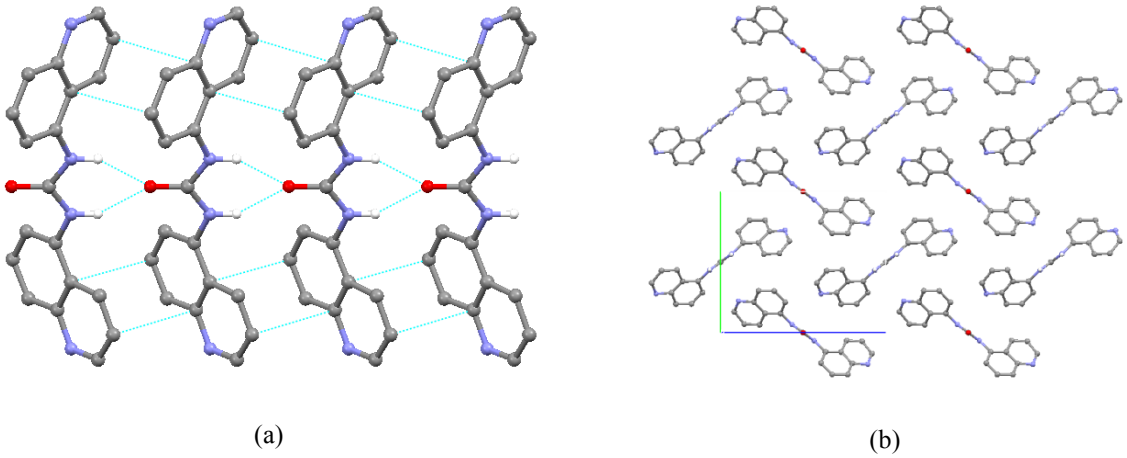

(a) (b)

Fig.35. (a) Urea tape motif present in crystal structure of DQ5U together with the π-stacking interactions and (b) crystal packing of DQ5U viewed down the *a*-axis. H_{CH} omitted for clarity.

A comparison between the XRPD patterns measured on complex DQ5U and that simulated on the basis of the single crystal structure confirm the exact nature of the polycrystalline sample (see figure 36).

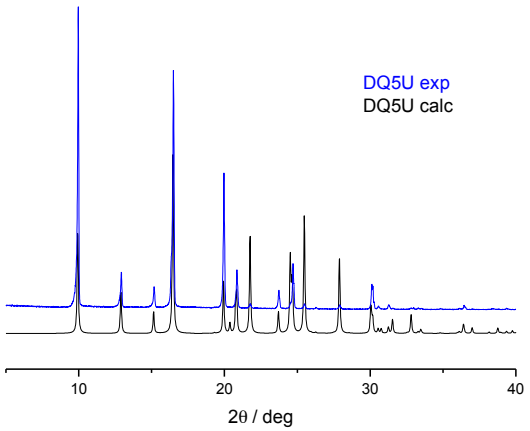

Fig.36. Comparison between diffraction patterns for DQ5U, calculated on the basis of single crystal structure (black-line) and experimental recorded at RT (blue-line).

5.4 Gelation tests and gel characterization

In a typical gelation experiment an amount of a finely ground ligand:$AgNO_3$ mixture in 1:2 (for PiQ5U and PQ6U), or 1:1(for DQ5U) molar ratio was suspended in 5 mL of a pure solvent or in a solvent mixture in a 2 cm ∅ diameter vial, and the vial was heated up to obtain a boiling solution/suspension. Table 5 lists the results of the tests.

Table 5. Results of the gelation experiments, in different solvents and solvent mixtures; (S = clear solutions; I = insolubility; P = precipitate; C = crystals G = gel formation). Concentrations expressed in percentage weight/volme (% w/v).

	PiQ5U:$AgNO_3$ 2:1			PQ6U:$AgNO_3$ 2:1			DQ5U:$AgNO_3$ 1:1		
Solvent	0.25%	0.50%	1.00%	0.25%	0.50%	1.00%	0.25%	0.50%	1.00%
Water	I	I	I	I	I	I	I	I	I
Methanol	I	I	I	S→C	S→C	S→C	I	I	I
Ethanol	I	I	I	I	I	I	I	I	I
n-propanol	I	I	I	I	I	I	I	I	I
i-propanol	I	I	I	I	I	I	I	I	I
n-butanol	I	I	I	I	I	I	I	I	I
acetonitrile	S→P	S→P	S→P	S→C	S→C	S→C	I	I	I
DMF	S	S	S	S	S	S	I	I	I
toluene	I	I	I	I	I	I	I	I	I
Chloroform	I	I	I	I	I	I	I	I	I
Butyl-benzoate	I	I	I	I	I	I	I	I	I
DMF / ethanol 1:2	S	S	S	S	S	S	I	I	I
DMF / ehanol 2:1	S	S	S	S	S	S	G	G	G

In the whole set of synthesized ligands only compound [DQ5U] has proven capable of gelating the mixed solvent EtOH / DMF 1:2 (v/v) when mixed with 1 equivalent of $AgNO_3$. As evidenced by the "tube-inversion" test[2b] (see figure 37a), the critical gelation concentration (CGC, *i.e.* the lowest concentration at which gelation occours) at room temperature is 0.17% (w / v).

Once prepared, the gel is stable at room temperature in the presence of air and can be stored for about a week without showing any changes. The dropping-ball method[2b] was used to evaluate the gel to sol transition temperature as function of the gelator concentration (figure 37); gel formation is not fully thermoreversible (at maximum 3-4 gel to sol cycles then a degradation process takes place probably due to the reduction of the silver cation), with gel to sol transition temperatures ranging from 24.1°C for 0.17 % (w/v) to 37.2°C for a 0.325% (w/v).

(a)

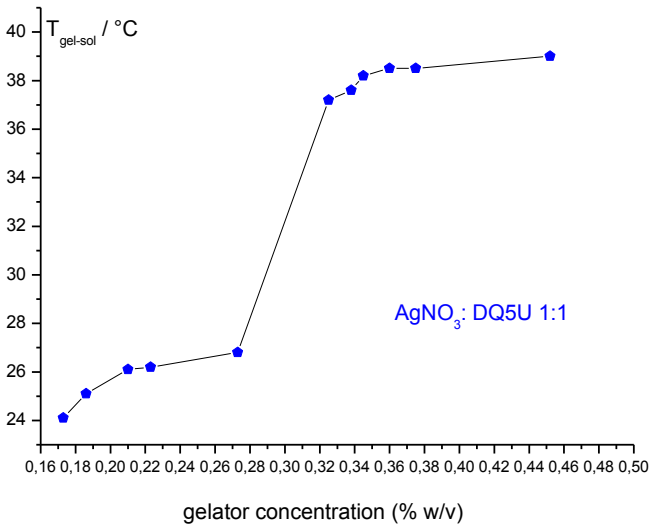

(b)

Fig.37. (a) "Tube-inversion" test. Photographs of $AgNO_3$ / DQ5U in the mixed solvent DMF / EtOH 1:2 v/v in the sol form at elevated temperature (left) and in the gel state at room temperature (right) and (b) plot of gel to sol transition temperature versus gelator concentration.

Fluorescence microscopy was employed to examine the aggregates microstructure (fibrils/fibers/strings) responsible for gelation. Figure 38 shows the concentration dependence of the fluorescence microscope images at increased concentrations. No morphological changes are observed upon increasing the concentation of the gelator. The length of the strings is several tens of μm, while the width is very narrow; sub or a few μm. the fibrous structure probably comes from anisotropic interactions between the ligand DQ5U, $AgNO_3$ and solvent molecules.

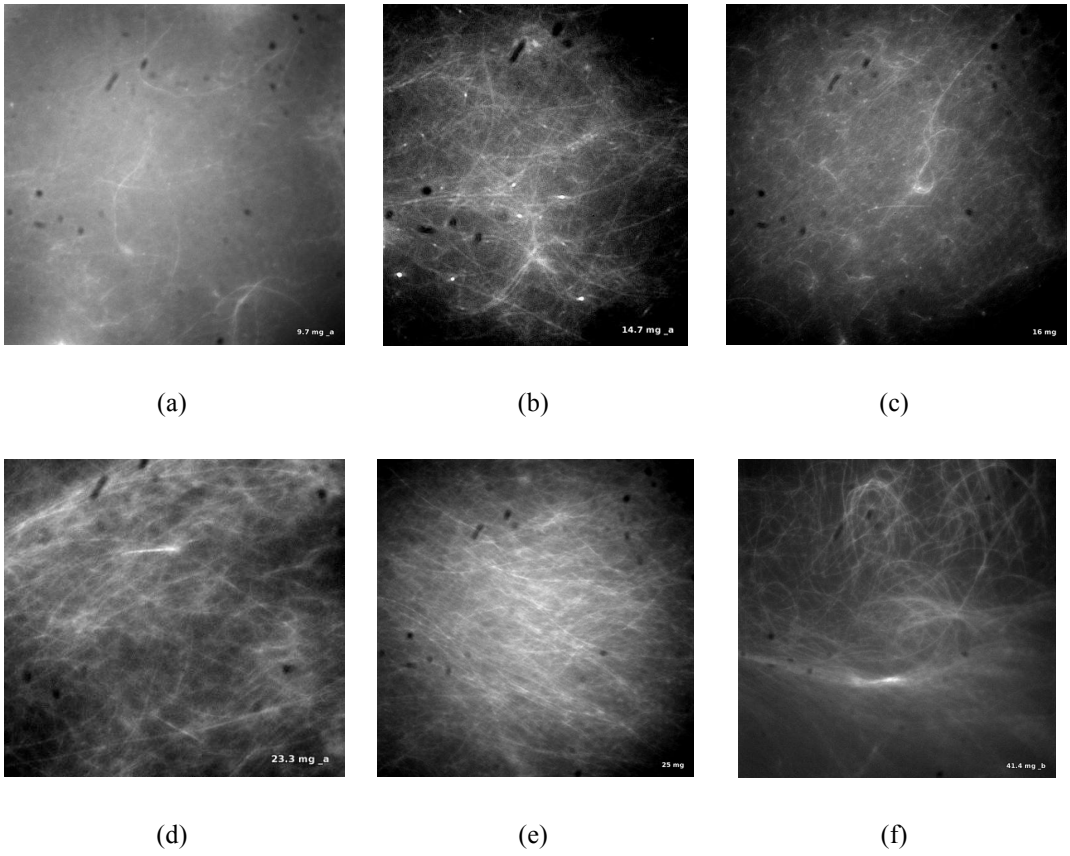

(a) (b) (c)

(d) (e) (f)

Fig.38. Fluoresce microscopy images of the gels at various concentrations: a) 0.16% w/v; b) 0.24% w/v; c) 0.26% w/v; d) 0.38% w/v; e) 0.41% w/v and f) 0.69% w/v. Note the presence of fibrillar aggregates. Courtesy of Dr. D. Genovese.

5.5 Structural description and characterization of the complexes obtained

In crystalline [Ag(PQ6U)2]NO_3·CH_3CN the Ag^+ ion is linearly coordinated by two nitrogen atoms from the quinoline units [Ag^+···N = 2.146(4) - 2.197(5) Å; N—Ag^+—N angle =180.0(2)°],see figure 39a.

The structure of [Ag(PQ6U)2]NO_3·CH_3CN is characterized by the presence of zig-zag chains held together by hydrogen bonds between the urea groups and the NO_3^- anions [O···N = 2.941(7) - 2.981(7) Å], see figure 39b. The chains stack in pairs leaving small holes filled by solvent molecules (acetonitrile) not involved in the coordination of the Ag^+ ion, see figure 39c.

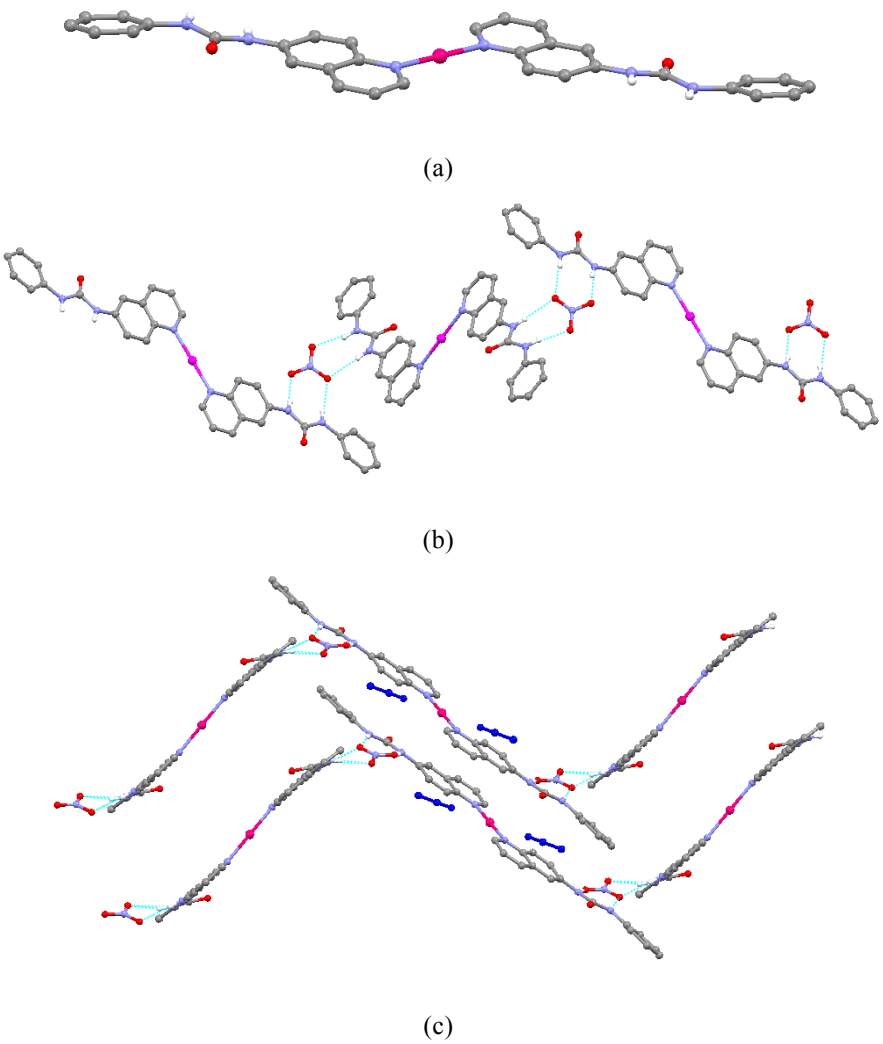

(a)

(b)

(c)

Fig.39. (a) Coordination sphere around the Ag^+ ion present in the cationic unit $[Ag(PQ6U)2]^+$; (b) hydrogen bonding ring motifs in crystalline [Ag(PQ6U)2]NO_3·CH_3CN involving urea groups and nitrate anions and (c) acetonitrile molecules trapped inside the cavities; note that these are not involved in any coordination interaction. H_{CH} atoms omitted for clarity.

A comparison between the XRPD patterns measured on complex $[Ag(PQ6U)2]NO_3 \cdot CH_3CN$ and that simulated on the basis of the single crystal structure confirms the exact nature of the polycrystalline sample (see figure 40a).

Thermal gravimetric analysis on a polycrystalline sample of $[Ag(PQ6U)2]NO_3 \cdot CH_3CN$ shows a weight loss of ca. 5% in the temperature range 100-175 °C, in agreement with the evaporation of one mole of acetonitrile, see figure 40b.

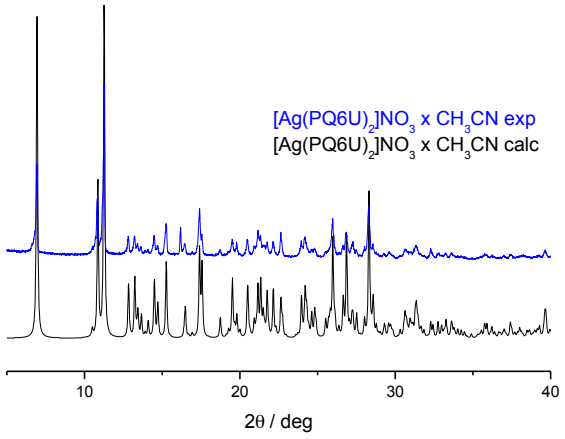

(a)

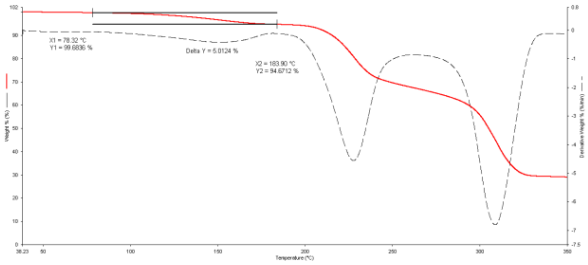

(b)

Fig.40. (a) Comparison between diffraction patterns for $[Ag(PQ6U)2]NO_3 \cdot CH_3CN$, calculated on the basis of single crystal structure (black-line) and experimental recorded at RT (blue-line); (b) the TGA trace for complex $[Ag(PQ6U)2]NO_3 \cdot CH_3CN$.

Unlike the previously described acetonitrile solvated complex, in crystalline $[Ag(PQ6U)2]NO_3$ the coordination geometry around the Ag^+ ion is distorted trigonal. The nitrate anion coordinates to the silver as an asymmetrically chelating bidentate ligand [$Ag^+ \cdots O$ = 2.743(3) - 2.821(3) Å]; two nitrogen atoms from the quinoline units complete the coordination around the cation [$Ag^+ \cdots N$ = 2.146(3) - 2.151(3) Å], see figure 41a.

Between the urea groups and the NO_3^- anions there are hydrogen bonding interactions [O···N = 2.922(5) - 2.929(4) Å], see figure 41b.

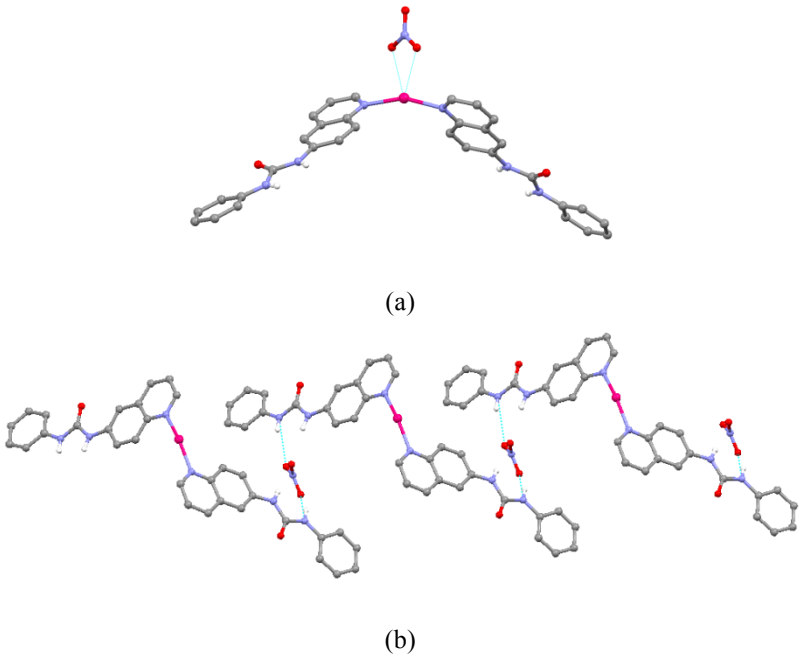

(a)

(b)

Fig.41. (a) Coordination sphere around the Ag^+ ion present in crystalline $[Ag(PQ6U)2]NO_3$ and (b) hydrogen bonding ring motifs in crystalline $[Ag(PQ6U)2]NO_3$ involving urea groups and nitrate anions.

A comparison between the XRPD patterns measured on complex $[Ag(PQ6U)_2]NO_3 \cdot CH_3CN$ and that simulated on the basis of the single crystal structure confirms the exact nature of the polycrystalline sample (see figure 42).

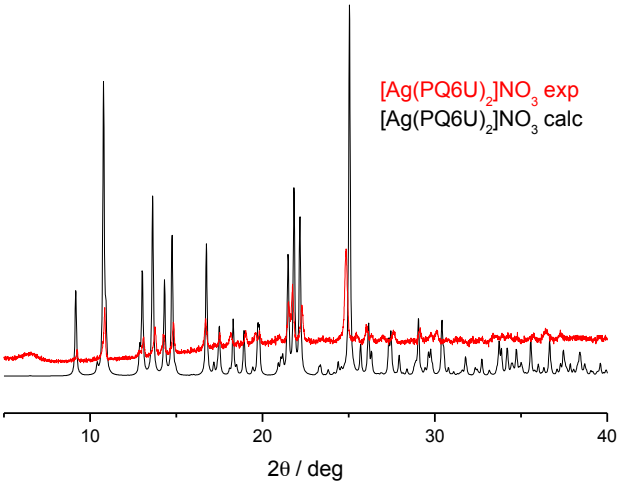

Fig.42. Comparison between diffraction patterns for $[Ag(PQ6U)2]NO_3$, calculated on the basis of single crystal structure (black-line) and experimental recorded at RT (blue-line).

A more detailed view of the behavior with temperature of $[Ag(PQ6U)2]NO_3 \cdot CH_3CN$ and its desolvated form is obtained by variable temperature powder diffraction measurements. Figure 43 provides clear indication of the transition $[Ag(PQ6U)2]NO_3 \cdot CH_3CN$ → $[Ag(PQ6U)2]NO_3$, associated with acetonitrile removal.

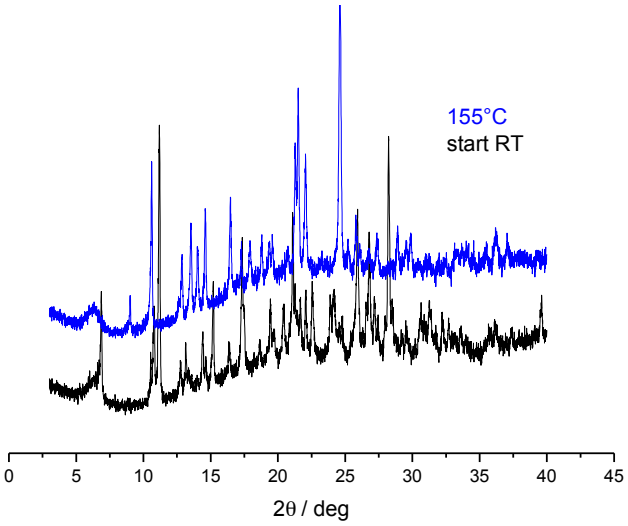

Fig.43. Variable temperature powder diffraction measurements for the process $[Ag(PQ6U)2]NO_3 \cdot CH_3CN$ → $[Ag(PQ6U)2]NO_3$.

6 Application of supramolecular gels as media for the crystal growth of APIs

The reversible nature of supramolecular gels can be used to allow easy recovery of crystals in contrast to conventional polymeric gel in which removal of the gel matrix may involve either acid hydrolysis or heating, both of which may dissolve or disrupt the crystals of interest grown inside. Moreover, unlike conventional hydrogels that are limited to water or aqueous solutions as solvents, LMWGs allow us to make gels with almost any solvent,[24] thus enlarging the "window" that can be explored.

In this part the potentiality of LMWGs as a medium for influencing crystal growth and form has been explored, particularly with active pharmaceutical ingredients (APIs), for which crystal habit and polymorphism are key economic and formulation problems.[25]

To this end we selected an API prone to polymorphism, as piracetam. Piracetam is a nootropic agent, currently marketed by UCB Pharma as Nootropil1, that is used to treat conditions of age-associated mental decline and disorders of the nervous system (see scheme 6 for molecular structure).

Four polymorphs of piracetam have been identified and structurally characterized (see Table 6). Forms II and III can be prepared by recrystallization from various solvents (e.g. methanol, iso-propanol) under ambient conditions and crystal structures for both forms have been reported.[26,27] Both forms transform above 400 K into the high-temperature phase denoted as form I. This can be obtained under ambient conditions by quenching, but it transforms within a few hours into form II. All polymorphs have been studied by thermochemical methods and shown to be enantiotropically related.[28-31] The hierarchical stability of these polymorphs was studied by relating sublimation vapour pressures to measurements made by differential scanning calorimetry.[31] At ambient temperatures these studies concluded that the stability order is II > III Z I, whilst above 399 K the stability order is I > II > III.[31] Polymorph IV can be obtained *via* high-pressure recrystallization of aqueous and ethanolic solutions of piracetam contained in a diamond-anvil cell at pressures spanning in the range of 0.07–0.4 Gpa. Piracetam posseses also a monohydrate form.[32] The transformations between the polymorphs and hydrate of piracetam are summarized in Scheme 6.

The coordination compound of silver(I) nitrate with 1-phenyl-3-(quinolin-5-yl)urea[17] (PQ5U), [Ag(PQ5U)2]NO_3,[22d] acts as a supramolecular supergelator[11] in the presence of polar solvents such as alcohols and acetonitrile, and matches fairly well the crystallization conditions of the API of interest.

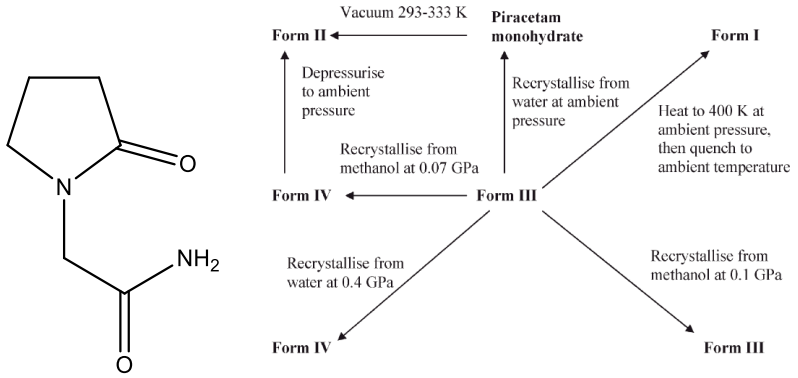

Scheme 6. (a) Molecular structure of piracetam and (b) transformations between all the known polymorphic and solvated forms of piracetam.

6.1 - Crystallization of Piracetam in supramolecular gels of LMWGs [Ag(P5QU)$_2$]NO$_3$ - Experiments were undertaken running in parallel crystallization of piracetam either in gel and solution media (also denoted as blank). Solvents used are methanol, ethanol, *n*-propanol, *i*-propanol and *n*-butanol.

Little amounts of piracetam were placed in vials containing the alcoholic solvents in order to reach a concentration of 4% w/v, either in the blank solvent and in presence of the gelator complex; the suspensions were boiled up until a clear solution was obtained, which was tehn allowed to cool to room temperature.

For the blanks precipitation of piracetam was observed after 12-18 hours. In all cases the polycrystalline materials obtained were identified via X-ray powder diffraction as piracetam form II, with exception of the sample obtained from *i*-propanol which was a mixture of form II and form III (see figure 44).

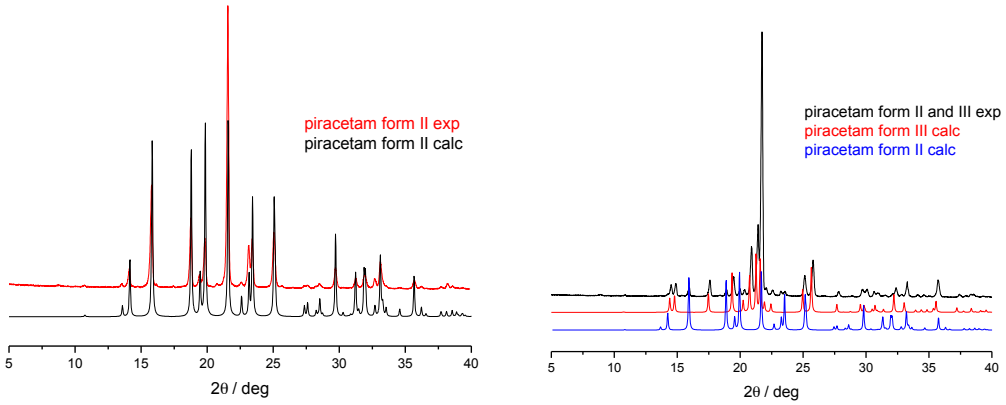

(a) (b)

Fig.44. Comparison of X-ray powder diffraction patterns for piracetam precipitated from alcoholic solutions: (a) piracetam form II obtained from methanol, ethanol, *n*-propanol and *n*-butanol and (b) piracetam as a mixture of forms II and III obtained from *i*-propanol.

Results of crystallization experiments in gels are summarized in table 6 together with those obtained from the blank solutions, and are as follows: in the case of methanol and n-propanol gel formation or crystallization/precipitation was not observed upon cooling to room temperature (permanence of clear solutions); for the other cases after 30 minutes transparent gels were formed and after other 18-20 hours block-shaped crystals grew inside the gel matrix (see figure 45).

Crystals obtained were recovered exploiting the tixotropy[33] of the gel, *i.e.* simply by shaking the gel gel → sol transition is observed. Crystals were identified, by means of single crystal X-ray diffraction, as piracetam form II.

(a) (b)

Fig.45. (a) Piracetam form II obtained as polycrystalline powder from the blank solution and (b) Piracetam form II obtained as single crystals from gel. Concentration of piracetam (4% w/v) is the same in the two experiments, concentration of gelator is 0.35% w/v, solvent is ethanol.

Table 6. Results of the crystallization experiments, in different solvents (blank and in gel), concentration of piracetam and gelator are 4% w/v and 0.35% w/v, respectively. (S = clear solutions; P = polycrystalline precipitate; G = gel formation and C = crystal formation).

Solvent	**Solution (blank)**	**Gel**
MeOH	Form II ^{P}	S
EtOH	Form II ^{P}	G + Form II ^{C}
n-PrOH	Form II ^{P}	S
i-PrOH	Form II / III ^{P}	G+ Form II ^{C}
n-BuOH	Form II ^{P}	G+ Form II ^{C}

7 Conclusions

In summary, we have prepared a series of ligands belonging to the family of di-substituted ureas. In particular we have prepared and characterized by X-ray techniques the following compounds: 1-phenyl-3-(pyridin-2-ylmethyl)urea [PPmU], 1-phenyl-3-(quinolin-5-yl)urea [PQ5U], 1-phenyl-3-(3,5-di(pyridin-2-yl)-4H-1,2,4-triazol-4-yl)urea [PDDPTU], di-3-(3,5-di(pyridin-2-yl)-4H-1,2,4-triazol-4-yl)urea [DDDPTU] and urea, N,N''-1,2-ethanediylbis(N'-phenyl-) [UEBP]. Both PDDPTU and UEBP exists in two polymorphic forms.

Then we have tested them, alone and in combination with metal salts, as low molecular weight gelators of water and organic solvents. Among them only PQ5U shows gelator properties *via* the formation of a complex with the Ag^+ cation, thus we have prepared a supergelator silver(I) complex $[Ag(PQ5U)_2]NO_3$ active in the presence of polar solvents, such as MeOH, EtOH, i-PrOH, n-butanol and CH_3CN. In the air the gels partially lose solvent by forming xerogels that can be reverted to gel by adding solvent, but when the gels are kept in a sealed vial for a week, they are unstable towards crystallization of the gelling coordination compounds. Four different crystal forms of the same gelator could be obtained from four different gelling solvents.

To investigate the relationship between molecular structure and gelation properties we also have synthesized and tested the isomers 1-phenyl-3-(isoquinolin-5-yl)urea [PiQ5U] and 1-phenyl-3-(quinolin-6-yl)urea [PQ6U] and the ligand 1,3-di(quinolin-5-yl)urea [DQ5U]. Gel formation with $AgNO_3$ has been observed only for the latter compound, while reaction of the silver salt with the other ligands isomers only yields complexes. Efforts are in progress to investigate the role of the coordination geometry around the cation during gelation, and the possinility of obtaining gelation with different complexes of formula $[M(PQ5U)_2]NO_3$, where M = copper (I) and gold(I).

In the last section of this chapter we have seen how LMWGs can be used as a medium for crystal growth of organic molecules, such as APIs. The nature of this kind of gels allows easy recovery of the single crystals grown within the gel medium, only by shaking. The complex $[Ag(PQ5U)_2]NO_3$ acts as an inert matrix, slowing down the crystallization rate, thus allowing the formation of large and good quality crystals. In particular we have seen the case of piracetam; in the case of methanol and *n*-propanol probably the interactions arisen in solution between piracetam and the complex hinder the hierarchical assembly of the latter, thus inhibiting gel formation. With other solvents gel formation promotes the growth of the thermodynamic polymorph piracetam form II.

The vast body of literature on supramolecular gels provides a library of gelators that can be chosen to match the crystallization conditions of interest. Supramolecular gels could find application as an important tool within the context of the polymorph screening methodologies. In this direction work is in progress to see if it is possible to extend this method of crystal growth to the preparation of new polymorphic modifications of APIs.

Experimental section

All reactants and reagents, purchased from Sigma-Aldrich, were used without further purification. Reagent grade solvents were used.

Synthesis of 1-phenyl-3-(pyridin-2-ylmethyl)urea [PPmU]. A solution of 0.27 mL (2.5 mmol) of phenyl isocyanate in *ca.* 5 mL of dichloromethane was added dropwise to a stirring solution of 0.24 mL (2.5 mmol) of 2-picolylamine in *ca.* 5 mL of dichloromethane. After 2 hours solvent was removed by rotary evaporation yielding 0.40 g of a white solid. Yield = 80 %, m.p. = decomposes above 200°C. Re-crystallization from methanol gave crystals suitable for SCXRD.

Synthesis of 1-phenyl-3-(quinolin-5-yl)urea [PQ5U].[17] The ligand PQ5U was prepared according to the reported procedure.[x] 5-aminoquinoline (72.3 mg, 5 mmol) was dissolved in dry dichloromethane (ca. 15 mL), then a solution of phenylisocyanate (0.54 mL, 5 mmol) in dichloromethane was added dropwise over two hours, the resulting mixture was stirred at RT for other two hours. The product formed (white powder) was filtered and washed with cold dichloromethane (5 x 2 mL). Yield: 85%. Re-crystallization from methanol gave crystals suitable for SCXRD.

Synthesis of 1-phenyl-3-(3,5-di(pyridin-2-yl)-4H-1,2,4-triazol-4-yl)urea [PDDPTU]. A solution of 0.27 mL (2.5 mmol) of phenyl isocyanate in *ca.* 8 mL of dichloromethane was added dropwise to a stirring solution of 0.6 g (2.5 mmol) of 4-amino-3,5-di-pyridyl-4H-1,2,4-triazole in *ca.* 25mL of dichloromethane over a period of 2 hours. The formed precipitate was collected through filtration and washed with dichloromethane yielding 0.88 g of a white solid. Yield = 98%, m.p. = decomposes above 200°C.

Crystals suitable for SCXRD can be growth by recrystallization from acetonitrile or methanol. Two polymorphs have been obtained: PDDPTU I and PDDPTU II.

Synthesis of di-3-(3,5-di(pyridin-2-yl)-4H-1,2,4-triazol-4-yl)urea [DDDPTU]. To a solution of 4-amino-3,5-di-pyridyl-4H-1,2,4-triazole (16.2 mg, 0.68 mmol) in dry dichloromethane (ca. 10 mL) were added 0.2 mL of tri-ethylamine, followed by 67.3 mg (0.226 mmol) of triphosgene. The mixture had been stirred for at RT for 1 hour, the yellow precipitate formed was recovered through filtration and washed with cold dichloromethane (5 x 2 mL) yielding 0.1819 g. Yield: 22 %. Recrystalization from nitromethane afforded crystals suitable for SCXRD.

Synthesis of Urea, N,N''-1,2-ethanediylbis(N'-phenyl-) [UEBP]. A solution of 0.27 mL (2.5 mmol) of phenyl isocyanate in *ca.* 10 mL of dichloromethane was added dropwise to a stirring solution of 75 mg (1.25 mmol) of ethane-1.2-di-amine in *ca.* 5 mL of dichloromethane over a period of 1 hour. The formed precipitate was collected through filtration and washed with dichloromethane yielding 0.88 g of a white solid. Yield = 90%, m.p. = decomposes above 260°C.
Crystals suitable for SCXRD can be growth by slow evaporation of a DMSO solution, or by vapour diffusion of water into the DMSO solution. Two polymorphs have been obtained: UEBP I and UEBP II.

Synthesis of 1-(isoquinolin-5-yl)-3-phenylurea [PiQ5U]. 5-aminoisoquinoline (72.1 mg, 5 mmol) was dissolved in dry acetone (ca. 15 mL), than a solution of phenylisocyanate (0.54 mL, 5 mmol) in acetone was added dropwise over two hours, the resulting mixture was stirred at RT for other four hours. The product formed (brownish powder) was recovered by filtration and washed with cold acetone (5 x 2 mL). Colourless crystals (needles) suitable for X-ray diffraction were obtained by vapor diffusion of water into a dimethylsulfoxyde solution of the freshly synthesized ligand. Yield: 75%.

Synthesis of 1-phenyl-3-(quinolin-6-yl)urea [PQ6U]. 6-aminoquinoline (72.3 mg, 5 mmol) was dissolved in dry dichloromethane (ca. 15 mL), than a solution of phenylisocyanate (0.54 mL, 5 mmol) in dichloromethane was added dropwise over two hours, the resulting mixture was stirred at RT for other two hours. The product formed (white powder) was recovered by filtration and washed with cold dichloromethane (5 x 2 mL). Re-crystallization from alcohols (methanol or ethanol) or acetonitrile afforded only a polycrystalline powder. Yield: 85%.

Synthesis of 1,3-di(quinolin-5-yl)urea [DQ5U]. To a solution of 5-aminoquinoline (98.4 mg, 0.68 mmol) in dry dichloromethane (ca. 10 mL) were added 0.2 mL of tri-ethylamine, followed by 67.3 mg (0.226 mmol) of triphosgene. The mixture had been stirred for at RT for 1 hour, the off-white precipitate formed was recovered through filtration and washed with dichloromethane (5 x 2 mL). Slow evaporation of a dimethyl sulfoxide solution gave small block-shaped colourless crystals. Yield: 20 %.

Hot stage Microscopy. Hot Stage experiments were carried out using a Linkam TMS94 device connected to a Linkam LTS350 platinum plate. Images were collected with the imaging software Cell, from an Olympus BX41 stereomicroscope.

Fluorescence microscopy. The fluorescence images were obtained with an inverted microscope (Olympus IX71) equipped with a cooled CCD camera (Princeton Instruments, Photon Max 512) and using as excitation light the 488nm laser emission of an Ar^+ ion laser (Melles Griot, IMA1-Multiwavelength, 43 series ion laser).

UV-VIS spectra was recorded on a Perkin-Elmer LS 50 with cuvettes of 1cm; luminescence spectra were recorded on a *Perkin-Elmer LS 50*.

Mass spectroscopy. Samples of gels for ESI-MS have been prepared as follow: $AgNO_3$ and PQ5U were ground in the stoichiometric ratio 1:2, 9.8 mg of the mixture were suspended in 12 mL of acetonitrile and warmed up to reach a clear solution (0.82 mg mL^{-1}).

X-ray diffraction. Single-crystal data for synthesized compounds and complexes were collected on an Oxford X'Calibur S CCD diffractometer equipped with a graphite monochromator (Mo-Kα radiation, λ = 0.71073Å) and operating at room temperature. Crystal data and details of measurement for all compounds are listed in Table 1. All non-hydrogen atoms were refined anisotropically; H_{OH} atoms were either directly located or added in calculated positions; H_{CH} atoms for all compounds were added in calculated positions and refined riding on their respective carbon atoms. SHELX97[34a] was used for structure solution and refinement on F^2, PLATON[34b], Mercury[34c] and SCHAKAL99[34d] were used for hydrogen bonding analysis and molecular graphics, respectively.

For structure solution and refinement purposes, X-ray powder diffractograms in the 2θ range 5-70° (step size, 0.01°; time/step, 50 s; 0.02 rad soller; VxA 40 x 40) were collected on a Panalytical X'Pert PRO automated diffractometer equipped with an X'Celerator detector. For phase identification purposes, X-ray powder diffractograms in the 2θ range 5-40° (step size, 0.02°; time/step, 20 s; 0.04 rad soller; VxA 40 x 40) were collected on a Panalytical X'Pert PRO automated diffractometer equipped with an X'Celerator detector. All data were collected in Bragg_Brentano geometry, using Cu Kα radiation without a monochromator. The program PowderCell[34e] was used for calculation of X-ray powder patterns on the basis of single crystal data. The identity between bulk materials and single crystals was always verified by comparing calculated and experimental powder diffraction patterns.

Structure determination of PQ6U. Powder diffraction data were analyzed with the software expo2010,[35a] which is designed to analyze either monochromatic and nonmonochromatic data. Peaks were automatically chosen in the 2θ range 5-40°, and a monoclinic cell was found, using the algorithm N-TREOR,[35b] with a volume of 1282.65 $Å^3$. The structure was then solved by simulated annealing using as molecular model built with Avogadro[36] software and refined by Rietveld analysis with the software GSAS.[37] A spherical orientation model was used to describe preferred orientation. Soft constrains were applied on bond distances and angles. Refinement converged with $\chi^2 = 8.5\%$, $R_{wp} = 9.14\%$ and $R_p = 7.08\%$.

Table 1a. Crystal data and details of measurements for compounds **PPmU PQ5U and PDDPTU** form **I and II.**

	PPmU	**PQ5U**	**PDDPTU I**	**PDDPTU II**
Formula	$C_{13}H_{13}N_3O$	$C_{16}H_{13}N_3O$	$C_{19}H_{15}N_7O$	$C_{19}H_{15}N_7O$
Z	4		4	2
a (Å)	11.9622(19)	12.3447(3)	11.1275(13)	6.1197(4)
b (Å)	18.072(2)	4.5957(10)	10.2052(9)	8.0872(7)
c (Å)	21.450(4)	11.4845(3)	16.4320(17)	17.6755(13)
α (deg)	90	90	90	90
β (deg)	90	95.416(2)	105.398(11)	91.449(6)
γ (deg)	90	90	90	90
fw	227,26	263.29	357.38	357.38
V ($Å^3$)	4637.23	648.64(3)	1799.0(3)	874.50(11)
D_{calc} (Mg/m^3)	1.302	1.348	1.268	1.357
μ (mm^{-1})	0.086	0.087	0.084	0.091
Cryst. System	Orthorhombic	Monoclinic	Monoclinic	Monoclinic
Space group	Pbca	Pc	$P2_1/c$	$P2_1$
n° of collected reflns	17743	5296	7850	4122
n° of indep. reflns	8981	1935	4037	2847
R1[on F_0^2,I>2sigma(I)]	0.0844	0.0260	0.0554	0.0560
wR2 (all data)	0.1896	0.0272	0.1072	0.0790

Table 1b. Crystal data and details of measurements for compounds: **DDDPTU** and **UEBP** form **I** and **II.**

	DDDPTU ·2H_2O	**UEBP I**	**UEBP II**
Formula	$C_{25}H_{22}N_{12}O_3$	$C_{16}H_{18}N_4O_2$	$C_{16}H_{18}N_4O_2$
Z	8	4	8
a (Å)	13.8049(11)	9.704	10.3482(11)
b (Å)	13.2395(10	4.669	9.1848(9)
c (Å)	15.7491(14)	16.807	15.903(2)
α (deg)	90	90	90
β (deg)	113.570(10)	102.61	90
γ (deg)	90	90	90
fw	538,52	298.34	298.34
V ($Å^3$)	2638.3(4)	743.1	1511.5(3)
D_{calc} (Mg/m^3)	1.401	1.333	1.311
μ (mm^{-1})	0.101	0.091	0.090
Cryst. System	Monoclinic	Monoclinic	Orthorhombic
Space group	C2/c	$P2_1/n$	Pbca
n° of collected reflns	5716	2168	3615
n° of indep. reflns	2964	1224	1647
R1[on F_0^2,I>2sigma(I)]	0.0403	0.0454	0.0631
wR2 (all data)	0.0902	0.1107	0.1380

Table 1c. Crystal data and details of measurements for compounds PiQ5U, PQ6U, DQ5U and complexes obtained with the ligand PQ6U.

	PiQ5U	**PQ6U**	**DQ5U**	**[Ag(PQ6U)2]NO_3·CH_3CN**	**[Ag(PQ6U)2]NO_3**
Formula	$C_{16}H_{13}ON_3$	$C_{16}H_{13}ON_3$	$C_{18}H_{14}ON_2$	$C_{34}H_{27}O_5N_8Ag$	$C_{32}H_{26}O_5N_7Ag$
Z	4	4	4	2	8
a (Å)	24.0204(1)	19.2919(9)	4.593	7.3672(2)	12.9856(7)
b (Å)	4.5893(3)	4.58451(3)	11.696	9.0123(4)	16.9749(10)
c (Å)	11.8276(1)	14.6857(1)	13.723	25.5246(8)	27.0605(13)
α (deg)	90	90	90	85.865(3)	90
β (deg)	96.411(7)	99.062(9)	90	87.607(3)	90
γ (deg)	90	90	90	69.359(3)	90
fw	263.29	263.29	314.34	735.51	696.47
V ($Å^3$)	1295.68(6)	1282.65	737.2	1581.56	5964.9(6)
D_{calc} (Mg/m^3)	1.350	-	1.416	1.544	1.551
μ (mm^{-1})	0.087	-	0.092	0.694	0.730
Cryst. System	Monoclinic	Monoclinic	Orthorhombic	Triclinic	Orthorhombic
Space group	$P2_1/c$	$P2_1/n$	$P22_12_1$	P-1	Pbca
n° of collected reflns	4414	-	2002	23963	25623
n° of indep. reflns	2641	-	1386	7541	7150
R1[on F_0^2,I>2sigma(I)]	0.0651	-	0.0503	0.0973	0.0605
wR2 (all data)	0.01469	-	0.076	0.1832	0.1083

Table 1d. Crystal data and structure refinement details for $[Ag(PQ5U)_2]NO_3$ for Forms I, II, III and IV.

	I	**II**	**III**	**IV**
Chemical formula	$C_{32}H_{26}N_7O_5Ag$	$C_{32}H_{26}N_7O_5Ag$	$C_{32}H_{26}N_7O_5Ag$	$C_{32}H_{26}N_7O_5Ag$
fw	696.47	696.47	696.47	696.47
Crystal System	Monoclinic	Monoclinic	Triclinic	Triclinic
Space group	$P2_1/_n$	C2/c	P-1	P-1
Z	4	4	1	2
Z'	1	0.5	0.5	1
a (Å)	14.9972(7)	13.842(1)	6.2652(2)	7.6870(3)
b (Å)	9.1664(5)	8.3439(7)	7.8792(2)	10.5157(4)
c (Å)	21.561(1)	25.208(2)	15.022(1)	18.9647(8)
α (deg)	90	90	95.156(6)	100.092(3)
β (deg)	101.587(5)	98.141(7)	91.583(6)	101.640(3)
γ (deg)	90	90	94.165(6)	99.170(3)
V ($Å^3$)	2903.6(3)	2882.0(4)	736.1	1447.8(1)
D_{calc} (Mg/m^3)	1.593	1.605	1.571	1.598
μ (mm^{-1})	0.750	0.756	0.740	0.752
n° of collected reflns	12854	6327	5778	10982
n° of indep. reflns	6146	3262	3315	6475
R1[on F_0^2,I>2sigma(I)]	0.0457	0.0415	0.0630	0.0375
wR2 (all data)	0.1098	0.0959	0.2091	0.0485

Gelation tests. In a typical gelation experiment an amount, in the range 10-25, mg of a finely ground metal transition salt:ligand mixture in 1:2; 1:1 or 0:1 molar ratio was suspended in 5 mL of an organic solvent in a 2 cm diameter vial, and the vial was heated until clear a solution was obtained, which was allowed to cool to room temperature. Gelation was complete when the vial could be inverted without liquid flow ("tube inversion test").[2] Minimum gelation concentration was determined by adding 0.1 mL aliquotes of solvent and repeating the inversion test.

Gel preparation, determination of the gel-sol dissociation temperatures and construction of a sol-gel plot. A plot of the gel-sol dissociation temperature (T_{gel}) in alcohols (for gels obtained with $AgNO_3$:PQ5U) or solvent mixture ethanol:dmf (for gels obtained with $AgNO_3$:DQ5U) versus the gelator concentration was constructed by using the "dropping ball" method,[2] in which a 0.5 g steel ball was placed on the gel surface in 2 cm diameter vials. The vials were slowly heated in an oil-bath (ca. 1 deg min^{-1}). The temperature at which the steel ball fell to the bottom of the vial was taken as *the gel dissociation temperature* (T_{gel}), see figure ES1.

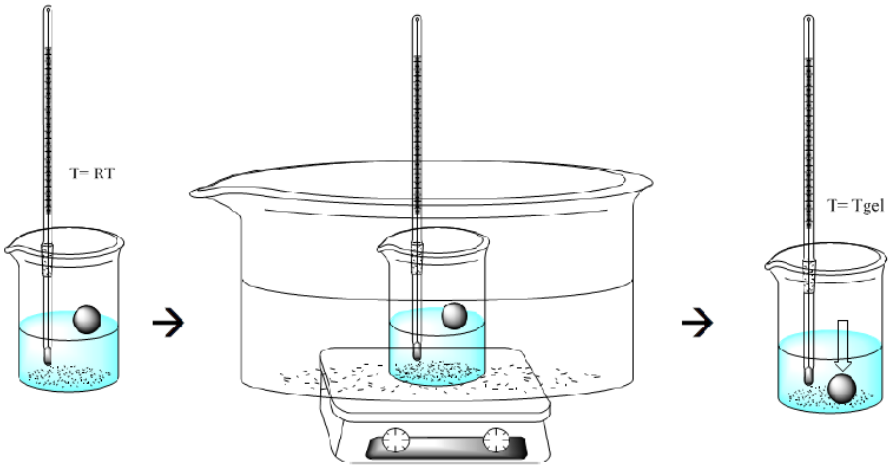

Fig.ES1. Representation of the determination of the T_{gel} by using the dropping ball method.

References

[1] J. D. Ferry, *Viscoelastic Properties of Polymers*. New York: Wiley, 1980.

[2] (a) R. G. Weiss and P. Terech, *Molecular Gels Materials with Self-Assembled Fibrillar* Networks, Springer, Dordrecht, 2006; (b) D. K. Smith, in *Organic Nanostructures*, ed. J. L. Atwood and J. W. Steed, WILEY-VCH, Weinheim, 2008, pp. 111–148.

[3] P. J. Flory, Faraday Discuss. *Chem. Soc.*, 1974, **57**, 7–18.

[4] P. Dastidar, *Chem. Soc. Rev.*, 2008, **37**, 2699–2715.

[5] (a) M. M. Piepenbrock, N. Clarke and J. W. Steed, *Langmuir*, 2009, **25**, 8451–8456; (b) N. N. Adarsh, P. Sahoo and P. Dastidar, *Cryst. Growth Des.*, 2010, **10**, 4976–4986.

[6] M. M. Piepenbrock, G. O. Lloyd, N. Clarke and J. W. Steed, *Chem. Rev.*, 2010, **110**, 1960–2004.

[7] A. R. Hirst, B. Escuder, J. F. Miravet and D. K. Smith, *Angew. Chem., Int. Ed.*, 2008, **47**, 8002–8018.

[8] J. A. Foster, M. M. Piepenbrock, G. O. Lloyd, N. Clarke, J. A. K. Howard and J. W. Steed, *Nat. Chem.*, 2010, **2**, 1037–1043.

[9] (a) D. Braga, F. Grepioni and L. Maini, *Chem. Commun.*, 2010, **46**, 6232–6242; (b) J. Bernstein, *Polymorphism in Molecular Crystals*, Clarendon Press, Oxford, 2002; (c) U. Griesser, *Polymorphism in the Pharmaceutical Industry*, ed. R. Hilfiker, Wiley VCH, Weinheim, 2006, pp. 211–234; (d) S. L. Childs and M. J. Zaworotko*, Cryst. Growth Des.*, 2009, **9**, 4208–4211; (e) G. R. Desiraju, *Cryst. Growth Des.*, 2008, **8**, 3–5.

[10] G. C. Maity, *Journal of Physical Sciences*, 2007, **11**, 156-171.

[11] P. J. Flory, *Faraday Discuss*. 1974, ***57***, 7.

[12] (a) J. N. Israelachvili, *Intermolecular and Surface Fources*, 2nd ed.; *Academic Press: New York*, 1991. (b) J. M. Schnur, *Science* 1993, **262**, 1669. (c) N. Nandi, B. J. Bagchi, *J. Am. Chem. Soc*. 1996, **118**, 11208.

[13] P. Jonkheijm, P. van der Schoot, A.P.H.J. Schenning and E. W. Meijer, *Science*, 2006, **313**, 80–83.

[14] A. Aggeli, I. A. Nyrkova, M. Bell, R. Harding, L. Carrick, T. C. B. McLeish, A. N. Semenov N. Boden, *Proc. Natl. Acad. Sci. USA*, 2001, **98**, 11857–11862.

[15] F. Fages, F. Vogtle, M. and Zinic, *Top. Curr. Chem.*, 2005, **256**, 77–131.

[16] (a) I. A. Coates, A. R. Hirst and D. K. Smith, *J. Org. Chem.*, 2007, **72**, 3937–3940. (b) K. Tomioka, T. Sumiyoshi, S. Narui, Y. Nagaoka, A. Iida, Y. Miwa, T. Taga, M. Nakano and T. Handa, *J. Am. Chem. Soc.*, 2001, **123**, 11817–11818. (c) K. Hanabusa, R. Tanaka, M.

Suzuki, M. Kimura and H. Shirai, *Adv. Mater.*, 1997, **9**, 1095–1097; (d) X. Luo, C. Li and Y. Liang, *Chem. Commun.*, 2000, 2091–2092. (e) J. J. van Gorp, J. A. J. M. Vekemans, and E. W. Meijer, *J. Am. Chem. Soc.*, 2002, **124**, 14759–14769. (f) K. Hanabusa, M. Yamada, M. Kimura and H. Shirai, *Angew. Chem. Int. Ed. Engl.*, 1996, **35**, 1949–1951.

[17] D. Kalita, R. Sarma and J. B. Baruah, *CrystEngComm*, 2009, **11**, 803–810.

[18] (a) J. Bernstein, R. E. Davis, L. Shimoni and N.-L. Chang, *Angew. Chem. Int. Ed. Eng.*, 1995, **34**, 1555–1573. (b) M. C. Etter, *Acc. Chem. Res.*, 1990, **23**, 120. (c) M. C. Etter, J. C. MacDonald and J. Bernstein, *Acta Cryst.* 1990, **B46**, 256-262 .

[19] H. Brittain, in *Methods for the characterization of polymorphs and solvates*.Ed. In H. G. Brittain. *Polymorphism in Pharmaceutical Solids*. Marcel Dekker, Inc., New York, 1999, pp. 227-278.

[20] C. Six, F. Richter, *Isocyanates, Organic* in Ulmann's Encyclopedia of Industrial Chemistry, 2005, Wiley-VCH, Weinheim.

[21] Critical gelator concentrations (% w/v) are 0.08, 0.16, 0.20, 0.30 and 0.36 for 1-butanol, ethanol, i-propanol, methanol and acetonitrile, respectively.

[22] (a) K. D. Krishna, J. D. Amilan, A. Das and P. Dastidar*, Chem. Commun.*, 2005, 4059–4061. (b) N. N. Adarsh, P. Sahoo and P. Dastidar, *Cryst. Growth Des.*, 2010, **10**, 4976–4986. (c) D. Braga, S. d'Agostino, E. D'Amen and F. Grepioni, *Chem. Commun.*, 2011, **47**, 5154–5156.

[23] (a) D. Braga, F. Grepioni and L. Maini, *Chem. Commun.* 2010, **46**, 6232–6242; b) J. Bernstein, *Polymorphism in Molecular Crystals*, Clarendon Press, Oxford, 2002; c) U. Griesser, *Polymorphism in the Pharmaceutical Industry*, ed. R. Hilfiker, Wiley VCH, Weinheim, 2006, pp. 211–234; d) S. L. Childs and M. J. Zaworotko, *Cryst. Growth Des.* 2009, **9**, 4208–4211; e) G. R. Desiraju, *Cryst. Growth Des*. 2008, **8**, 3–5.

[24] B. Moulton and M. J. Zaworotko, *Chem. Rev.,* 2001, **101**, 1629-1658.

[25] (a) M. M. Piepenbrock, G. O. Lloyd, N. Clarke and J. W. Steed, *Chem. Rev.*, 2010, **110**, 1960–2004. (b) P. Dastidar, *Chem. Soc. Rev.*, 2008, **37**, 2699–2715.

[26] Stahly, G. P. *Cryst. Growth Des.,* 2007, **7**, 1007–1026.

[27] G. Bandoli, D. A. Clemente, A. Grassi and G. C. Pappalardo, *Mol. Pharmcol.*, 1981, **20**, 558–564.

[28] G. Admiraal, J. C. Eikelenboom and A. Vos, *Acta Crystallogr., Sect. B*, 1982, **38**, 2600–2605.

[29] S. Toscani, *Thermochim. Acta*, 1998, **321**, 73–79.

[30] M. Kuhnert-Brandstatter, A. Burger and R. Vollenkee, *Sci. Pharm*., 1994, **62**, 307–316.

[31] R. Ceolin, V. Agafonov, D. Louer, V. A. Dzyabchenko, S. Toscani and J. M. Cense, *J. Solid State Chem.*, 1996, **122**, 186–194.

(32) F. P. A. Fabbiani, D. R. Allan, S. Parsons and C. R. Pulham, *CrystEngComm*, 2005, **7**(29), 179–186.

[33] Tixotropy is the property of certain gels or fluids that are thick (viscous) under normal conditions, but flow (become thin, less viscous) over time when shaken, agitated, or otherwise stressed.

[34] (a) G. M. Sheldrick, SHELX97, *Program for Crystal Structure Determination*; University of Gottingen: Gottingen, Germany, 1997. (b) A. L. Speck, PLATON; *Acta Crystallogr., Sect. A*, 1990, 46, C34; (c) C. F. Macrae, I. J. Bruno, J. A. Chisholm, P. R. Edgington, P. McCabe, E. Pidcock, L. Rodriguez-Monge, R. Taylor, J. van de Streek and P. A. Wood, *J. Appl. Cryst.*, 2008, **41**, 466-470 (d) E. Keller, *SCHAKAL99*, *Graphical Representation of Molecular Models*; University of Freiburg: Freiburg, Germany, **1999** . (e) PowderCell programmed by W. Kraus and G. Nolze (BAM Berlin) subgroups derived by Ulrich Muller (Gh Kassel).

[35] (a) A. Altomare, M. Camalli, C. Cuocci and R. Rizzi, *J.Appl. Cryst.stallog.*, 2009, **42**, 1197-1202. (b) A. Altomare, C. Giacovazzo A. Molinterni and R. Rizzi, *J.Appl. Cryst.stallog.*, 2001, **34**, 704-709.

[36] see http://avogadro.openmolecules.net

[37] A. C. Larson and R. B. von Dreele, General Structure Analysis System (GSAS); Los Alamos National Laboratory LAUR86-748: Los Alamos, NM, 2000.

Aknowledgements

First of all I would like to thank my supervisors Prof. Dario Braga and Prof. Fabrizia Grepioni, for all the helps and the trust they gave me in these years. I also would like to thank Prof. Stuart Batten for the hospitality in Melbourne and for allowing me to synthesize some coordination polymers and to use their amazing toy, that is the Australian Synchrotron.

Thank you to all my collegues and all the students that shared with me this trip in the world of crystals and gels.

Special thanks go to my fiancée, Piera, and to my family. I would like to dedicate this work to my niece born "Down Under" in January.

Ciao Sophia.